
Doctoral Dissertations

Student Theses and Dissertations

1952

An investigation of the deformation textures of titanium

Dean Nesbit Williams

Follow this and additional works at: https://scholarsmine.mst.edu/doctoral_dissertations



Part of the [Metallurgy Commons](#)

Department: **Materials Science and Engineering**

Recommended Citation

Williams, Dean Nesbit, "An investigation of the deformation textures of titanium" (1952). *Doctoral Dissertations*. 986.

https://scholarsmine.mst.edu/doctoral_dissertations/986

This thesis is brought to you by Scholars' Mine, a service of the Missouri S&T Library and Learning Resources. This work is protected by U. S. Copyright Law. Unauthorized use including reproduction for redistribution requires the permission of the copyright holder. For more information, please contact scholarsmine@mst.edu.

Blk 710

T1036

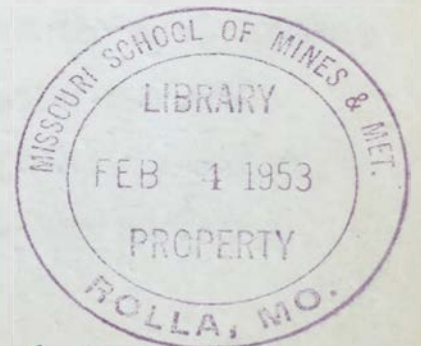
10710

AN INVESTIGATION OF THE DEFORMATION TEXTURES
OF TITANIUM

An Abstract
of a Dissertation
Presented to
the Faculty of the Graduate School
University of Missouri

In Partial Fulfillment
of the Requirements for the Degree
Doctor of Philosophy

by
Dean Nesbit Williams
May 1952



81370

AN INVESTIGATION OF THE DEFORMATION TEXTURES
OF TITANIUM

The textures of deformed titanium were determined using a modification of the Schulz-Decker Geiger counter technique. This technique allowed semiquantitative pole figures of high accuracy to be constructed. Pole figures were constructed for the $10\bar{1}0$, 0001 , and $10\bar{1}1$ planes.

Samples of iodide titanium deformed in compression by compression between parallel plates and by compression rolling were examined after reductions in thickness varying from 24.1 to 98.9 percent. A $[0001]$ texture rotated up to thirty degrees from the compression axis was found. As the amount of reduction increased, the angle of the $[0001]$ rotation decreased, reaching seventeen and one-half degrees at 98.9 percent. The final texture was independent of the method of compression.

Cold rolled textures of iodide titanium and of three grades of commercial titanium were determined. The iodide titanium and two of the three grades of commercial titanium showed a $(0001)[10\bar{1}0]$ texture rotated thirty degrees or more toward the transverse direction. The greatest preferred orientation was found in the $10\bar{1}0$ pole figure in which a $\langle 10\bar{1}0 \rangle$ direction tended strongly to be located in the rolling direction. The third commercial titanium sample showed a second texture, in addition to the above texture, in which the (0001) rotation was twenty degrees toward the rolling

direction.

The deformation process in titanium was examined theoretically using the method developed by Calnan and Clews and the necessary modes of slip and twinning to give the observed compression and cold rolling textures and the reported drawing texture were determined. The $\{0001\}\langle 11\bar{2}0 \rangle$, $\{10\bar{1}1\}\langle 11\bar{2}0 \rangle$, and $\{10\bar{1}0\}\langle 11\bar{2}0 \rangle$ slip systems and the $\{10\bar{1}2\}$, $\{11\bar{2}2\}$, and $\{11\bar{2}1\}$ twinning systems were considered individually and the textures which would result from their action determined. By combining the slip and twinning systems so that the critical shear stress for slip, C_s , and for twinning, C_t , were related as follows,

$$C_{s0001} = 1.1 C_{s10\bar{1}1} = 1.02 C_{s10\bar{1}0} = C_{t10\bar{1}2} = C_{t11\bar{2}2}.$$

The observed tension and compression textures could be explained. These modes of slip and twinning were also used successfully to develop a theoretical 0001 pole figure for cold rolled titanium which was similar in form to the measured texture.

AN INVESTIGATION OF THE DEFORMATION TEXTURES
OF TITANIUM

A Dissertation
Presented to
the Faculty of the Graduate School
University of Missouri

In Partial Fulfillment
of the Requirements for the Degree
Doctor of Philosophy

by
Dean Nesbit Williams
May 1952

ACKNOWLEDGEMENTS

The author would like to thank the Titanium Alloy Manufacturing Division of the National Lead Company for support of the research fellowship under which this work was conducted and to express his gratitude to Dr. S. F. Urban, Director of Research of the Titanium Alloy Manufacturing Division, for his aid in procuring the samples of titanium examined and for furnishing the analysis of the samples of commercial titanium.

The author would also like to acknowledge the aid and advice given by Dr. D. S. Eppelsheimer, Professor of Metallurgical Engineering, and to thank him for his enthusiasm and for the manner in which he made available his vast familiarity with the literature.

TABLE OF CONTENTS

CHAPTER		PAGE
I	INTRODUCTION	1
	A. THE PROBLEM	1
	Statement of the problem	1
	Importance of the study	2
	B. OUTLINE OF THE STUDY	3
II	REVIEW OF THE LITERATURE	4
	Literature of the deformation of titanium	4
	Literature on the determination of pole figures	6
	Literature of the origin of textures.	9
III	DESCRIPTION OF THE METAL INVESTIGATED	17
	A. SOURCE OF THE METALS EXAMINED	17
	Iodide titanium	17
	Commercial titanium grade number one	18
	Commercial titanium grade number two	18
	Commercial titanium grade number three	18
	B. COMPOSITION OF TITANIUM SAMPLES	18
	C. ANNEALING PROCEDURES	20
	Procedure for air annealing	21
	Procedure for inert gas annealing	21
	Procedure for vacuum annealing	22

CHAPTER		PAGE
	D. HARDNESS, GRAIN SIZE, AND MICROSTRUCTURE OF ANNEALED TITANIUM	23
	Annealed hardness of titanium samples	23
	Microstructure of annealed titanium samples	25
	Grain size determination	28
IV	THE PREPARATION AND X-RAY EXAMINATION OF SPECIMENS	30
	A. COMPRESSION METHODS	30
	Preparation of compression samples	31
	Compression between parallel plates	31
	Compression by compression rolling	32
	B. COLD ROLLING METHODS	32
	Preparation of the samples for cold rolling	34
	Cold rolling of samples	34
	C. PREPARATION OF X-RAY SAMPLES	36
	Preparation of transmission samples	36
	Preparation of reflection samples	38
	Etching techniques	39
	D. THE X-RAY TECHNIQUE	39
	Measurement of X-ray intensity	40
	Plotting of the pole figures	41
V	THE COMPRESSION TEXTURE OF IODIDE TITANIUM	42
	A. EXPERIMENTAL RESULTS	43
	0001 pole figures of compressed titanium	43

CHAPTER

PAGE

	Relative intensity of the 0001 maximum	50
	Effect of grinding or filing after compression	51
	Evidence of a preferred axis of rotation	53
	B. DISCUSSION OF RESULTS	55
	C. SUMMARY	57
VI	THE COLD ROLLED TEXTURE OF TITANIUM	59
	A. EXPERIMENTAL RESULTS	60
	Cold rolled texture of iodide titanium	62
	Cold rolled texture of commercial titanium	64
	Changes in texture with amount of deformation	67
	B. DISCUSSION OF RESULTS	69
	C. SUMMARY	73
VII	THEORETICAL ANALYSIS OF THE DEFORMATION TEXTURES OF TITANIUM	74
	A. GENERAL PRINCIPLES OF THE CALNAN AND CLEWS METHOD	75
	B. CALCULATION OF RESOLVED SHEAR STRESS VALUES	83
	C. DEFORMATION BY SLIP	84
	$\{0001\}\langle 11\bar{2}0 \rangle$ slip	85
	$\{10\bar{1}1\}\langle 11\bar{2}0 \rangle$ slip	85
	$\{10\bar{1}0\}\langle 11\bar{2}0 \rangle$ slip	95
	Combined slip system	95

CHAPTER

PAGE

D. DEFORMATION BY TWINNING 105

 {10 $\bar{1}$ 2} twinning 107

 {11 $\bar{2}$ 2} twinning 108

 {11 $\bar{2}$ 1} twinning 111

E. THE DEFORMATION TEXTURES OF TITANIUM . 114

 The tension texture of titanium . . . 114

 The compression texture of titanium . 116

 The cold rolled texture of titanium . 118

F. DISCUSSION 122

VIII SUMMARY AND CONCLUSIONS 126

A. SUMMARY 126

B. CONCLUSIONS 127

BIBLIOGRAPHY 129

APPENDIX 135

I X-RAY TECHNIQUE 136

A. CONSTRUCTION OF THE SPECIMEN MOUNT . . 137

B. USE OF THE SPECIMEN MOUNT 140

 Making transmission patterns 141

 Making reflection patterns 144

 Plotting of the data 150

II INTERPRETATION AND ADJUSTMENT OF DATA 151

A. TABULATION OF INTENSITY DATA 151

B. CORRECTION OF TRANSMISSION READINGS
 FOR ABSORPTION 155

C. CORRELATION OF PATTERNS 158

CHAPTER	PAGE
D. PLOTTING OF DATA	159
III THE RECRYSTALLIZATION TEXTURE OF COMMERCIAL TITANIUM	164
A. EXPERIMENTAL PROCEDURE	164
B. DISCUSSION OF RESULTS	165
C. SUMMARY	170
VITA	171

LIST OF TABLES

TABLE	PAGE
I	Reported Analysis of Titanium Samples 19
II	Grain Size and Hardness of Annealed Titanium 24
III	Dimensional Changes During Rolling of Titanium 35
IV	Textures Developed by Compressed Iodide Titanium 44
V	Percent Reduction of Cold Rolled Titanium Samples 61
VI	Active Slip Elements in the $\{0001\}\langle 11\bar{2}0 \rangle$ Slip System 87
VII	Active Slip Elements in the $\{10\bar{1}1\}\langle 11\bar{2}0 \rangle$ Slip System 92
VIII	Active Slip Elements in the $\{10\bar{1}0\}\langle 11\bar{2}0 \rangle$ Slip System 97
IX	Active Slip Elements in the Combined Slip System 102
X	Intersections of Twin-Slip Boundaries for $\{10\bar{1}2\}$ Twinning 109
XI	Intersections of Twin-Slip Boundaries for $\{11\bar{2}2\}$ Twinning 112
XII	$10\bar{1}1$ Intensities From Transmission Pattern 154
XIII	$10\bar{1}1$ Intensities From Reflection Pattern 154
XIV	Correction Factor For Transmission Intensities 156
XV	Corrected Transmission Intensities 157
XVI	Correlated Intensity Values 160
XVII	Final Adjusted $10\bar{1}1$ Intensity Values 161

LIST OF FIGURES

FIGURE		PAGE
1.	Annealed iodide titanium--100X	26
2.	Annealed commercial titanium grade number one--100X	26
3.	Annealed commercial titanium grade number two--250X	27
4.	Annealed commercial titanium grade number three--250X	27
5.	Iodide titanium compression rolled 89.6 percent reduction in thickness	33
6.	Edge cracking and increase in width during cold rolling	33
7.	0001 pole figure of compressed iodide titanium--24.1 percent reduction	46
8.	0001 pole figure of compressed iodide titanium--34.3 percent reduction	46
9.	0001 pole figure of compression rolled iodide titanium--50.0 percent reduction	47
10.	0001 pole figure of compressed iodide titanium--80.1 percent reduction	47
11.	0001 pole figure of compressed iodide titanium--86.3 percent reduction	48
12.	0001 pole figure of compression rolled iodide titanium--89.6 percent reduction	48
13.	0001 pole figure of compression rolled iodide titanium--96.2 percent reduction	49
14.	0001 pole figure of compression rolled iodide titanium--98.9 percent reduction	49
15.	Comparison of the 0001 patterns of compressed iodide titanium (34.3 percent reduction) after various methods of specimen preparation	52

FIGURE	PAGE
16.	Pole figures of iodide titanium reduced 98.9 percent by compression rolling showing the tendency for 0001 rotation to occur about a $\langle 10\bar{1}0 \rangle$ rotation axis 54
17.	Cold rolled iodide titanium 63
18.	Cold rolled commercial titanium sample number one 65
19.	Cold rolled commercial titanium sample number three 66
20.	0001 pole figures of cold rolled commercial titanium sample number three 68
21.	Position of the ideal textures 70
22.	Sample resolved shear stress contour diagram plotted in the hexagonal unit stereographic triangle 77
23.	Resolved shear stress contours for $\{0001\}$ $\langle 11\bar{2}0 \rangle$ slip 86
24.	Tension slip rotations and tension texture resulting from $\{0001\}\langle 11\bar{2}0 \rangle$ slip 88
25.	Compression slip rotations and compression texture resulting from $\{0001\}\langle 11\bar{2}0 \rangle$ slip 89
26.	Resolved shear stress contours for $\{10\bar{1}1\}$ $\langle 11\bar{2}0 \rangle$ slip 91
27.	Tension slip rotations and tension texture resulting from $\{10\bar{1}1\}\langle 11\bar{2}0 \rangle$ slip 93
28.	Compression slip rotations and compression texture resulting from $\{10\bar{1}1\}\langle 11\bar{2}0 \rangle$ slip 94
29.	Resolved shear stress contours for $\{10\bar{1}0\}$ $\langle 11\bar{2}0 \rangle$ slip 96
30.	Tension slip rotations and tension texture resulting from $\{10\bar{1}0\}\langle 11\bar{2}0 \rangle$ slip 98
31.	Compression slip rotations and compression texture resulting from $\{10\bar{1}0\}\langle 11\bar{2}0 \rangle$ slip 99

FIGURE	PAGE
32. Tension slip rotations and tension texture resulting from the combined slip system . . .	103
33. Compression slip rotations and compression texture resulting from the combined slip system	104
34. Twinning shear direction of twinning of $\{10\bar{1}2\}$, $\{11\bar{2}2\}$, and $\{11\bar{2}1\}$ planes of titanium	106
35. Reorientation resulting from $\{10\bar{1}2\}$ twinning from the combined slip system	110
36. Reorientation resulting from $\{11\bar{2}2\}$ twinning from the combined slip system	113
37. Tension texture resulting from combined slip on the $\{0001\}\langle 11\bar{2}0\rangle$, $\{10\bar{1}1\}\langle 11\bar{2}0\rangle$, and $\{10\bar{1}0\}\langle 11\bar{2}0\rangle$ slip planes and twinning from the $\{10\bar{1}2\}$ and $\{11\bar{2}2\}$ planes	115
38. Compression texture resulting from combined slip on the $\{0001\}\langle 11\bar{2}0\rangle$, $\{10\bar{1}1\}\langle 11\bar{2}0\rangle$, and $\{10\bar{1}0\}\langle 11\bar{2}0\rangle$ slip systems and twinning from the $\{10\bar{1}2\}$ and $\{11\bar{2}2\}$ planes	117
39. Stereographic plot of the compression texture of titanium	120
40. Form of the 0001 pole figure of titanium resulting from tension in the rolling direction and compression along the rolling plane normal .	121
41. The five parts of the universal specimen mount .	139
42. Graph showing the optimum values of μT for various values of θ	142
43. Location of the various elements in the transmission method	145
44. Location of the various elements in the reflection method	146
45. The universal specimen mount in position for measurement of transmission intensities . . .	149
46. The universal specimen mount in position for measurement of transmission intensities . . .	149

FIGURE	PAGE
47. Part of the transmission pattern of a cold rolled sample of commercial titanium	152
48. Part of the reflection pattern of a cold rolled sample of commercial titanium	153
49. 1011 pole figure resulting from a plot of the intensity values given in Table XVII	162
50. Pole figures of commercial titanium annealed one-half hour at 650°C	166
51. Pole figures of commercial titanium annealed one-half hour at 800°C	167
52. Pole figures of commercial titanium annealed one-half hour at 880°C	168

CHAPTER I

INTRODUCTION

With the increase in production of titanium in recent years has come a great interest in the mechanical properties and in the possible uses of this metal. Due to the affinity of titanium for oxygen, nitrogen, carbon, and hydrogen, and the marked effect of these elements on the mechanical properties, much of the work previously reported is unreliable. As purer commercial grades of titanium and high purity iodide titanium have become available for examination, research has been undertaken to correct and expand the knowledge of the properties of titanium. Although the uses of titanium are limited at the present time, a considerable amount of time and money is being spent to thoroughly exploit its possibilities and it is expected that titanium will soon hold an established position as one of the more important light metals.

A. THE PROBLEM

Statement of the problem. This study was undertaken (1) to determine the textures developed in titanium during cold rolling, (2) to determine why the observed textures of titanium differ from those of other hexagonal metals, and (3) to develop a satisfactory explanation of the deformation

textures of titanium.

Importance of the study. The presence of preferred orientation in a metal can cause marked changes in mechanical properties with direction. This is especially true in the hexagonal close-packed metals due to their marked anisotropy. A knowledge of the type of preferred orientation which will result from various treatments is therefore essential for the fabrication industries.

In the absence of any extensive data on formability, a complete texture study is almost a necessity before any new type of forming process is considered. Since most forming operations are carried out using metal initially in the cold rolled state, the cold rolled texture is particularly important. Although annealing a cold rolled sheet may completely change the type of preferred orientation, the annealed texture is determined by the cold rolled texture.

The metals of the hexagonal system are generally divided into two groups, those with a c/a ratio greater than 1.633, the value for ideal close packing, and those with a c/a ratio less than 1.633. The deformation textures of both zinc, with a high c/a ratio, and magnesium, with a low c/a ratio, have been extensively studied and the general behavior of deformed close-packed hexagonal metals predicted from these studies. Recent texture studies of titanium, zirconium, and beryllium

have indicated that these three metals, although of low c/a ratio, do not behave in the predicted manner.

The older idea of classifying hexagonal close-packed metals according to the c/a ratio into two groups is evidently in error. Since the texture of titanium shows the greatest deviation from the predicted texture, the explanation of the new deformation behavior should be most easily found by careful study of titanium.

B. OUTLINE OF THE STUDY

The material presented in this thesis is divided into four sections; review of previous work, experimental technique, results of experimental work, and theoretical interpretation of the experimental results.

The experimental techniques are discussed in Chapter III, in which the metal and its annealing characteristics are considered, and Chapter IV, in which the rolling procedures and X-ray techniques are considered. A discussion of the special pole figure specimen mount developed for use with the Schulz-Decker X-ray technique is given in Appendix I. A complete pole figure calculation is included in Appendix II.

A complete listing of experimental results and a critical discussion of these results are given in the next two chapters. Chapter V is devoted to the results of the study

of the compression texture and Chapter VI to the results of the study of the cold rolled texture. A brief examination of the recrystallisation texture of titanium is discussed in Appendix III.

In Chapter VII a new method of texture analysis is applied to the observed titanium texture. By use of this method of analysis a theoretical mechanism of deformation was developed which would result in a texture very similar to that found for both cold rolling and compression. This method, due to its recent development, is discussed quite thoroughly and several illustrations included for clarity.

CHAPTER II

REVIEW OF THE LITERATURE

The literature on titanium, pole figure techniques, and X-ray techniques is such too voluminous to permit a complete coverage of even one of these topics. Only a brief summary of the more important basic papers and those directly related to the problem studied can be given.

Literature of the deformation of titanium. Only two texture studies of titanium have been reported in the literature.

Clark (1) examined the cold rolled texture of titanium and reported that titanium showed a new type texture which can be described as a $(0001)[10\bar{1}0]$ rotated thirty degrees toward the transverse direction. This texture is similar to that reported for zirconium (2) and beryllium (3). The amount of transverse spread is apparently greatest in titanium and least in beryllium.

Comparison of these three textures with the cold rolled

(1) H. T. Clark, Jr., "The textures of cold rolled and annealed titanium." TRANS AIME, Vol 188, pp. 1154-56, 1950

(2) R. K. McGeary and B. Lustman, "Preferred orientation in zirconium." ARSD-2951, March 1950

(3) A. Smigelkas and C. S. Barrett, "Preferred orientation in rolled and recrystallized beryllium." TRANS AIME, Vol 185, pp. 145-8, 1949

textures of magnesium (4) and zinc (5) shows that there is a decided difference. Both magnesium and zinc show a tendency for the 0001 poles to be spread toward the rolling direction rather than toward the transverse direction as is the case in titanium, zirconium, and beryllium.

A brief examination was made by Yen (6) of the drawing, compression, and cold rolling textures of some titanium being prepared for other work. His results showed titanium to exhibit a $[10\bar{1}0]$ drawing texture, a rolling texture similar to that reported by Clark, and a compression texture which was described as $\{0001\}$ up to eighty-five percent reduction with a $[0001]$ rotated up to thirty degrees from the compression axis at higher reductions.

Literature on the determination of pole figures. The use of pole figures to describe the orientation of metal crystals in a polycrystalline material was first suggested by Wever (7). This method made it possible to represent the orientations of all the crystals in the metal by means of an

(4) P. W. Sakarian, "Preferred orientation in rolled magnesium and magnesium alloys." Trans AIME, Vol 147, pp. 266-72, 1942

(5) V. Caglioti and G. Sachs, "The structure of rolled zinc and magnesium." Metallwirtschaft, Vol 11, pp. 1-4, 1932

(6) M. E. Yen, "Interim report to Watertown Arsenal." WRL 401/14-4, March 20, 1950

(7) F. Wever, "The structure of cubically crystallizing metals after rolling." Z. Physik, Vol 28, pp. 69-90, 1924

intensity distribution instead of merely designating the position in which the majority of the crystals seemed to be located.

There were only minor changes in the pole figure techniques during the following years. Almost all pole figures were made using a standard X-ray or optical method (8). The only changes in technique involved slight modifications of sample preparation, mounting, etc.

In 1948 two articles were published giving a method of determining pole figures using a Geiger counter spectrometer (9)(10).

The method developed by Decker et al (9) requires a thin sheet X-ray sample which is placed in a special sample holder such that transmission intensities can be read with the sample at various positions. Unfortunately, this method was unable to cover the central portion of the pole figure.

The Norton method (10) uses a small cylindrical specimen which is rotated in the path of the X-ray beam. Although this method has the advantage of complete pole figure cover-

(8) C. S. Barrett, The Structure of Metals, (New York: McGraw-Hill Book Company, 1943), pp. 154-73

(9) S. F. Decker, E. T. Asp, and D. Harker, "Preferred orientation determination using a Geiger counter X-ray diffraction goniometer." J. Appl. Phy., Vol 19, pp. 388-92, 1948

(10) J. T. Norton, "A technique for quantitative determination of textures of sheet metals." J. Appl. Phy., Vol 19, pp. 1176-78, 1948

age, a number of delicate samples have to be prepared. A second disadvantage of the method is that there is a low surface area exposed to the incident beam with respect to the thickness so that the diffracted beam intensity is weak.

The American Society for Testing Materials examined the Decker method and in 1949 issued a tentative standard (11) based on that method.

In late 1949 two articles were published by Schulz which greatly increased the applicability of the Decker method (12) (13). By use of the reflection method suggested by Schulz in conjunction with the transmission method of Decker it is possible to obtain complete pole figure coverage while retaining the advantage of a sheet sample which is easy to prepare and which allows a very intense diffracted beam to be obtained. This combined method is referred to hereafter as the "Schulz-Decker" technique. In his analysis of the Decker reflection technique Schulz has shown that by proper control of the thickness of the transmission sample the intensity correction necessary in the Decker method may be

(11) "Preparing quantitative pole figures of metals." ASTM Designation: E81-49T, 1949

(12) L. G. Schulz, "A direct method of determining preferred orientation of a flat reflection sample using a Geiger counter X-ray spectrometer." J. Appl. Phy., Vol 20, pp. 1030-33, 1949

(13) L. G. Schulz, "Determination of preferred orientation in a flat transmission sample using a Geiger counter X-ray spectrometer." J. Appl. Phy., Vol 20, pp. 1033-36, 1949

eliminated.

Literature of the origin of textures. Since the earliest observations that deformation of a metal caused the Laue pattern to change from that common to a random orientation (14)(15), there has been complete agreement among crystallographers that this change in the X-ray pattern is a direct result of the deformation process and that it should provide important information about the basic mechanism of slip.

Although there have been many theoretical studies of single crystals and their behavior (16), the problem of slip in polycrystalline material is more difficult to study. In general, the method of attack has been to study carefully the deformation characteristics of single crystals and then to rationalize their behavior to form a picture of what might possibly occur in polycrystals. The problem must be considerably oversimplified for any results to be obtained.

In 1923 a mechanism of deformation texture formation involving the assumption that each grain acted essentially

(14) N. Uspinskij and Konobejewski, Lecture before the Russian Physical Lebedev Society, April 30, 1920, Moscow

(15) K. Becker, R. O. Herzog, W. Jancke, and M. Polanyi, "Methods for the arrangement of crystal elements." Z. Physik, Vol 5, pp. 61-2, 1921

(16) E. Schmid and W. Boas, Plasticity of Crystals, (London: F. A. Hughes and Company, 1950) English translation

like a single crystal was suggested by Mark et al (17). The basis of their explanation was the occurrence of bend slipping or "Biegegleitung". Since it is apparent that slip on a single set of slip planes can not account for the adjustment of the crystal to the external changes in shape being forced upon it by the applied stress, it is assumed that the bending moments produced by the applied stress cause the slip plane to rotate in such a direction that the active slip direction approaches the direction of flow. The rotation of slip direction toward flow direction causes the formation of the deformation texture. This idea of slip rotation or bend slipping has been retained in most of the subsequent texture studies.

Wever and Schmid (18) suggested in 1930 that the deformation of a polycrystalline material in tension or compression occurred by slip on the planes of maximum resolved shear stress and that each crystallite rotates during slip about an axis which lies in the slip plane and is perpendicular to the slip direction. Thus initial slip occurs with single slip rotation to a boundary line between two slip systems where the resolved shear stresses for both systems are equal, at

(17) H. Mark, M. Polanyi, and E. Schmid, "Processes in the stretching of zinc crystals." Z. Physik, Vol 12, pp. 58-72, 78-110, 111-6, 1923

(18) F. Wever and W. E. Schmid, "Texture of cold-deformed metals." Z. Metallkunde, Vol 22, pp. 133-40, 1930

which point duplex slip occurs. Thus single and duplex slip occur in the crystal to bring the crystal to the ideal end orientation. To consider cold rolling Wever and Schmid assumed that the rolling stresses can be approximated by tension in the rolling direction and compression along the rolling plane normal. This was called plane parallelepipedal deformation by the authors. The agreement of the predicted and observed textures was rather good.

Boas and Schmid (19) developed a theory of texture formation in 1931 which was based on the assumption that the three most favorably oriented slip systems must be oriented in the final stable end texture so that all three are equally favored and the rotation tendencies cancel each other. Thus the final deformation texture is that which is stable for all three orientations. The resolved shear stresses were calculated for each position in the unit stereographic triangle and the three slip systems with the highest resolved shear stresses assumed to be active. This divided the unit triangle into several areas each with different rotational tendencies. This method of deformation texture analysis was successful in predicting the observed tension and compression textures for several face-centered and body-centered

(19) W. Boas and E. Schmid, "The interpretation of the deformation textures of metals." Z. tech. Physik, Vol 12, p. 71, 1931

cubic metals. Rolling textures were predicted using the plane parallelepipedal deformation concept plus an added restriction which excluded all slip systems in tension which did not also cause the sheet to decrease in thickness.

Taylor (20) developed a mathematical theory based on homogeneous deformation. This treatment was based on the fact that for homogeneous deformation to occur five special slip systems must be active simultaneously. The five active systems were calculated using the principle of virtual work. This method of analysis successfully predicted the texture of face-centered cubic metals plus the stress-elongation curve but was too difficult mathematically to be applied to more complicated systems.

Pickus and Mathewson (21) have developed a theory of rolling textures requiring that the operating slip systems be symmetrically positioned in the final texture so that the resolved shear stresses are equal and the rotation tendencies cancel and that the operating slip systems be symmetrically oriented with respect to the flow direction. The operating slip systems are chosen by calculating the value of the

(20) G. I. Taylor, "Mechanics of plastic deformation of crystals." Proc. Royal Soc. (London), Vol 145, pp. 362-404, 1934

(21) M. R. Pickus and C. H. Mathewson, "On the theory of the origin of rolling textures in face-centered cubic metals." J. Inst. Met., Vol 64, pp. 237-60, 1939

product of the resolved shear stress and the cosine of the angle between the slip direction and the flow direction. The three systems for which this function is largest are considered to be the operating slip systems. This method of analysis successfully predicted the various ideal cold rolled textures of face-centered cubic metals and also the relative frequency of occurrence of each.

Polanyi (22) and Barrett (23) have concluded that deformation in polycrystalline metals occurs by simultaneous slip on many slip planes. Barrett, in his analysis of iron under compression, concluded that as many as thirty-two different slip systems were active at one time. These slip systems were necessary to explain the crystal rotation observed experimentally. The resultant rotation tendency was determined by examination of a plot of the magnitude and direction of the rotation tendency for each individual slip system.

A semi-graphical method of predicting ideal orientations developed by Hibbard and Yen (24) has been used successfully

(22) M. Polanyi, "Structure changes in metals through cold working." Z. Physik, Vol 17, pp. 42-53, 1923

(23) C. S. Barrett, "Structure of iron after compression." Trans AIME, Vol 135, pp. 296-326, 1939

(24) W. R. Hibbard and M. K. Yen, "Wire textures of copper and its binary and solid solution alloys with aluminum, nickel, and zinc." Trans AIME, Vol 175, pp. 126-40, 1948

to predict textures of the face-centered and body-centered cubic systems and also in metals of the hexagonal system in which twinning is unimportant. This method is based primarily on the assumption that for an orientation to be favorable--that is to remain unchanged by further deformation--the slip direction must be within a definite angle of the flow direction. For example, in tension the slip direction must be within forty-five degrees of the flow direction. This article presents an interesting method of tabulating orientations and of predicting ideal textures.

In three recent articles Calnan and Clews have developed a graphical method of texture analysis which has satisfactorily predicted the tension, compression, and cold rolling textures of face-centered cubic (25), body-centered cubic (26), and close-packed hexagonal (27) metals. This method, which resembles that suggested by Wever and Schmid (28) in that only the slip system or systems of maximum resolved

(25) E. A. Calnan and C. J. B. Clews, "Deformation textures in face-centered cubic metals." Phil. Mag., Vol 41, pp. 1085-1100, 1950

(26) E. A. Calnan and C. J. B. Clews, "The development of deformation textures in metals. Part II. Body-centered cubic metals." Phil. Mag., Vol 42, pp. 616-35, 1951

(27) E. A. Calnan and C. J. B. Clews, "The development of deformation textures in metals. Part III. Hexagonal structures." Phil. Mag., Vol 42, pp. 919-31, 1951

(28) Wever and Schmid, loc. cit.

shear stress are considered active at any one point in the deformation process. The method deviates from all previous methods in that the actual position of the crystallite is not considered the only criterion for the number of active slip systems which will operate at any point. It is assumed that the effective stress position may move away from the applied stress position without actual physical movement of the crystal due to lateral stresses from grain boundaries, etc. Thus a region of duplex slip may be reached by the effective stress when only single slip should occur according to the position of the actual stress. This factor permits the variations in textures in metals of the same crystal class to be considered. Rotation of the crystal is assumed to follow the laws established for single crystals rather than to be fixed by a constant axis of rotation such as Wever and Schmid suggested. Thus the method also retains the advantage of that of Boas and Schmid (29) in that the direction of rotation may vary considerably with the orientation of the crystallites within the unit triangle.

One of the outstanding successes of the method of deformation texture analysis developed by Calnan and Glews is that metals of all three common lattice types have been treated successfully. No other method has yet been able to

(29) Boas and Schmid, loc. cit.

develop a satisfactory quantitative explanation of the textures of hexagonal close-packed metals.

As is apparent from the above discussion, the theory of the origin of deformation textures is still in its early stages. Various authors have given evidence that two, three, five, and almost all slip systems must be active to develop the deformation textures observed in metals. In addition to the lack of agreement about the number of active slip systems, no final conclusion has yet been reached about the individual grain rotations in a polycrystalline matrix or about the importance of resolved shear stress in determining the active slip systems.

It is hoped that re-examination of the deformation textures of the various metals using the more quantitative Geiger counter techniques recently developed will furnish evidence from which an all-inclusive theory of the origin of textures in metals may be developed.

CHAPTER III

DESCRIPTION OF THE METAL INVESTIGATED

In this chapter the four samples of titanium metal which were used in the deformation texture study are discussed. All available information on chemical analysis, previous work history, and any treatment given to the samples to prepare them for the deformation study is given. The various annealing procedures used are outlined and the properties of the annealed samples discussed.

A. SOURCE OF THE METALS EXAMINED

Four samples of titanium metal were examined in this investigation. Each of these metals was of different origin. One of the metals examined was high purity iodide titanium. The other three were commercial grades of titanium and are designated as commercial titanium grade number one, two, and three in the following rather than by the original source name.

Iodide titanium. A crystal bar of high purity iodide titanium, produced by the New Jersey Zinc Company, was furnished for this examination by the Titanium Alloy Manufacturing Division of the National Lead Company. This bar was received in the original form and was not melted and recast before using.

Commercial titanium grade number one. This sample of commercial titanium was obtained from the Argonne National Laboratory in the form of a square bar. Although the previous history is unknown, the titanium bar appeared to have been cast and then ground to give a clean surface. This bar was designated as Kroll titanium by Argonne National Laboratory.

Commercial titanium grade number two. This sample of titanium was also obtained from Argonne National Laboratory. The sample had been machined to a circular section and was in an annealed condition as received. The sample was produced by the Titanium Metals Corporation.

Commercial titanium grade number three. Eight strips of a commercial grade of titanium which had been previously worked were donated by the Titanium Alloy Manufacturing Division of the National Lead Company. These strips had been prepared by rolling of arc melted titanium and required annealing before rolling for the final texture examination.

B. COMPOSITION OF TITANIUM SAMPLES

An analysis of the iodide titanium crystal bar was furnished with the bar. This analysis was run by the New Jersey Zinc Company. The results of the analysis are given in Table I. Although the analysis did not include an oxygen, hydrogen, or carbon determination, the low hardness

TABLE I
 REPORTED ANALYSIS OF TITANIUM SAMPLES

Element	Iodide Titanium	Commercial Titanium Grade		
		No. 1	No. 2	No. 3
Hydrogen	-	0.014	0.013	0.023
Oxygen	-	0.109	0.141	0.119
Nitrogen	0.001	0.024	0.027	0.021
Carbon	-	0.02	0.03	0.10
Silicon	-	0.08	0.04	0.12
Zirconium	-	0.01	0.01	0.01
Iron	0.0085	0.02	0.06	0.09
Chromium	-	-	0.01	0.10
Manganese	0.067	0.005	0.01	0.03
Magnesium	-	0.01	0.01	0.01
Tin	0.002	0.002	0.002	-
Aluminum	0.014	0.25	0.01	0.05
Calcium	-	0.03	0.03	0.03
Vanadium	-	0.001	0.001	0.005
Copper	0.005	0.003	0.003	0.003
Nickel	-	-	-	0.01
Molybdenum	0.002	-	-	-
Lead	0.0035	-	-	-
Non-metallic	0.001	0.167	0.211	0.263
Metallic	0.102	0.411	0.186	0.453
Titanium	99.897	99.422	99.603	99.284

indicated that these elements were present only in small amounts.

Analyses of the three commercial grades of titanium were made by the Titanium Alloy Manufacturing Division of the National Lead Company. These analyses were made to determine if there was any significant difference between the composition of grades one and two and the composition of grade three which could account for the difference in annealed hardness. Examination of the analyses given in Table I shows no large difference in composition. Commercial titanium grade number three is slightly higher in non-metallics with the major difference being in carbon content. Commercial grade number one has a much higher aluminum content than the other two commercial grades but the difference apparently had little effect on the ability to be cold rolled.

C. ANNEALING PROCEDURES

Titanium absorbs considerable hydrogen at the lower annealing temperatures and also considerable carbon, nitrogen, and oxygen at annealing temperatures above 700°C (30). For this reason either vacuum or inert gas annealing is generally recommended. In the absence of either of these,

(30) A. M. Bounds and H. W. Cooper, "Annealing of titanium and zirconium." Metal Prog., Vol 59, pp. 69, 100-2, 1951

air annealing may be used if the annealing temperature is below 700°C.

Samples were annealed in air, helium, and vacuum before rolling to determine if annealing atmosphere had any noticeable effect on the deformation texture.

Procedure for air annealing. Samples to be annealed in air were placed in a tube furnace with one end of the tube open to the air. The furnace was brought to temperature and the sample inserted when the desired temperature was reached. Samples were either air cooled in a cool part of the tube or water quenched.

A scale formed on all of the samples annealed in air. This scale was not dissolved by a strong hydrofluoric acid bath but could be removed by allowing the acid to attack the titanium beneath the scale and removing the loosened scale by wiping frequently. If the scale was rather heavy, a preliminary light polish to expose some metal to the acid was usually necessary.

Procedure for inert gas annealing. A tank of high purity helium was obtained from the Bureau of Mines and was used as the atmosphere in annealing several samples. Both a slow rate of flow and a static gas atmosphere were used. Each produced satisfactory results.

The helium was passed directly from the tank into the furnace with no purification. Samples to be annealed were

placed in the furnace and heated to temperature with the furnace when annealing time was not critical. When annealing time was critical, the furnace was flushed with helium while heating to temperature, and the sample placed in the furnace when the desired temperature was reached. Samples were removed by opening the furnace and pulling the sample into a cool part of the tube where it was exposed to a strong flow of helium or by quenching in water immediately upon opening the furnace. Both methods allowed a very light scale to form but this scale was easily removed.

The helium was kept at a slight positive pressure within the annealing chamber by using a mercury seal. This seal also prevented leaking of air into the furnace when using a static helium atmosphere.

Procedure for vacuum annealing. Several samples of titanium were sealed in a vacuum furnace and annealed at a pressure of forty microns. When using the vacuum furnace it was necessary to bring the furnace to temperature and to cool it to room temperature without breaking the vacuum seal. This prevented accurate control of annealing time and temperature since the sample had to be sealed in the furnace during heating and cooling.

There was no evidence of scale on these samples annealed in vacuum. Although vacuum annealing produced the best surfaces, the inability to control the annealing process accurately in vacuum restricted its use.

D. HARDNESS, GRAIN SIZE, AND MICROSTRUCTURE
OF ANNEALED TITANIUM

Since the previous history of three of the titanium samples was unknown, the samples were given an initial cold reduction of approximately fifty percent reduction in area by rolling and then annealed to give a uniform basis from which comparisons of the results of the deformation texture studies could be made. Hardness readings, grain size determinations, and microstructure examinations were made on each annealed sample. The effect of annealing for one hour in vacuum at 800°C on these properties is shown in Table II.

Annealed hardness of titanium samples. As was expected, the hardness of the commercial grades of titanium was considerably higher than that of iodide titanium. The annealed hardness of these samples was not sufficiently affected by change in annealing atmosphere for any difference to be noticed in the hardness readings among samples of any one type of titanium annealed in different atmospheres.

Examination of Table II shows that the commercial grade number three had a much higher hardness than the other two commercial grades of titanium. This sample when it was cold worked hardened to approximately RB 110 and when annealed softened only to RB 102. Although the other commercial grades of titanium cold worked to the same hardness, their

TABLE II

GRAIN SIZE AND HARDNESS OF ANNEALED TITANIUM

Sample	Grain Size	Rockwell B Hardness
Iodide titanium	0.102 mm	< 0
Commercial grade No. 1	0.045 mm	83
Commercial grade No. 2	0.011 mm	84
Commercial grade No. 3	0.010 mm	102

annealed hardness was RB 83 and 84. Analyses were made for the three commercial grades of titanium to determine if there was any marked composition difference. The analyses, as already mentioned, did not indicate any reason for the observed difference in hardness. Although the reason for the higher hardness is not apparent from Table I, it must be assumed that the cause is to be found in some difference in composition.

Microstructure of annealed titanium samples. A typical microstructure of each of the four samples examined is given in Figures 1 through 4. The samples were mechanically polished and etched in a solution of hydrofluoric acid, nitric acid, and water (1:12:87 by volume).

The above etching solution gave the best results of all of those tried but still was not completely satisfactory. It tended to etch certain planes preferentially and caused severe pitting, particularly in fine grained samples. In addition, it developed only certain of the grain boundaries, probably only those separating grains with rather large differences in orientation. Thus some grain boundaries were severely etched while others were untouched.

Figure 1 shows the microstructure of annealed iodide titanium at 100X. The grains are large and regular. The surface shows the effects of mechanical polishing even after repeated polishing and etching. The uneven etch due to shearing during polishing is clearly visible.

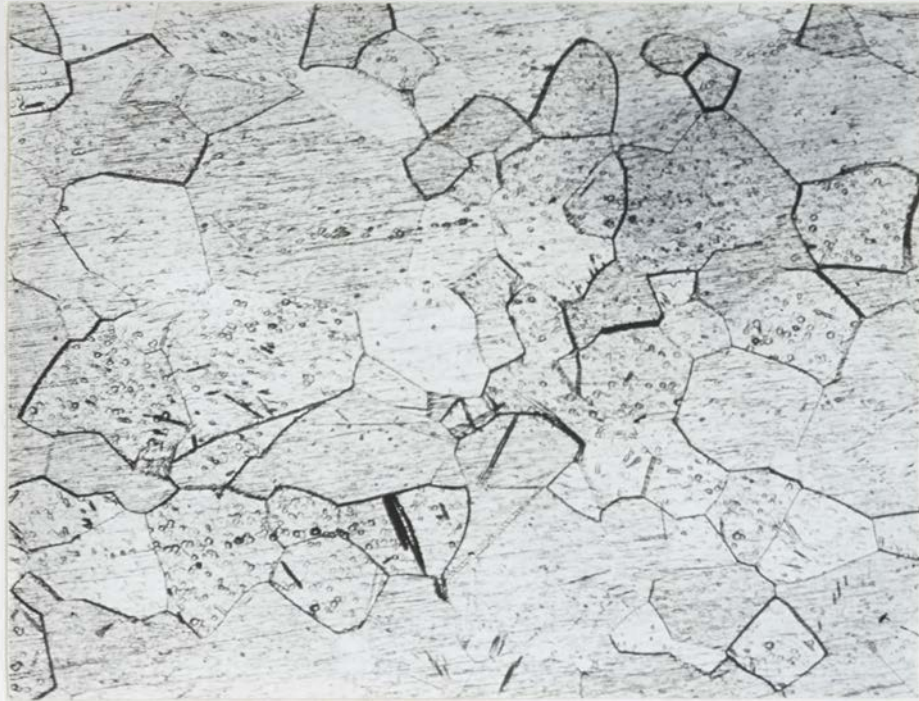


Figure 1. Annealed iodide titanium--100X.

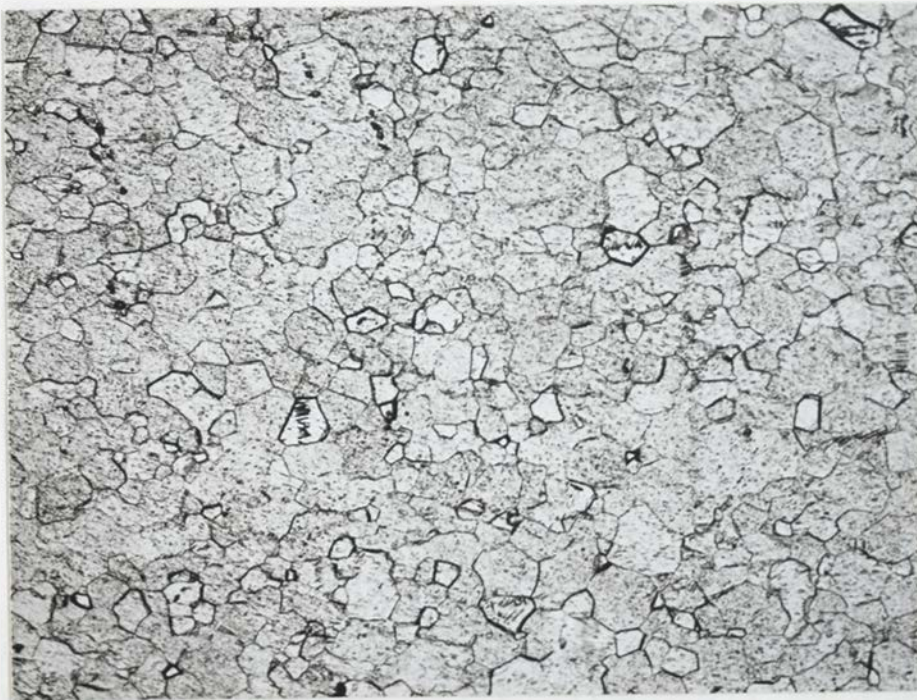


Figure 2. Annealed commercial titanium grade number one--100X.

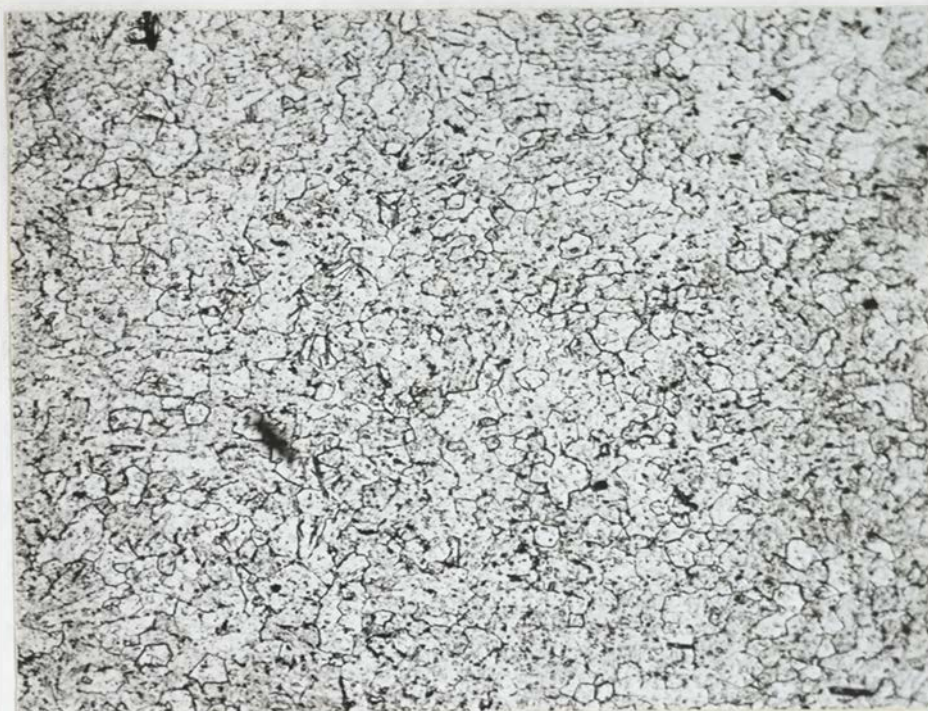


Figure 3. Annealed commercial titanium grade number two--
250X.

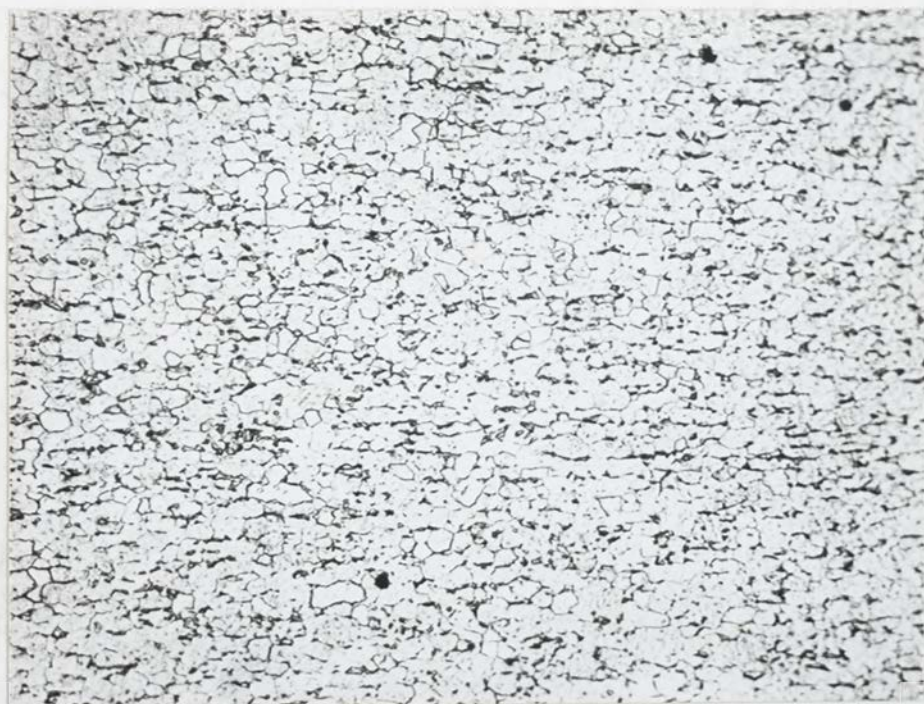


Figure 4. Annealed commercial titanium grade number three--
250X.

Figure 2 shows the structure of commercial titanium grade number one at 100X. This structure is similar to the iodide titanium structure except that the grain size is smaller.

The most difficult of the samples to prepare was commercial titanium grade number two. The best microstructure obtained for this sample is shown in Figure 3. It was necessary to etch this specimen in an etch of hydrofluoric acid, nitric acid, and glycerol (1:1:2 by volume) to develop the structure. The sample pitted so severely with only short etches that it was very difficult to develop a good grain structure. The finer grain size may have contributed to the pitting tendency but the relative ease of preparing the samples of commercial titanium grade number three, also of fine grain size, suggests that some difference in composition may have been the cause.

Figure 4 shows the microstructure of commercial titanium grade number three at 250X. A small amount of grain boundary material is seen in this sample. This material had been oriented by the initial cold rolling to some extent. The appearance of a second phase indicates, as did the hardness data, that this sample is different in composition from the other two commercial grades of titanium. No evidence of a second phase was seen in other samples.

Grain size determination. Grain size determinations

were made using the formula given by Dunkerley et al (31),

$$D \text{ (mm)} = \frac{1.075}{M} \sqrt{\frac{A \text{ (mm)}^2}{n}}$$

where D is the distance between opposite flats of uniform hexagonal grains in millimeters, M is the magnification of the photomicrograph used in making the grain count, and n is the number of grains counted in an area A measured in square millimeters. The area was made large enough to include at least sixty grains and the n value used in the formula obtained from averaging at least three separate n values.

The results of grain size determinations made on each of the four different samples of titanium are shown in Table II. The grain size of each titanium sample was relatively independent of annealing time, annealing temperature, and amount of prior cold rolling as long as the sample was annealed below the transformation temperature. Grain growth above this temperature (882°C) was quite rapid however. No difference in grain size was noted with change in annealing atmosphere in any of the titanium samples examined.

(31) F. J. Dunkerley, F. Fledger, V. Damiano, and J. Fulton, "Grain-growth and recrystallization characteristics of zirconium." Trans AIME, Vol 191, pp. 1003-8, 1951

CHAPTER IV

THE PREPARATION AND X-RAY EXAMINATION OF SPECIMENS

The samples of titanium discussed in Chapter III were deformed either by compression or by cold rolling. The deformed material was then etched to a sufficient thickness for X-ray examination and pole figures determined using the Schultz-Decker pole figure technique.

In this chapter the experimental techniques involved in compression, cold rolling, etching of X-ray specimens, and X-ray examination are discussed. For convenience, much of the more detailed information about the X-ray technique is placed in two of the appendixes.

A. COMPRESSION METHODS

Compression texture studies were made using the iodide titanium. Compression specimens were prepared by cutting samples directly from the crystal bar. Due to the crystalline nature of the iodide titanium bar, some difficulty with separation of the crystals during compression was encountered.

Samples were compressed by compression between parallel plates and by compression rolling. The reductions by the two methods were made so that the ranges covered overlapped. Any differences in texture due to method of compression would then be immediately seen. The cone compression method,

probably the most reliable of the compression methods (32), could not be used due to the necessity of obtaining thin, parallel-sided samples for X-ray examination.

Preparation of compression samples. Samples of iodide titanium were prepared by cutting a section from the crystal bar. This formed a cylindrical sample approximately 1.9 centimeters in diameter and from 0.60 to 0.25 centimeter in thickness depending upon the final reduction required.

The ends of the sample were polished carefully until they were parallel. After the ends were parallel, they were alternately etched and lightly polished to remove as much of the deformed material as possible. After the final light polish, the thickness of the samples was measured to the nearest thousandth of a centimeter. A second measurement was made after compression and the deformation reported as percent reduction in thickness.

Compression between parallel plates. An Olsen testing machine of 60,000 pound capacity was used to compress these samples subjected to compression between parallel plates. During the compression process the samples were frequently removed from the machine for reduction of the area of the sample and for lubrication. The removal of the samples was made necessary by the low load limit of the machine which

(32) G. S. Barrett, "The structure of iron after compression." Trans AIME, Vol 135, pp. 296-326, 1939

required that the area be frequently reduced before further compression could be obtained. The approach to uni-axial compression was better than expected. The external shape of the sample after compression showed rather uniform lateral spread. The possibility of secondary stresses can not be overlooked however.

Compression by compression rolling. A set of two inch laboratory rolls were used to roll the samples. Both rolls were driven and the roll speed was 14 R.p.m. The rolls were lubricated with a light oil during rolling.

A small reduction per pass was used during compression rolling with a clockwise rotation of from three to five degrees after each pass. Each compression rolled sample was rotated completely around the compression axis at least twice. The compression rolled samples showed a circular section after rolling indicating that uniform compression was obtained.

A picture of a sample of iodide titanium reduced 89.6 percent by compression rolling is shown in Figure 5. The separation of the crystals along the circumference of the sample is clearly visible. For this reason, only the center part of the compressed iodide titanium crystal could be used for X-ray samples.

B. GOLD ROLLING METHODS

Gold rolled specimens of all four titanium samples

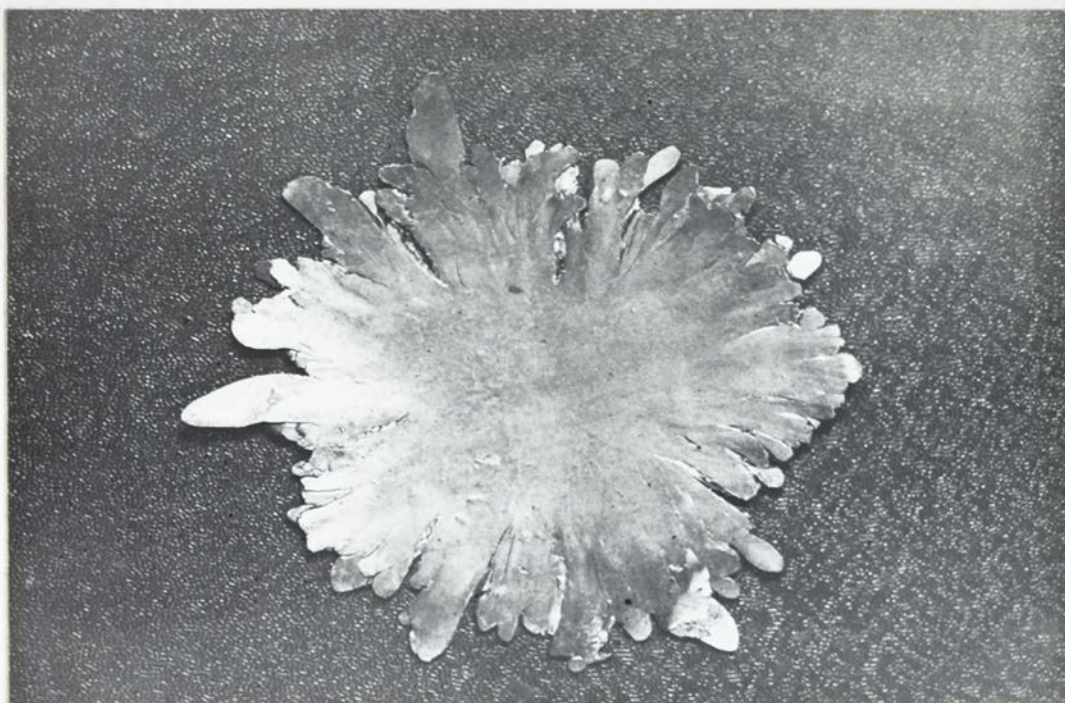


Figure 5. Iodide titanium compression rolled to 89.6 percent reduction in thickness.

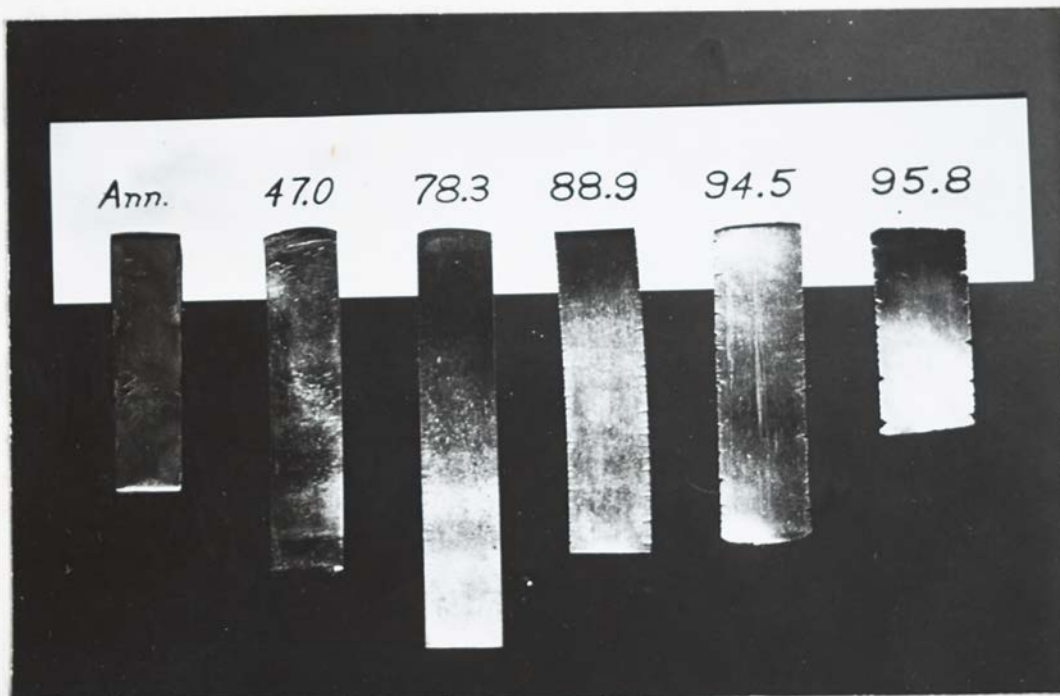


Figure 6. Edge cracking and increase in width during cold rolling. Figures give percent reduction in area.

were prepared. All four titanium samples were given a prior cold rolling and annealing treatment as discussed in Chapter III before being cold rolled for the texture study.

Preparation of the samples for cold rolling. After the initial annealing treatment discussed in Chapter III had been carried out, the annealed sample was carefully cut and polished to give a sample of rectangular shape. After this treatment the sample was lightly etched to remove any worked metal resulting from the shaping operations.

Measurements of the width and thickness of the sample were made after etching for use in calculating the percent reduction in area. The samples before cold rolling were approximately 0.3 centimeter thick, 1.5 centimeters wide, and three centimeters long.

Cold rolling of samples. The set of two inch laboratory rolls described previously was used to prepare the cold rolled specimens. The titanium samples were passed through the rolls in one direction only but were inverted after each pass. Only slight reductions per pass were made. From sixty to ninety passes were usually necessary to obtain a final reduction of more than ninety percent. The samples were allowed to cool after each pass to prevent temperature effects.

In Table III the measurements made during a typical cold rolling reduction are shown. These results were ob-

TABLE III

DIMENSIONAL CHANGES DURING ROLLING OF TITANIUM

Sample	Width (cm)	Thickness (cm)	Reduction in Area	Increase in Width	Number of passes
Ann.	1.080	0.233	0%	0%	0
C.R.	1.128	0.108	47.0%	4.4%	20
C.R.	1.182	0.046	78.3%	9.4%	34
C.R.	1.260	0.022	88.9%	16.6%	46
C.R.	1.378	0.010	94.5%	27.6%	60
C.R.	1.465	0.007	95.8%	35.6%	76

tained in rolling commercial titanium grade number three. Similar results were obtained with the other samples. Of particular interest in this table is the increase in width of the samples during rolling. As is shown by the figures in Table III, the sample increased in width 35.6 percent on rolling to a reduction in area of 95.8 percent.

In Figure 6 a photograph of the cold rolled samples used in obtaining the data in Table III is shown. Edge cracking can be seen in the sample cold rolled 78.3 percent and grows progressively worse as the reduction increases. Edge cracking was absent in the rolled iodide titanium samples but was evident in all three commercial grades rolled beyond sixty percent reduction in area.

C. PREPARATION OF X-RAY SAMPLES

The Schulz-Decker X-ray technique requires the preparation of two separate samples--one for transmission intensity determination and one for reflection intensity determination. Because of the tendency of titanium to form a subsidiary surface texture if the surface is mechanically polished, it was necessary to prepare the X-ray samples by etching alone.

Preparation of transmission samples. Schulz (33) has

(33) L. G. Schulz, "Determination of preferred orientation in flat transmission samples using a Geiger counter X-ray spectrometer." J. Appl. Phys., Vol 21, pp. 1033-36, 1949

shown that if the value of μt is controlled by control of the sample thickness, a correction for absorption is unnecessary when the angle of rotation is less than twenty degrees. Examination of the graph showing maximum value of μt for a given value of θ given by Schulz and reproduced in Appendix I shows that for the 0002 line of titanium a sample thickness of less than 0.00065 centimeter would be required. (This value is obtained as follows: Since the value of θ for the 0002 line of titanium is 19.17° , μt from the graph in Appendix I must be less than 0.6. Since μ is 918 per centimeter for titanium, t must be less than 0.00065 centimeter.)

This value of t is rather small and it was usually necessary to prepare a thicker transmission sample and to apply a correction for absorption to the transmission intensity readings.

The value of t was measured using a micrometer on the thicker samples and using the method suggested by Decker et al (34) on the thin samples. Using the Decker method the value of a strong brass reflection was measured at the counter. The counter was then covered with the transmission sample and the new value of intensity measured. The value of μt can be calculated from the two measured intensities.

(34) E. F. Decker, E. T. Asp, and D. Harker, "Preferred orientation determination using a Geiger counter X-ray diffraction goniometer." J. Appl. Phys., Vol 19, pp. 388-92, 1948

(This calculation is made in the following manner: The value of the unabsorbed brass reflection is I_0 . The value of the brass reflection after passing through the titanium sample is I . Using the equation of absorption, $\ln I_0/I = \mu t$, and knowing that μ for titanium is 918 per centimeter, t is easily calculated.)

The thickness values of the samples obtained by measurement were found to be in error when checked by the above method. The mechanically measured values were always too high, probably due to pitting of the surface of the titanium sample. Thus in those samples which were too thick for the Decker method of measurement of t to be practical, an error may be expected in the correction factor.

Preparation of reflection samples. The Schulz reflection technique is based on the assumption that the reflection sample is sufficiently thick for the incident beam to be completely absorbed in the sample (35). For the purpose of calculation, it was assumed during this examination that the absorption could be considered as total absorption when the ratio of I_0 to I was 1000 to 0. Using this ratio the minimum value of t was found to be 0.0076 centimeter.

(When I_0 is 1000 and I is 1, $\ln I_0/I = \ln 1000 = 2.303 \times \log 1000 = 2.303 \times 3 = 6.909$. Since $\ln I_0/I = \mu t$ and μ for

(35) L. G. Schulz, "A direct method of determining preferred orientation of a flat reflection sample using a Geiger counter X-ray spectrometer." J. Appl. Phys., Vol 20, pp. 1030-33, 1949

titanium is 918 per centimeter, t equals 6.909 divided by 918 or 0.0075 centimeter.)

For additional assurance that complete absorption could be assumed, all reflection specimens were made at least 0.015 centimeter thick, using a laminated sample if the sample was thinner than this after etching. The reflection samples were prepared by etching with at least one-third of the original sample thickness removed to eliminate the possibility of surface effects.

Etching techniques. The etching solution used was composed of hydrofluoric acid, nitric acid, and water. Several different ratios of the components of the solution were tried. A ratio of 1:2:5 by volume gave the most uniform etch of any of those tested and was used in preparing the transmission and reflection samples discussed above.

The etching rate was found to vary with the ratio of the acids as well as with the amount of acid present. Continuous agitation of the samples in the etching solution was necessary to prevent pitting or grooving.

D. THE X-RAY TECHNIQUE

Pole figures were made using the Schulz-Decker Geiger counter technique. A universal specimen mount was constructed for use in the pole figure determination which allowed the best features of the specimen mounts suggested for the

Schulz reflection method (36) and the Decker transmission method (37) to be combined. The application of this specimen mount is discussed thoroughly in Appendix I.

Intensity readings from the $10\bar{1}0$, 0002 , and $10\bar{1}1$ lines were measured and, after suitable corrections had been made to adjust for absorption, the pole figures were drawn. An example of the necessary adjustment of data is given in Appendix II in which a complete pole figure determination is carried out.

Measurement of X-ray intensity. Measurements of the intensities of the diffracted α -ray from the $10\bar{1}0$, 0001 , and $10\bar{1}1$ planes were made at every ten degree interval of latitude and longitude in one quadrant of a polar stereographic net for the pole figures of the cold rolled samples. Readings along the circumference and across diameters passing through the rolling direction and the transverse direction were made to establish symmetry. Readings at two and one-half degree intervals along from two to four diameters of the polar stereographic net were made to determine the pole figures of the compressed titanium samples.

Transmission intensity readings were made on the latitude circles from 0° to 50° . Reflection intensity readings

(36) Schulz, loc. cit.

(37) Decker, Asp, and Harker, loc. cit.

were made from 20° to 90° . The region between 20° and 50° overlapped and served as a means of correlating the transmission and reflection data. (See Appendix II for an example of this correlation.)

All X-ray examinations were made using filtered copper radiation from a North American Philips X-ray Goniometer Unit. The required slit systems and counter movements are discussed in Appendix I.

Plotting of the pole figures. Two methods of presenting the data are used in this report. In plotting the compression textures the shading method--in which the most intense region is made darkest--is used. In plotting the cold rolled textures the intensity contour system is used. The second method allows more complete information to be given but is difficult to read when used for compression textures. For this reason, the compression textures are all given using the first method of plotting.

CHAPTER V

THE COMPRESSION TEXTURE OF IODIDE TITANIUM

Knowledge of the compression texture of a metal has been found to be helpful in understanding the cold-rolled texture. As was mentioned in Chapter II, rolling has often been considered as tension in the rolling direction and compression on the rolling plane. Since the rolling texture of titanium was shown to be different from the rolling textures reported for most other hexagonal close-packed metals (38), the compression texture of titanium was expected to differ from the normal [0001] hexagonal close-packed compression texture.

The compression texture of titanium was examined by Yen (39)(40). His results showed titanium to exhibit the normal [0001] texture up to eighty-five percent reduction. At higher reductions a double texture appeared in which the 0001 planes were rotated from ten to thirty degrees from the plane of compression. This change in the compression texture seemed unusual since the tendency for hexagonal

(38) H. T. Clark, "The textures of cold-rolled and annealed titanium." Trans AIME, Vol 188, pp. 1154-6, 1950

(39) M. K. Yen, Interim report submitted to Watertown Arsenal, WHL No. 401-14/4, (March 20, 1951)

(40) M. K. Yen and J. P. Nielsen, Discussion of paper by Clark (38), J. of Metals, Vol 3, No. 7, pp. 549-50, 1951

close-packed metals is to approach the [0001] texture as the ideal compression texture. Mechanical twinning generally occurs over a considerable range of reductions beginning at a rather low reduction.

The samples used by Yen in his investigations were prepared by two methods. Compression in a testing machine was used up to a reduction of eighty-five percent. Compression by compression rolling was used at higher reductions. Since the change in texture occurred at the same reduction as the change in the method of compression, a connection between the two seemed likely. To check this possibility and to locate the position of the change in texture definitely, if it was found to exist, the compression texture of titanium was re-examined.

Samples of iodide titanium were used in the investigation of the compression texture of titanium.

A. EXPERIMENTAL RESULTS

The samples of iodide titanium were either compressed or compression rolled as discussed in Chapter IV. The diffracted intensities from the $10\bar{1}0$, 0001, and $10\bar{1}1$ planes of the deformed sample were recorded using the Schulz-Decker technique and the pole figures plotted.

0001 pole figures of compressed titanium. The various reductions given the iodide titanium samples and the method

TABLE IV

TEXTURES DEVELOPED BY COMPRESSED IODIDE TITANIUM

Percent Reduction	Method of Compression	Angle between 0001 max and comp. axis	Relative intensity of maximum
24.1	Compressed	32.5°-25°	30*
34.3	Compressed	30°	100**
50.0	Comp Rolled	30°	35
80.1	Compressed	27.5°	40
86.3	Compressed	25°	35
89.6	Comp Rolled	24°	42
96.2	Comp Rolled	20°	39
98.9	Comp Rolled	17.5°	35

* From deformed material only.

** Probably in error.

used to compress each of the samples are given in Table IV. The reductions made by the two methods of compression were chosen so that they overlapped.

The 0001 pole figures of the samples listed in Table IV are shown in Figures 7 through 14. The plane of the pole figure corresponds to the plane of compression and the axis of compression is perpendicular to the plane of the pole figure. Thus the pole figures consisted of a series of concentric intensity rings centered on the axis of compression.

After correction of the transmission patterns for absorption, the readings were compared with those obtained from the reflection patterns in the overlapping region and a uniform correction applied. The final readings were then reduced so that all readings fell within the range of 0 to 50 intensity units, the maximum having an intensity reading of 50 units. These readings were plotted in the pole figure using the shading method with five degrees of intensity as follows: 0 to 10 units--blank, 10 to 20 units--dotted, 20 to 30 units--wide lining, 30 to 40 units--medium lining, and 40 to 50 units--narrow lining. The position of the maximum reading was shown by a dashed line when a definite maximum existed.

The texture produced by compression could not be distinguished from that produced by compression rolling. The general appearance of the texture was the same in each case.

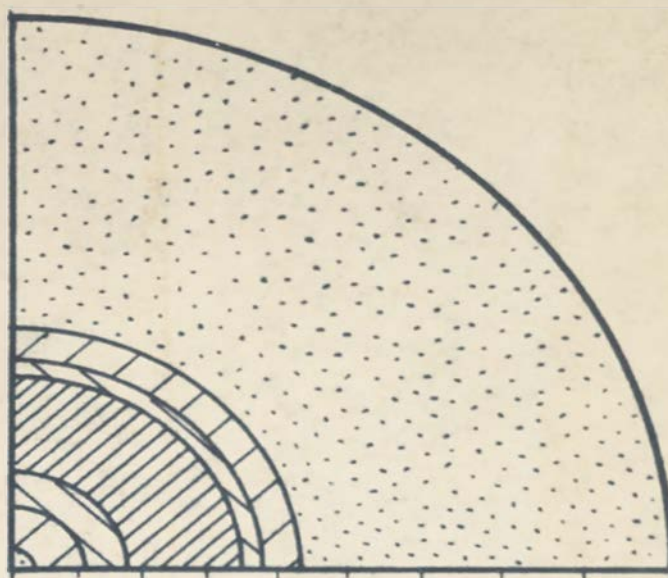


Figure 7. 0001 pole figure of compressed iodide titanium--
24.1 percent reduction.

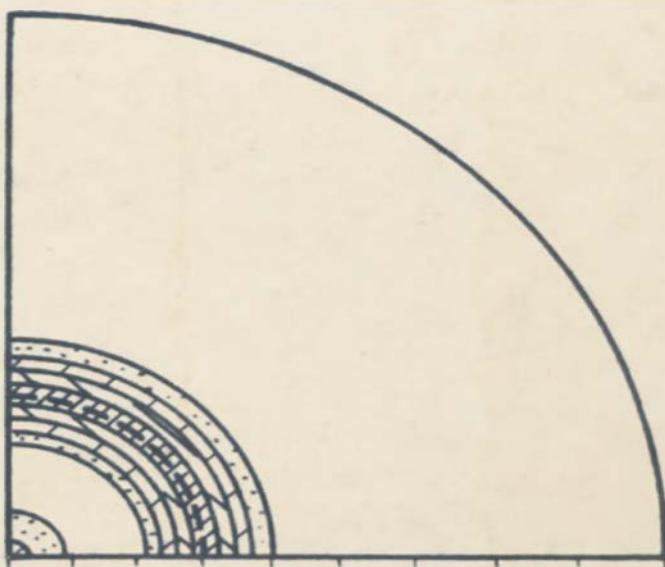


Figure 8. 0001 pole figure of compressed iodide titanium--
34.3 percent reduction.

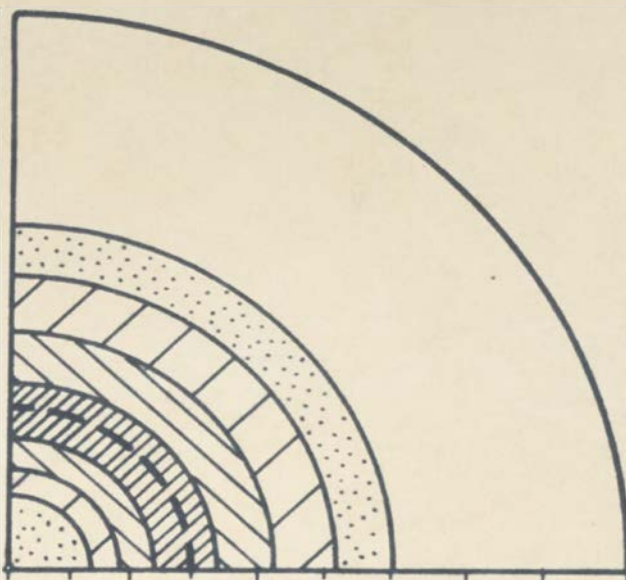


Figure 9. 0001 pole figure of compression rolled iodide titanium--50.0 percent reduction.

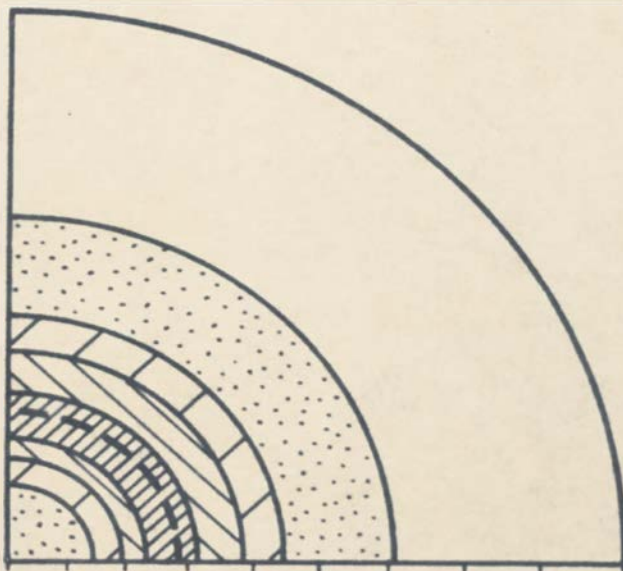


Figure 10. 0001 pole figure of compressed iodide titanium--80.1 percent reduction.

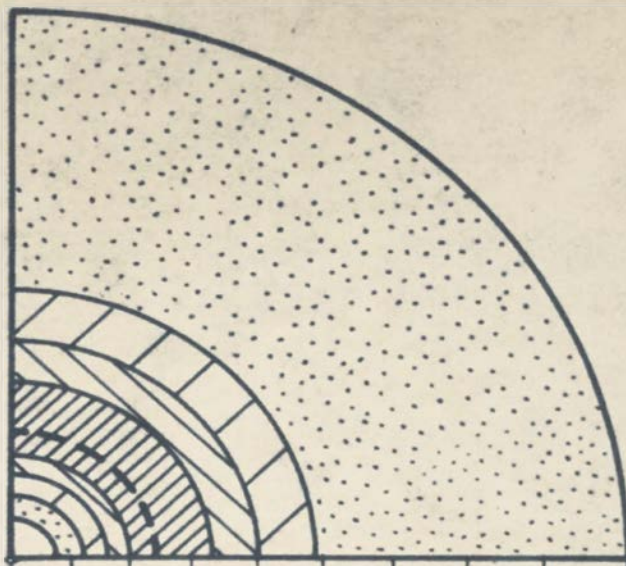


Figure 11. 0001 pole figure of compressed iodide titanium--86.3 percent reduction.

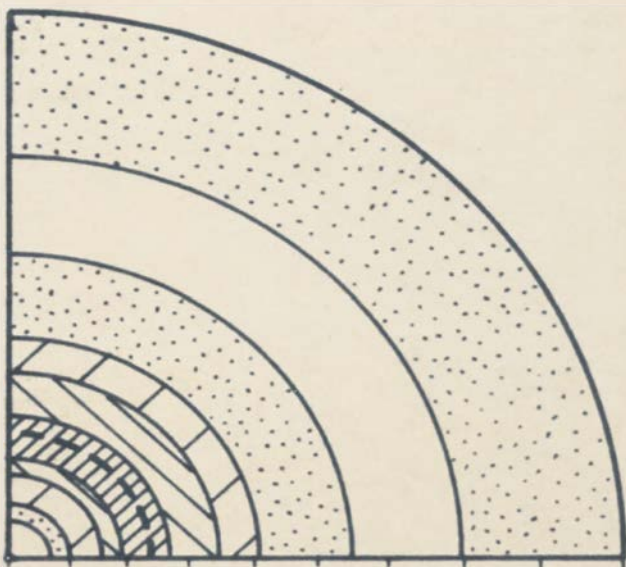


Figure 12. 0001 pole figure of compression rolled iodide titanium--89.6 percent reduction.

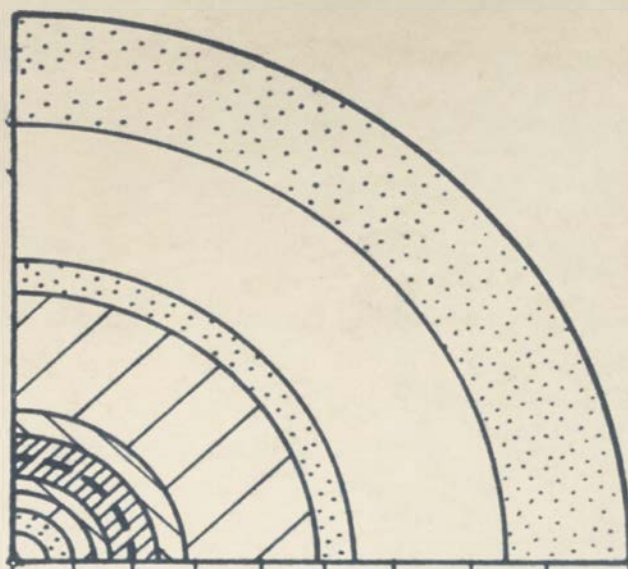


Figure 13. 0001 pole figure of compression rolled iodide titanium--96.2 percent reduction.

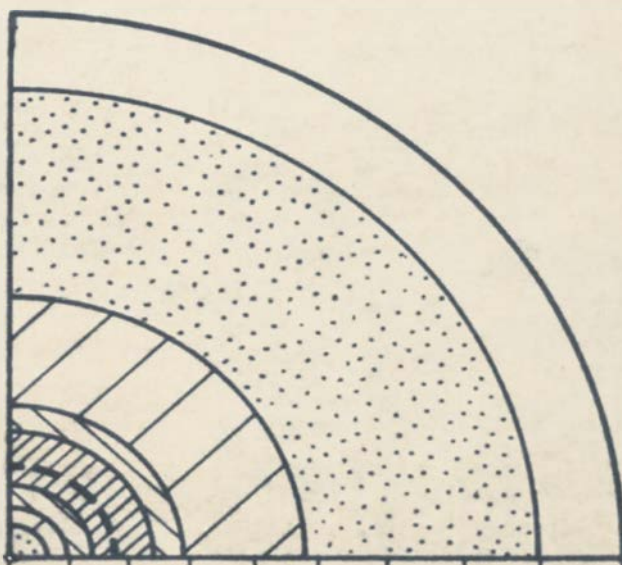


Figure 14. 0001 pole figure of compression rolled iodide titanium--98.9 percent reduction.

The texture can be described as a rotation of the 0001 planes from 15 to 30 degrees away from the plane of compression. Examination of the pole figures shows that as the reduction increased the angle of rotation decreased. The angle between the 0001 maximum and the compression axis for each reduction is given in Table IV. The maximum intensity occurred at an angle of rotation of 30 degrees at low reductions and at an angle of rotation of 17.5 degrees at 98.9 percent reduction. No definite maximum existed in the sample compressed 24.1 percent.

A second noticeable feature of these pole figures is the low intensity occurring at the center of the pole figures. This region corresponds to the position of the [0001] texture which is usually considered as the ideal compression texture for a hexagonal close-packed metal. The low intensity of this region indicates that some type of twinning is removing the 0001 poles from the ideal position.

Relative intensity of the 0001 maximum. The method used in plotting the pole figures in this chapter gives no indication of the relative intensity of the maximum. To determine the relative strength of each 0001 maximum reading the intensity distribution of each sample was adjusted to give a constant total intensity over the range examined. The maximum intensity was then measured for comparison with

the other samples. Corrected maximum intensities are given in Table IV.

The figure given in Table IV for the relative intensity of the maximum of the sample compressed 24.1 percent reduction is not strictly comparable with those from the other samples. This sample showed two distinct patterns. The first, which was used in plotting the pole figure given in Figure 7, arose from the deformed or fragmented structure of the metal. A second pattern, arising from a large block of relatively undeformed metal, was not included in the pole figure. This pattern showed the usual sharp, strong intensity readings of a single grain area. Only the intensity readings from the first pattern were used in determining the corrected intensity distribution and the value of the relative maximum intensity given in Table IV.

Effect of grinding or filing after compression. Figure 15 shows the 0001 intensity curves of the sample compressed 34.3 percent. The X-ray specimens of this sample were prepared by three methods. The original sample after compression had a thickness of approximately 0.35 centimeter. To reduce the opportunity for pitting during etching, the sample was filed to 0.15 centimeter and then reduced to 0.08 centimeter by alternate etching and light polishing. The X-ray examination of this sample showed the usual double texture plus a strong [0001] texture. The [0001] maximum did not occur at 90 degrees indicating that it may have been

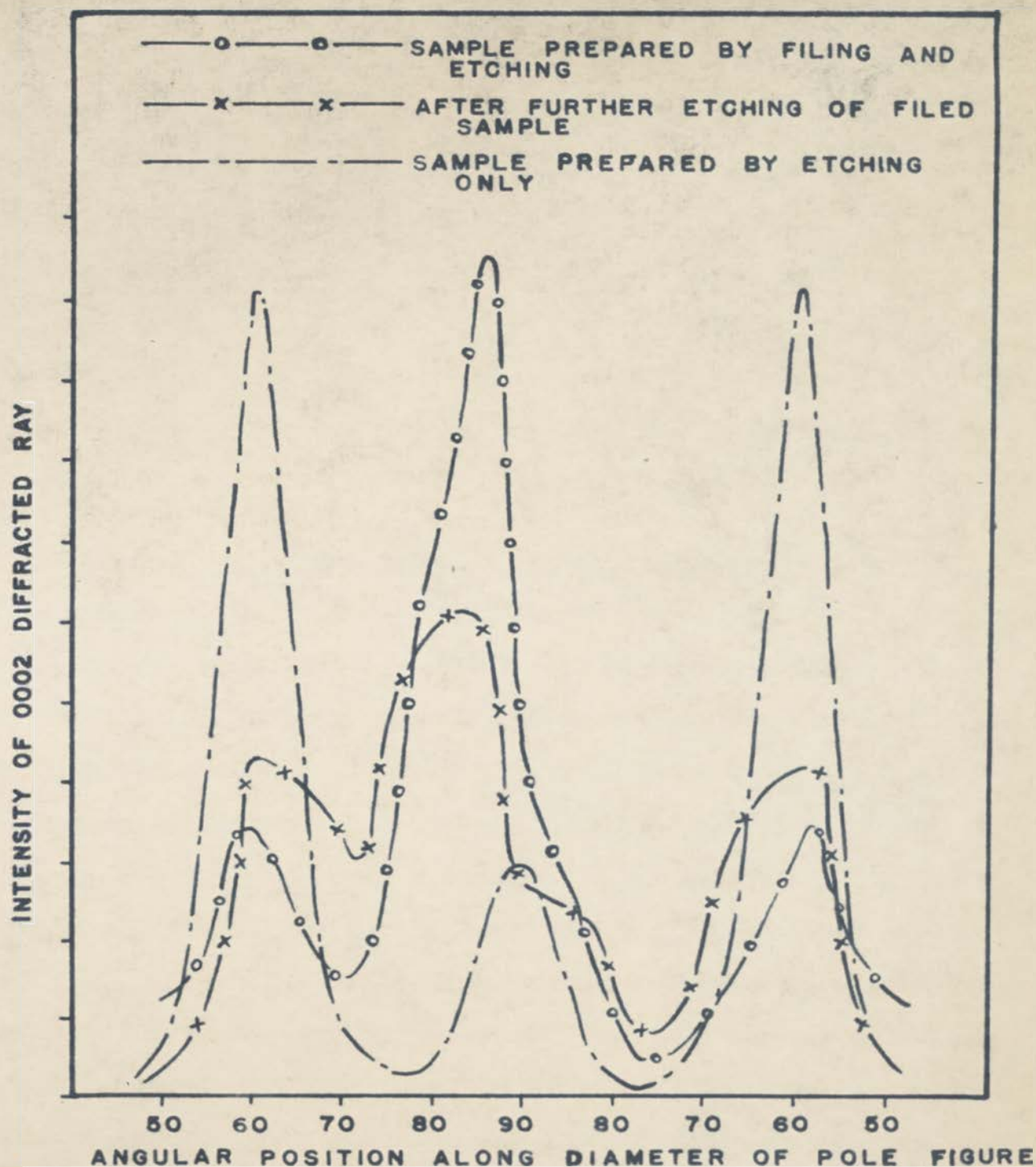
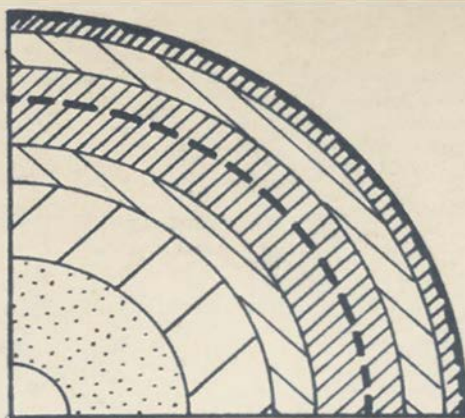


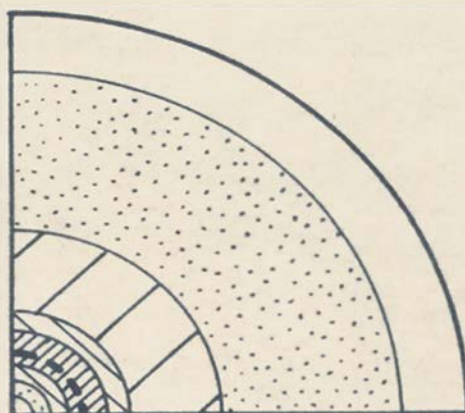
Figure 15. Comparison of the 0001 patterns of compressed iodide titanium (34.3 percent reduction) after various methods of specimen preparation.

a secondary texture produced by the filing operation. The sample was etched further to 0.065 centimeter and again examined. The unsymmetrical central maximum was much lower with a corresponding increase in the double maxima. A third specimen was prepared by etching alone. The readings obtained with this specimen are seen to be considerably different from those obtained using the previous methods of specimen preparation. The double texture is very pronounced with no maximum occurring at 85 degrees. A small [0001] maximum is seen at 90 degrees.

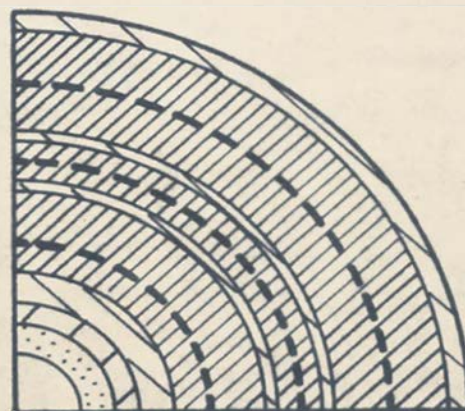
Evidence of a preferred axis of rotation. The $10\bar{1}0$, 0001, and $10\bar{1}1$ pole figures of the sample of iodide titanium compression rolled 98.9 percent are shown in Figure 16. The $10\bar{1}0$ and $10\bar{1}1$ pole figures show that there is a slight tendency for the rotation of the 0001 pole away from the compression axis to occur about a $\langle 10\bar{1}0 \rangle$ axis. This is shown by the appearance of slight $10\bar{1}0$ maxima at 0 and 15 degrees and $10\bar{1}1$ maxima at 12.5, 27.5, and 45 degrees. These maxima are marked by heavy dashed lines in Figure 16. For the 0001 maximum to appear at 72.5 degrees--a rotation of 17.5 degrees--by rotation about a $\langle 10\bar{1}0 \rangle$ rotation axis, the $10\bar{1}0$ maxima must appear at 0 and 15 degrees and the $10\bar{1}1$ maxima must appear at 13, 27, and 41 degrees. The agreement of the above values with the experimentally measured values is good.



10 $\bar{1}$ 0 POLE FIGURE



0001 POLE FIGURE



10 $\bar{1}$ 1 POLE FIGURE

Figure 16. Pole figures of iodide titanium reduced 98.9 percent by compression rolling showing the tendency for 0001 rotation to occur about a $\langle 10\bar{1}0 \rangle$ rotation axis.

This tendency for the 0001 rotation to occur about a $\langle 10\bar{1}0 \rangle$ rotation axis appeared in all of the samples examined. The intensity of the maxima in the $10\bar{1}0$ and $10\bar{1}1$ pole figures was usually about fifteen percent greater than that of the surrounding region in the pole figure.

B. DISCUSSION OF RESULTS

The appearance of a uniform texture over the complete range examined indicated that compression between parallel plates and compression rolling produce similar results as was found by Barrett (41) in the case of iron.

The compression texture of titanium is seen by the results plotted in Figure 15 to be sensitive to a shear stress parallel to the plane of compression. The effect of this stress is noted at a considerable distance into the sample. The [0001] texture reported by Yen (42) may possibly have been a result of this effect.

The results obtained from the examination of the sample compressed 34.3 percent are not reliable. The degree of preferred orientation of this sample is considerably higher than that of the other samples as is shown in Table IV. This difference is believed due to some deformation introduced into the sample during its original preparation.

(41) G. S. Barrett, "The structure of iron after compression." Trans AIME, Vol 135, pp. 296-326, 1939

(42) M. K. Yen, loc. cit.

Although it shows the usual double maxima it also has a distinct [0001] maximum (see Figure 15) which was absent in all other samples.

If the corrected intensity of the other seven samples is compared it is seen that the compression texture soon reached a more or less stable intensity and that the only change brought about by increased reduction was a shift in the position of the 0001 maximum. This suggests that the observed texture is an equilibrium texture existing between the stable end points of slip and twinning. A movement of the boundary between the slip and twinning regions due to unequal changes of the critical shear stresses would then account for the shift in the position of the 0001 maxima.

According to a recent analysis of the mechanics of twinning by Barrett (43), twinning on the $10\bar{1}2$ planes is not possible in close-packed hexagonal metals with a c/a ratio less than 1.732 if the axis of compression is along the hexagonal axis of the lattice. In titanium, with a c/a ratio of 1.601, $10\bar{1}2$ twinning, the usual type of hexagonal twinning, could not be the means by which the central low intensity region is kept depleted of 0001 planes. Since rotation by slip on the base planes should be continually moving planes into this region, an explanation of its low

(43) C. S. Barrett, "The crystallographic mechanisms of translation, twinning, and banding." Cold Working of Metals, (Cleveland: American Society for Metals, 1949), p. 84

intensity is required.

A recent investigation of the slip and twinning elements of titanium (44) has shown titanium to twin on the $10\bar{1}2$, $11\bar{2}2$, and $11\bar{2}1$ planes. Both $11\bar{2}2$ and $11\bar{2}1$ twinning are able to twin in compression from a $[0001]$ position and therefore to remove 0001 planes from the center of the pole figures in this paper.

Examination of the $10\bar{1}0$ and $10\bar{1}1$ pole figures of the samples showed a slight tendency for the 0001 rotation to occur about a $\langle 10\bar{1}0 \rangle$ axis. This type of preferred orientation would result from $\{10\bar{1}1\}\langle 11\bar{2}0 \rangle$ slip. The lack of any appreciable 0001 intensity along the circumference of the 0001 pole figures indicates that in compression $\{10\bar{1}0\}\langle 11\bar{2}0 \rangle$ slip is relatively unimportant. Both of these modes of slip have been reported for titanium (45).

C. SUMMARY

1. Compression samples with eight different reductions were prepared and the 0001, $10\bar{1}0$, and $10\bar{1}1$ pole figures determined.

2. A rotation of the base planes 30 degrees from the compression plane was found in the initial reductions. The

(44) F. D. Rosi, C. A. Dube, and B. H. Alexander, "Mechanism of plastic flow in titanium." J. of Metals, Vol 4, No. 2, pp. 145-6, 1952

(45) Loc. cit.

amount of rotation of the base plane from the compression plane decreased with increased reduction. A minimum angle of rotation of 17.5 degrees was found at a reduction of 98.9 percent.

3. Compression in a testing machine and by compression rolling were found to produce similar results.

4. The compression texture was found to be considerably changed by any shearing stress parallel to the plane of compression. This stress tended to produce a $[0001]$ texture.

5. A slight preference for a $\langle 10\bar{1}0 \rangle$ axis of rotation for movement of the 0001 poles from the $[0001]$ position was evident in the $10\bar{1}0$ and $10\bar{1}1$ pole figures.

CHAPTER VI

THE COLD ROLLED TEXTURE OF TITANIUM

The cold rolled texture of iodide titanium has been examined by Clark (46) who reported a $(0001)[10\bar{1}0]$ texture rotated thirty degrees toward the transverse direction. Clark used a photographic pole figure method in his examination.

The metals in the hexagonal lattice system are usually divided into two groups; those with a c/a ratio above the value for ideal close packing, 1.633, and those with a c/a ratio below this value. Titanium, with a c/a ratio of 1.601 (47) is a member of the latter group which also includes the common metals cobalt, magnesium, zirconium, and beryllium.

Both zirconium, with a c/a ratio of 1.590 (48), and beryllium, with a c/a ratio of 1.570 (49), would be expected to show deformation textures similar to those of titanium. The ideal cold rolled texture of zirconium has been described as $(0001)[10\bar{1}0]$ rotated thirty degrees in the transverse direction (50). This is similar to the ideal cold rolled

(46) H. T. Clark, "The textures of cold rolled and annealed titanium." Trans AIME, Vol 188, pp. 1154-6, 1950

(47) S. S. Sidhu, Personal communication

(48) Loc. cit.

(49) Loc. cit.

(50) R. K. McGeary and B. Lustman, "Preferred orientation in zirconium." AECD-2951, March 1950

texture reported for iodide titanium. The ideal cold rolled texture of beryllium on the other hand has been described as $(0001)[10\bar{1}0]$ with only a slight transverse spread (51). Thus it is apparent that the deformation textures of hexagonal close-packed metals may vary considerably with small differences in c/a ratio.

Since the previous work on titanium was conducted using the standard photographic X-ray methods, the degree of accuracy is rather low. The cold rolled texture of titanium was therefore re-examined using the more quantitative Geiger counter technique. Textures were determined for iodide titanium and for three grades of commercial titanium.

A. EXPERIMENTAL RESULTS

The methods used in the preparation of the titanium samples for the texture study and the cold rolling procedures are discussed in Chapters III and IV. The reduction given each of the samples examined is given in Table V which also includes data on the original hardness and grain size of the samples. The $10\bar{1}0$, 0001 , and $10\bar{1}1$ pole figures were determined using the Schulz-Decker technique. It was necessary to plot only one quadrant since the pole figures were symmetrical about the rolling direction and the transverse

(51) A. Smigelskas and C. S. Barrett, "Preferred orientation in rolled and recrystallized beryllium." Trans AIME, Vol 185, pp. 145-8, 1949

TABLE V

PERCENT REDUCTION OF COLD ROLLED TITANIUM SAMPLES

Sample	Annealed in,	Annealed Grain Size	Rockwell B Hardness	Percent Reduction
Iodide Ti	Vacuum	0.102 mm	< 0	93.2
Comm. Ti,				
No. 1	Vacuum	0.045 mm	83	95.8
No. 1	Air	0.045 mm	83	94.9
No. 2	Vacuum	0.011 mm	84	95.7
No. 3	Vacuum	0.010 mm	102	94.0
No. 3	Helium	0.008 mm	107	78.3
No. 3	Helium	0.008 mm	107	95.8

direction. The maximum intensity was reduced to seventy intensity units and all other readings reduced proportionally for convenience in plotting. The intensity contour system of plotting was used with the contours for sixty, fifty, etc., shown on the plot of the pole figure by the numbers 6, 5, etc.

Cold rolled texture of iodide titanium. The $10\bar{1}0$, 0001 , and $10\bar{1}1$ pole figures of iodide titanium reduced 93.2 percent are shown in Figure 17. The texture is seen to be primarily the $(0001)[10\bar{1}0]$ rotated thirty degrees or more in the transverse direction as previously reported by Clark (52).

The most noticeable feature of the cold rolled texture is that the highest degree of preferred orientation is in the $10\bar{1}0$ pole figure in which the $10\bar{1}0$ poles tend strongly to be located in the rolling direction. The 0001 pole figure shows a preferred orientation consisting of a spread along the transverse axis with a maximum about thirty degrees from the rolling plane normal. The low intensity of the 0001 pole figure at the rolling plane normal should be noted. The $10\bar{1}1$ pole figure shows a rather low degree of preferred orientation. The position of the $10\bar{1}1$ maxima correspond to the texture $(0001)[10\bar{1}0]$ rotated thirty degrees in the trans-

(52) Clark, loc. cit.

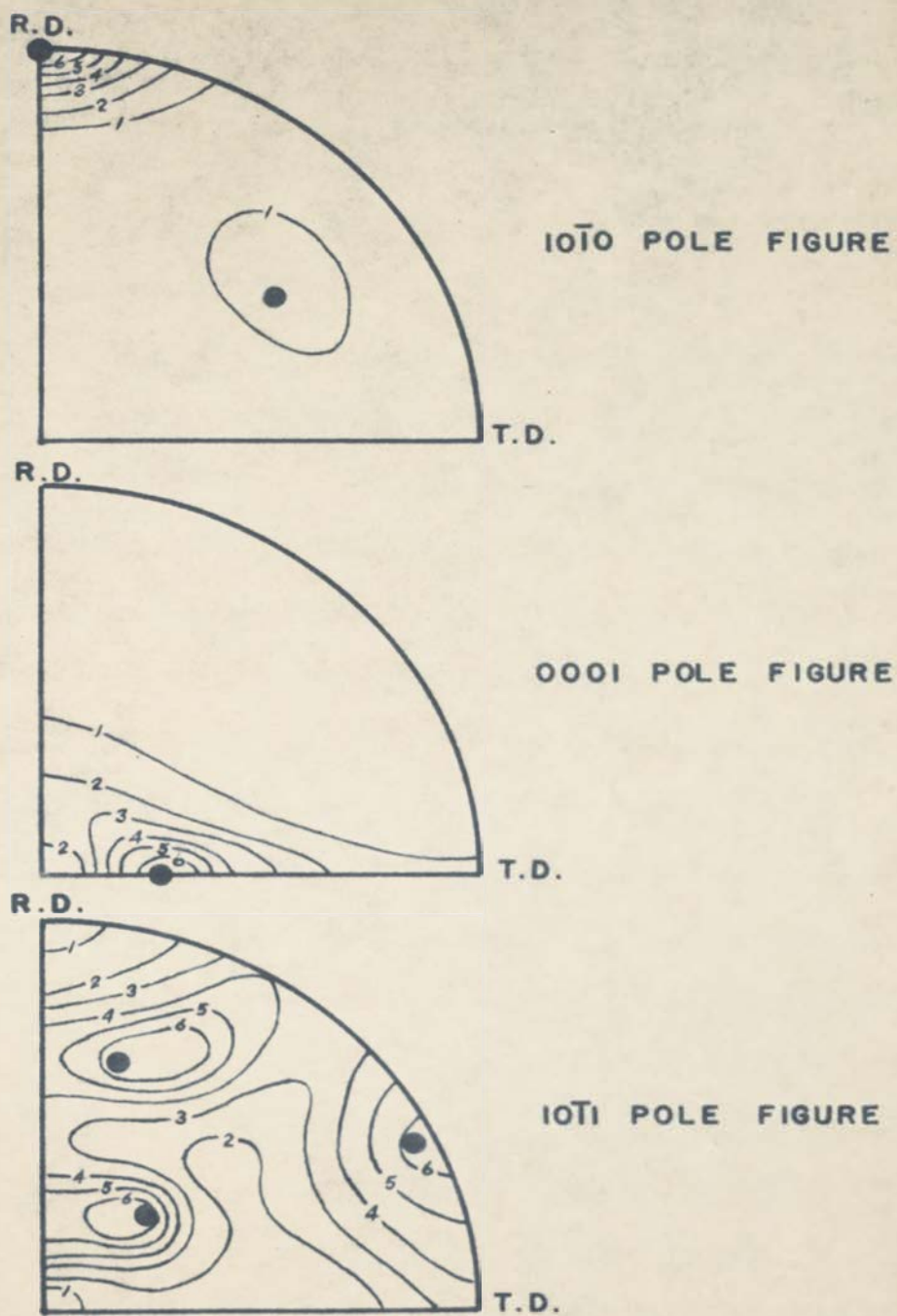


Figure 17. Cold rolled iodide titanium. ●--(0001)[1010] rotated thirty degrees in the transverse direction.

verse direction. The spread of orientations is large. Minimum intensity of the $10\bar{1}1$ poles was measured along the transverse axis and in the rolling direction.

Gold rolled textures of commercial titanium. No texture studies of commercial titanium were found in the literature. The three commercial grades examined were from different sources and had received different types of treatment before being used in this study. Commercial titanium sample number one and number two showed after annealing and cold rolling a texture almost identical with that of iodide titanium. The $10\bar{1}0$, 0001 , and $10\bar{1}1$ pole figures of the commercial titanium sample number one annealed in vacuum are shown in Figure 18. The pole figure of the commercial titanium sample number one annealed in air and the commercial titanium sample number two annealed in vacuum were practically identical with Figure 18 and are not shown.

Comparison of Figure 17 and Figure 18 shows that there is little significant difference between the iodide texture and that of the softer commercial grades of titanium. The extremely low intensity at the rolling plane normal in the 0001 pole figure should be noted. This position is that which usually shows highest intensity in hexagonal close-packed metals with a c/a ratio less than 1.633.

The $10\bar{1}0$, 0001 , and $10\bar{1}1$ pole figures of commercial titanium sample number three annealed in vacuum are shown in Figure 19. A noticeable difference in the 0001 pole figure

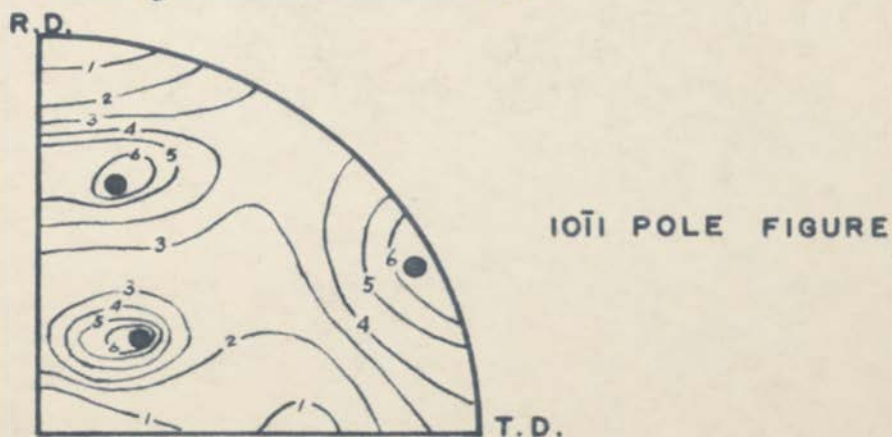
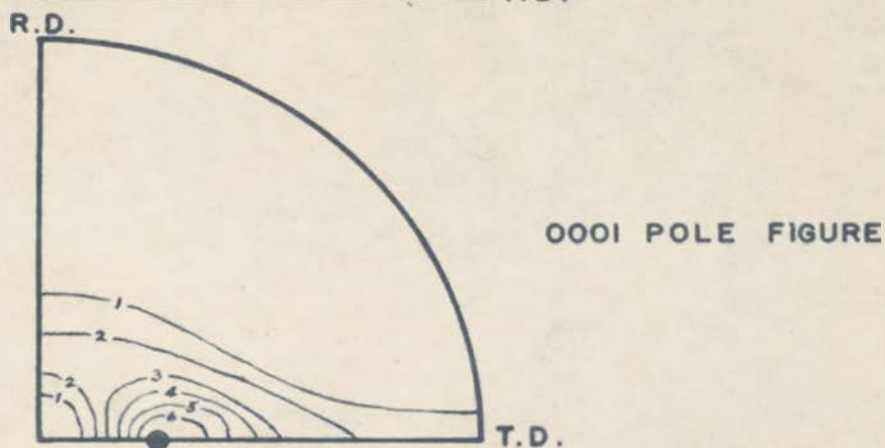
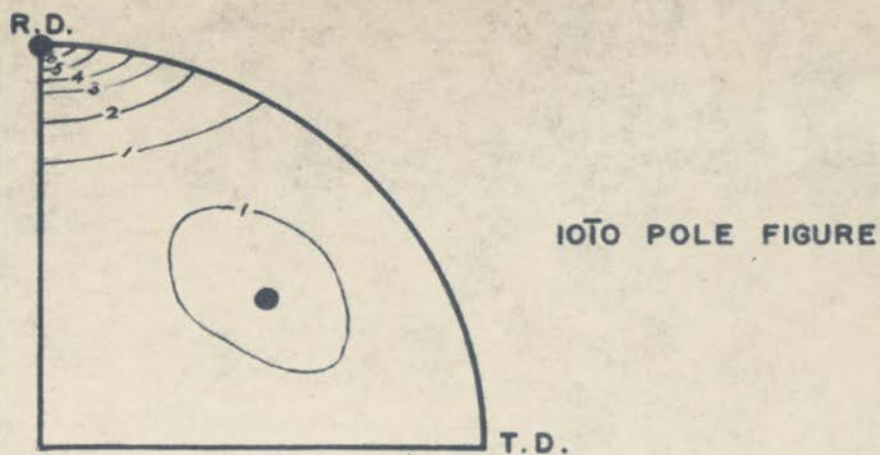


Figure 18. Cold rolled commercial titanium sample number one. ●--(0001)[1010] rotated thirty degrees in the transverse direction.

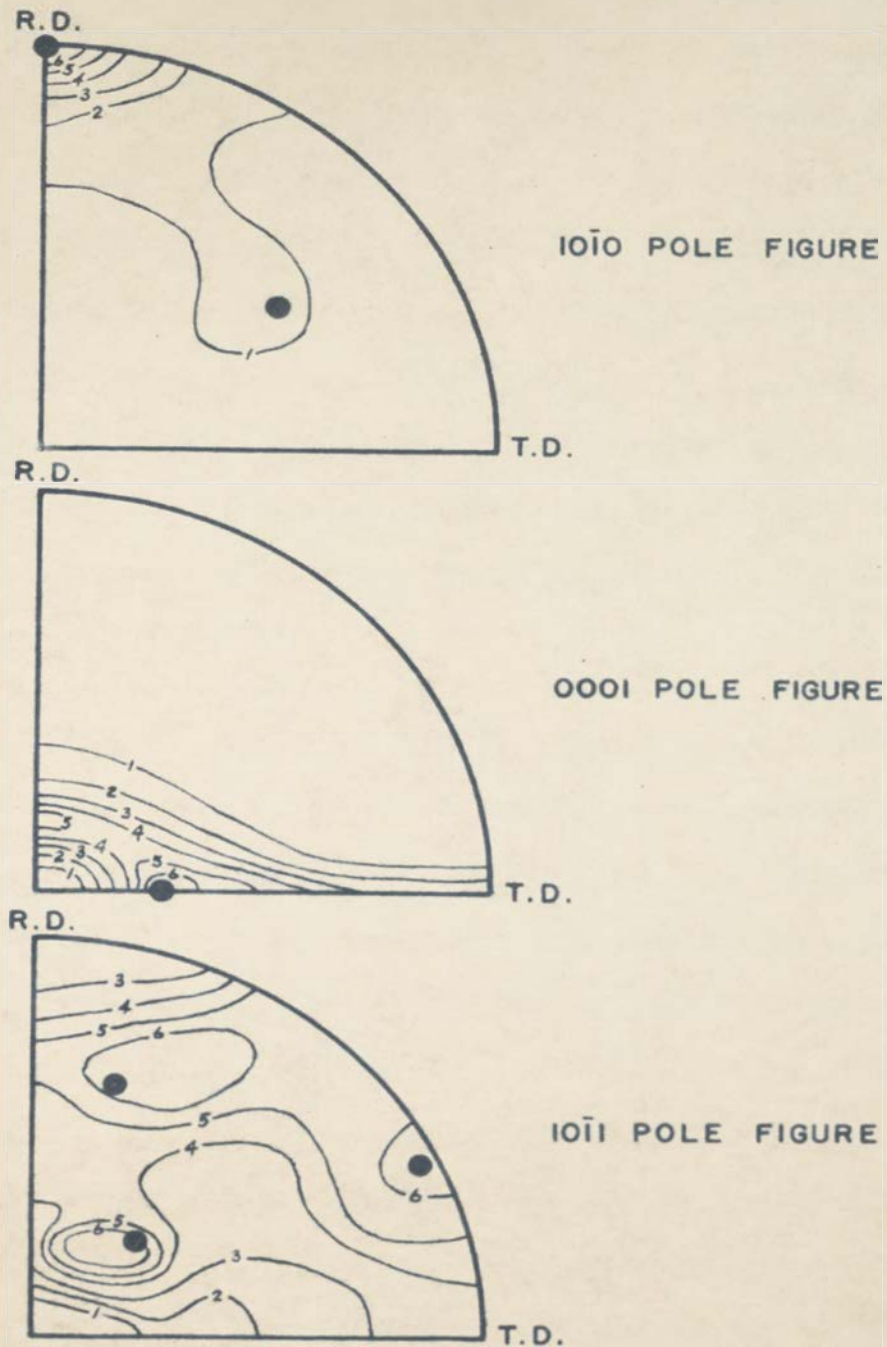


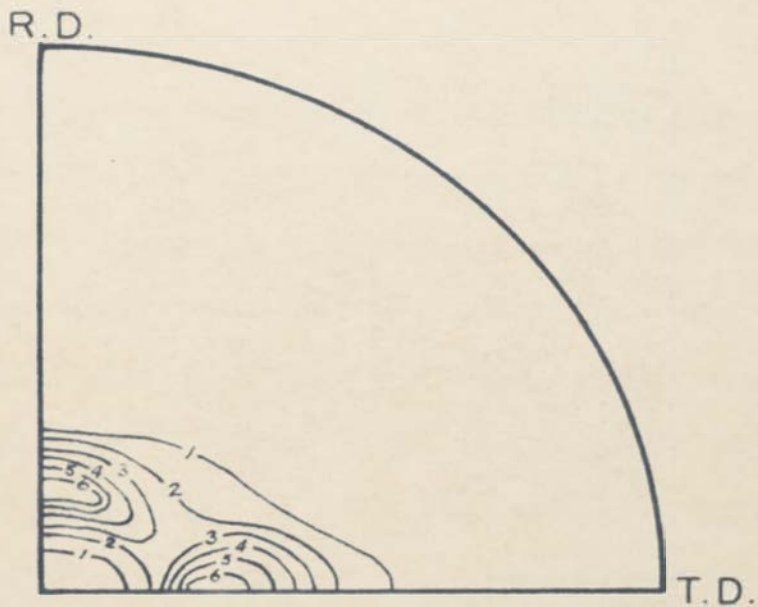
Figure 19. Cold rolled commercial titanium sample number three. ●--(0001)[1010] rotated thirty degrees in the transverse direction.

is seen in comparing Figure 19 with Figure 17 and Figure 18. In this sample of commercial titanium a second 0001 maximum was apparent in the rolling direction twenty degrees from the rolling plane normal. This maximum is superimposed on the normal 0001 texture. In the $10\bar{1}0$ pole figure the only noticeable change is a slight increase in intensity between the two $10\bar{1}0$ maxima regions causing them to be joined by the lowest intensity contour. The $10\bar{1}1$ pole figure shows less preferred orientation in Figure 19 than in Figure 17 or Figure 18. The rolling direction in particular is now more intensely populated.

Changes in texture with amount of deformation. Two 0001 pole figures of the commercial titanium sample number three annealed in helium are shown in Figure 20. These pole figures show the variation in texture with increased reduction. The double maxima noted in Figure 19 is apparent in both pole figures and the maximum in the rolling direction, twenty degrees from the rolling plane normal, is slightly more intense. Of particular interest in these two pole figures is the 0001 maximum in the transverse direction in the specimen reduced 78.3 percent. This maximum is an indication of $\{10\bar{1}0\}$ slip. A slight increase in the 0001 intensity was noticed in all of the pole figures near the transverse direction but in the case of higher reductions it was usually too slight to appear with the method of plotting. Although the intensity of the region along the transverse



a. 78.3 percent reduction in area



b. 95.8 percent reduction in area

Figure 20. 0001 pole figures of cold rolled commercial titanium sample number three.

axis near the transverse direction in the specimen reduced 95.8 percent was too low to fall within the lowest contour line, it was several units higher than that of the region about ten degrees from the transverse axis. The disappearance of the 0001 maximum in the transverse direction at high reductions indicates that $\{10\bar{1}0\}$ slip is of importance only in the earlier stages of deformation.

9. DISCUSSION OF RESULTS

From the cold rolled pole figures of the first two commercial grades of titanium and from the iodide titanium it seems apparent that the ideal texture can be described as a $(0001)[10\bar{1}0]$ texture rotated thirty degrees or more in the transverse direction.

In Figure 21 the positions of the $10\bar{1}0$, 0001, and $10\bar{1}1$ poles of the $(0001)[10\bar{1}0]$ texture before rotation (white circles) and after rotating thirty degrees toward the transverse direction (black circles) are plotted over a polar stereographic net. As the $(0001)[10\bar{1}0]$ texture is rotated toward the transverse direction the poles move along the dashed lines in Figure 21. By consideration of these movements it is seen how the determined texture developed.

As the 0001 pole moves from a position thirty degrees from the rolling plane normal to the transverse direction the $10\bar{1}0$ pole in the rolling direction stays fixed and acts as a rotation axis. The second $10\bar{1}0$ pole however rotates

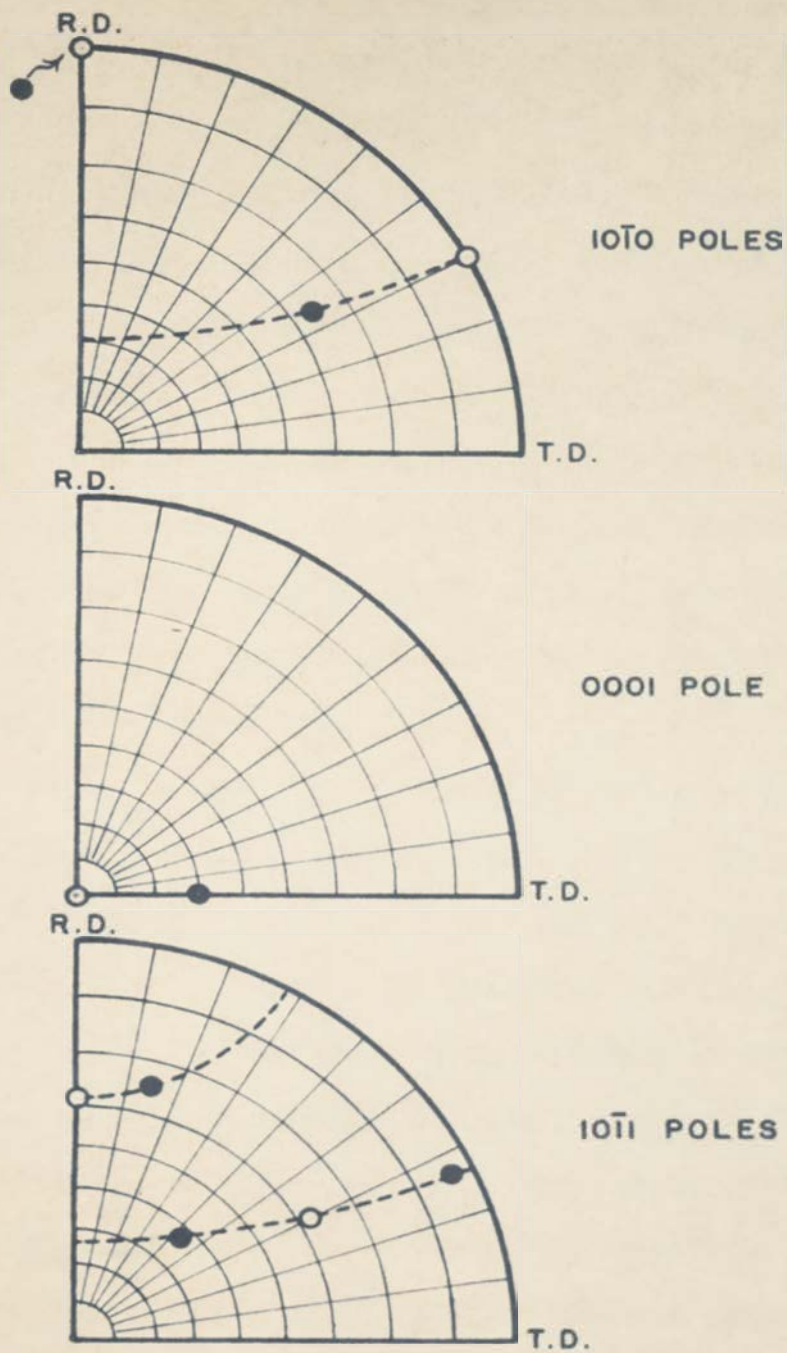


Figure 21. Position of the ideal textures: O--(0001) [10 $\bar{1}$ 0]; ●--(0001)[10 $\bar{1}$ 0] rotated thirty degrees toward the transverse direction.

from the position of the black circle to the intersection of the dashed line with the rolling axis. Thus the measured intensities of the two positions will be considerably different. The $10\bar{1}0$ pole not in the rolling direction will have maximum intensity at thirty degrees (the position of the black circle) to correspond to the maximum intensity in the 0001 pole figure. The intensity between this position and the center of the pole figure will decrease in proportion to the intensity of the 0001 poles along the transverse axis from thirty degrees to ninety degrees from the rolling plane normal. The $10\bar{1}0$ pole in the rolling direction remains in one position for all of these orientations and thus its intensity is proportional to the sum of all of the 0001 intensities between thirty degrees and ninety degrees.

The $10\bar{1}1$ rotations are shown in the same manner. In this case however it should be noted that a rotation thirty degrees to the right in the 0001 pole figure produces the black circles nearest the rolling direction and the transverse direction in the $10\bar{1}1$ pole figure. A rotation to the left is necessary for the black circle nearest the rolling plane normal in the $10\bar{1}1$ pole figure. Thus a rotation of the 0001 pole from thirty degrees to ninety degrees will spread orientations in the $10\bar{1}1$ pole figure from the black circle nearest the rolling direction to the circumference of the polar stereographic net, and from the black circle nearest the transverse direction to the circumference and

then back toward the white circle, but from the black circle to the left when considering the black circle nearest the rolling plane normal. Thus a spread of orientations is obtained with maxima at the black circles and minima near the rolling direction, along the transverse axis, and between the white circle and the black circle nearest the rolling plane normal. The pole figures of Figures 17 and 18 show this tendency. The positions of the rotated ideal texture are shown in the pole figures of Figures 17, 18, and 19 by black circles.

The origin of the second 0001 maximum in the commercial titanium sample number three is not apparent. No corresponding maxima are seen in the $10\bar{1}0$ or $10\bar{1}1$ pole figures. The higher annealed hardness of this sample plus the visible grain boundary phase seen in the microstructure (see Chapter III) suggests that the formation of the second maximum may be the result of foreign atoms present in the titanium lattice in sufficient amounts to alter the normal slip-twinning behavior.

The cold rolled pole figures of titanium are seen by the preceding results to be influenced by two main factors. The first is a very strong tendency for the $10\bar{1}0$ pole to be in the rolling direction. The second is the tendency for the 0001 pole to be thirty degrees or more away from the rolling plane normal. The first of these two conditions would be the result of either $\{10\bar{1}1\}$ or $\{10\bar{1}0\}$ slip while

the second apparently requires some type of mechanical twinning, such as $10\bar{1}1$, $11\bar{2}1$, or $11\bar{2}2$, which will remove the 0001 poles from the region around the rolling plane normal.

C. SUMMARY

1. The $10\bar{1}0$, 0001 , and $10\bar{1}1$ pole figures of iodide titanium and of three commercial grades of titanium were determined after cold rolling.

2. The cold rolled texture of iodide titanium and two of the three commercial grades of titanium were found to be similar to the texture reported by Clark.

3. The ideal texture was found to be a $(0001)[10\bar{1}0]$ rotated from thirty to ninety degrees in the transverse direction with the maximum concentration at thirty degrees.

4. The third commercial grade of titanium was found to exhibit a double texture with 0001 maxima rotated, from the rolling plane normal, thirty degrees toward the transverse direction and twenty degrees toward the rolling direction. The double texture was evidently the result of impurities in the lattice.

CHAPTER VII

A. THEORETICAL ANALYSIS OF THE DEFORMATION TEXTURES OF TITANIUM

In Chapter II the various theories for explaining the origin of deformation textures were discussed. Of these theories the only one able to explain texture formation when mechanical twinning was an important factor was that developed by Calnan and Clews (53)(54)(55). This method of texture analysis--referred to hereafter as the "Calnan and Clews method"--has been successful in predicting the textures of both magnesium and zinc. The successful application to the texture of zinc was particularly interesting since zinc showed no stable end texture due to mechanical twinning.

Because of its successful application to the study of zinc, it seemed likely that the Calnan and Clews method of analysis might prove equally satisfactory in explaining the origin of the deformation texture of titanium. During the course of the examination, tentative results of an investi-

(53) E. A. Calnan and C. J. B. Clews, "Deformation textures in face-centered cubic metals." Phil. Mag., Vol 41, pp. 1085-1100, 1950

(54) E. A. Calnan and C. J. B. Clews, "The development of deformation textures in metals. Part II. Body-centered cubic metals." Phil. Mag., Vol 42, pp. 616-35, 1951

(55) E. A. Calnan and C. J. B. Clews, "The development of deformation textures in metals. Part III. Hexagonal structures." Phil. Mag., Vol 42, pp. 919-31, 1951

gation of the elements of slip and twinning in titanium were published (56). These results confirmed several points predicted by the application of the Calnan and Clews method and aided materially in the successful conclusion of the study.

A. GENERAL PRINCIPLES OF THE CALNAN AND CLEWS METHOD

The following brief discussion will attempt to outline the essential portions of the method of texture analysis developed by Calnan and Clews. Their method provides a means of predicting the texture resulting from the deformation of polycrystalline materials from the behavior of single crystals. It is capable of handling inhomogeneous deformation and is based on the assumption that inhomogeneous deformation is occurring.

In homogeneous deformation multiple slip--slip on three or more slip systems at the same time--must occur to maintain the external shape and to prevent grain boundary separation. In the treatment of Calnan and Clews it is assumed that for multiple slip to occur the stress must be such as to give equal resolved shear stress simultaneously on all of the active slip planes. If the applied stress is directed so that the resolved shear stress is a maximum on

(56) F. D. Rosi, G. A. Dube, and B. H. Alexander, "Mechanism of plastic flow in titanium." J. of Metals, Vol 4, No. 2, pp. 145-5, 1952

one slip system, only one slip system will be active. If the resolved shear stress is maximum and equal in two slip systems, duplex slip--slip on two slip systems at the same time--will occur.

Slip on a single slip system will give rotation of the slip plane normal toward the stress axis in compression and of the slip direction toward the stress axis in tension. Duplex slip will give rotation of the great circle joining the two slip plane normals toward the stress axis in compression and the great circle joining the two slip directions toward the stress axis in tension. Thus single and duplex slip are tending to develop a deformation texture while multiple slip is necessary to maintain external shape and grain boundary cohesion. When a stereographic plot of the crystal is used, these rotations are shown by a movement of the stress axis while the slip plane normal and slip direction remain fixed.

In the method of Calnan and Clews the effect resulting from simultaneous operation of single, duplex, and multiple slip, thus inhomogeneous deformation, is predicted.

In Figure 22 a hypothetical slip system plotted in the unit stereographic triangle for the hexagonal system is shown. For the purpose of this discussion it will be assumed that duplex slip occurs along the $[0001]$ - $[10\bar{1}0]$ edge, multiple slip at $[10\bar{1}0]$, and single slip in the area of the unit triangle.

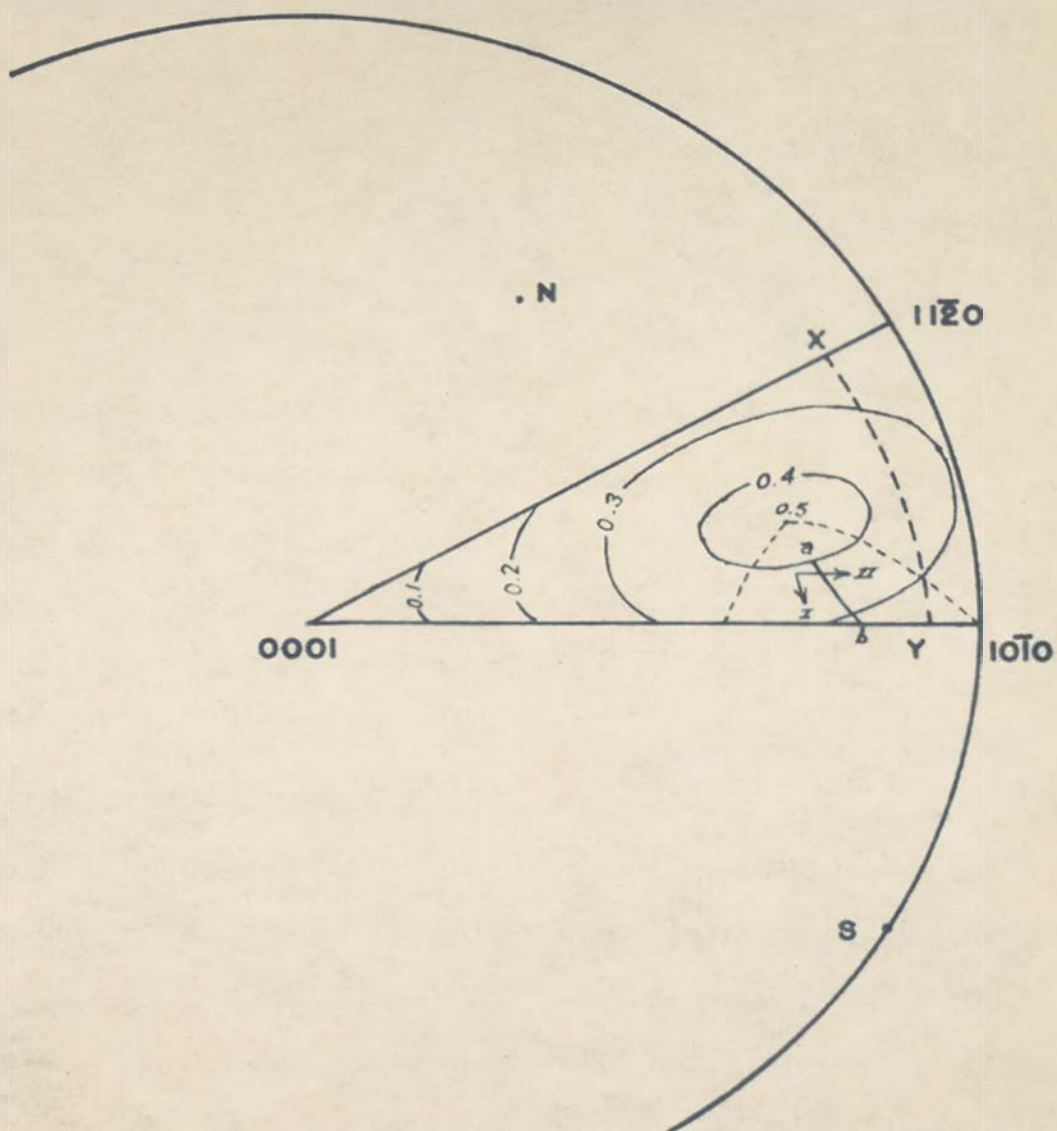


Figure 22. Sample resolved shear stress contour diagram plotted in the hexagonal unit stereographic triangle.

Hypothetical resolved shear stress contours are plotted for the active slip system in the unit triangle. These contour lines are obtained by joining all points in the unit triangle having equal resolved shear stress. The resolved shear stress is determined for any point in the unit triangle by calculating the value of the function, $\cos \times \cos \lambda$, where \times is the angle between the stress axis and the slip plane normal and λ is the angle between the stress axis and the slip direction. In Figure 22, the value of the resolved shear stress function for point a would be 0.4, obtained by substituting the measured angle between a and N for \times and of the angle between a and S for λ in the function, $\cos \times \cos \lambda$, where N and S are the slip plane normal and the slip direction respectively.

Since the active slip system is that for which the resolved shear stress function is maximum, all other possible slip systems in the same slip family will have lower values of resolved shear stress within the unit triangle. Along the $[0001]$ - $[10\bar{1}0]$ edge two slip systems will have equal resolved shear stress values and duplex slip will occur. At $[10\bar{1}0]$ the resolved shear stress is equal for more than two systems and multiple slip will occur.

If the stress axis lies at point a in Figure 22, slip will occur on the single slip system when the value of the resolved shear stress, $T_a \cos \times \cos \lambda$, where T_a is the applied stress, equals the critical shear stress, C_s . If the applied

stress, T_a , reaches a value greater than that necessary for slip at a , that is if $0.4 T_a > C_s$, and slip has not occurred, the effective stress, T_e , is no longer at a but must have moved to a position of lower resolved shear stress. This movement is assumed to be by the most direct route, thus a moves down a contour gradient toward point b . If T_e reaches b before slip occurs, any increase of T_a will cause either duplex slip at b or movement of T_e to a region of lower resolved shear stress--toward $[10\bar{1}0]$ in Figure 22. At $[10\bar{1}0]$ multiple slip will occur. The movement of T_e from T_a is considered to be the result of lateral stresses due to grain boundary effects, etc. Thus each grain and in some cases different parts of the same grain will have different positions of T_a as plotted in the unit triangle and therefore will have different amounts and directions of movement of T_e . It is this concept of movement of the effective stress which has enabled the Calnan and Clews method to successfully treat several previously unsolved problems in deformation texture study.

Assuming T_a to be a tensile stress, slip between a and b will result in single slip rotation toward S whenever $T_e \cos \lambda \cos \lambda$ becomes greater than C_s . When slip rotation occurs T_e returns to the new position of T_a and the process starts again. Thus the deformation proceeds in a series of steps and the texture resulting can be determined by considering the probability of the various steps.

Duplex slip rotation will occur if T_0 succeeds in reaching the $[0001]-[10\bar{1}0]$ boundary. Since the resolved shear stress is equal for both the slip system (N)[S] and the second active slip system, it follows that the second slip plane normal and slip direction are symmetrical with N and S about the $[0001]-[10\bar{1}0]$ line. Thus the second slip direction is $[11\bar{2}0]$. The great circle connecting these two slip directions crosses the $[0001]-[10\bar{1}0]$ edge at $[10\bar{1}0]$. Duplex rotation in tension will therefore be toward $[10\bar{1}0]$ which is also the direction of decreasing resolved shear stress. The single and duplex slip rotations are indicated for point a by the two arrows marked I and II respectively.

All points to the left of the contour gradient connecting $[10\bar{1}0]$ with the maximum resolved shear stress point and to the right of the contour gradient connecting the maximum resolved shear stress point on the $[0001]-[10\bar{1}0]$ edge to the maximum resolved shear stress point tend to move to the same point, $[10\bar{1}0]$. Since all orientations within these boundaries behave similarly, it is convenient to consider them as a group and to mark off all such areas by dashed lines as has been done for this area in Figure 22.

If the direction of single slip is the same general direction as the decrease in resolved shear stress, as in the example shown in Figure 22, there is a strong probability that the region of duplex slip will be reached either by single slip rotation or by movement of T_0 or by a combina-

tion of both. Similarly, if duplex slip rotation and the decrease in resolved shear stress both lead to a region of multiple slip, multiple slip is probable. Thus the orientations represented in the area marked in Figure 22 by the two dashed contour gradients have a strong probability of reaching $[10\bar{1}0]$ and multiple slip.

The formation of deformation textures can be predicted by consideration of the possible directions of single and duplex slip. In Figure 29 are shown the calculated resolved shear stress contours for $\{10\bar{1}0\}\langle 11\bar{2}0\rangle$ slip. In this illustration the shear stress contours are symmetrical about the line connecting $[0001]$ and the midpoint between $[10\bar{1}0]$ and $[11\bar{2}0]$. Thus T_e will tend to move toward the $[0001]$ - $[11\bar{2}0]$ edge if T_a is above this line and toward the $[0001]$ - $[10\bar{1}0]$ edge if T_a is below this line. The active slip systems for $\{10\bar{1}0\}\langle 11\bar{2}0\rangle$ slip are shown in Table VIII. Single slip rotations in tension are seen to be toward $[2\bar{1}\bar{1}0]$ and duplex rotations toward $[11\bar{2}0]$ along the $[0001]$ - $[11\bar{2}0]$ edge and toward $[10\bar{1}0]$ along the $[0001]$ - $[10\bar{1}0]$ edge. In Figure 30 single and duplex tension rotations on both sides of the dashed midpoint line are shown. Since T_e above the line moves toward $[0001]$ - $[11\bar{2}0]$, duplex slip rotations are toward $[11\bar{2}0]$. Similarly, duplex slip rotations below the dashed line are toward $[10\bar{1}0]$. It is seen from Figure 30 that all orientations originally located below the midpoint line will tend to rotate by slip to

$[10\bar{1}0]$. Since the direction of single slip rotation above the dashed line opposes the direction of movement of T_0 , there is a strong possibility that many orientations originally present above the dashed line will be rotated across the dashed line by single slip before the duplex slip region is reached. Those orientations close enough to the $[0001]$ - $[11\bar{2}0]$ edge to reach a region of duplex slip before occurrence of single slip will rotate toward $[11\bar{2}0]$. The lower diagram of Figure 30 shows the general tendency of both single and duplex slip rotations. Although the primary texture is $[10\bar{1}0]$, a noticeable $[11\bar{2}0]$ texture should be developed.

By similar analysis of the direction of movement of T_0 and the directions of single and duplex slip rotation, more complicated slip systems may be considered and the general slip rotation tendencies determined.

Twinning can also be considered using this method. For example, if the value of the resolved shear stress for twinning is $T_a \cos \gamma \cos \delta$, where γ is the angle between the twin plane normal and the stress axis and δ is the angle between the twinning shear direction and the stress axis, and the critical shear stress for twinning is C_t , twinning will occur when,

$$T_a \cos \lambda \cos \lambda / C_s < T_a \cos \gamma \cos \delta / C_t$$

If this equation is satisfied in the region X- $[11\bar{2}0]$ - $[10\bar{1}0]$ -Y in Figure 22, when T_0 reaches point Y twinning is favored

over slip. The twinned grain will then have a new orientation and a new position of T_a . Although the new value of T_a may fall outside the unit triangle, it is moved to its relative position within the unit triangle. The new position of T_a is then handled as if twinning had not occurred.

B. CALCULATION OF RESOLVED SHEAR STRESS VALUES

Values of α , λ , γ , and δ were determined by direct measurement over a seven inch Wulff net graduated in two degree intervals. Measurements were made by estimating to the nearest 0.2 degree and the results of the cosine function plotted. Shear stress contour diagrams were obtained by making sufficient measurements to locate the approximate position of each contour line. These diagrams are probably accurate at most to two degrees. Boundary lines between two slip systems or between slip and twinning systems were located by plotting the position of T_a and measuring the values of the angles until the following equations were solved,

$$\text{for slip: } \cos \alpha_1 \cos \lambda_1 / C_{S_1} = \cos \alpha_2 \cos \lambda_2 / C_{S_2} \quad 1.$$

$$\text{for twinning: } \cos \alpha \cos \lambda / C_S = \cos \gamma \cos \delta / C_t \quad 2.$$

A mathematical analysis (57) has shown that this boundary may have two possible forms. At least three points

(57) E. A. Calnan and C. J. B. Clews, "The development of deformation textures in metals. Part II. Body-centered cubic metals." Phil. Mag., Vol 42, pp. 616-35, 1951

were located on each boundary to determine its position.

Values for C_s and C_t had to be assumed. In some cases there is justification for the assumption made, in most cases, however, there is a considerable range of possible values. By examination of the textures it was possible to fix approximately either an upper or lower limit of the critical shear stress ratio, but seldom both.

C. DEFORMATION BY SLIP

The hexagonal metals subjected to critical study have been found to slip in the $\{0001\}\langle 11\bar{2}0 \rangle$ system (58). This system will tend to give a tension texture of the type $[11\bar{2}0]$. Examination of the wire texture of titanium (59) shows titanium to have a strong $[10\bar{1}0]$ texture. A preliminary report on the plastic flow of titanium (60) shows slip in titanium to occur on both the $\{10\bar{1}0\}$ and $\{10\bar{1}1\}$ planes. These tests have not yet led to a determination of the slip direction. Since the slip direction is usually retained in other metals which exhibit slip on several planes, a $\langle 11\bar{2}0 \rangle$ slip direction is assumed. Their results showed no evidence of $\{0001\}\langle 11\bar{2}0 \rangle$ slip but at the low reduction nec-

(58) C. S. Barrett, The Structure of Metals, (New York: McGraw-Hill Book Company, 1943) p. 289

(59) M. K. Yen, Interim report to Watertown Arsenal. WHL 401/14-4, March 20, 1950

(60) Rosi, Dube, and Alexander, loc. cit.

essary for location of slip elements by the trace method this mode of slip may be relatively inactive. As will be shown later, $\{0001\}$ slip is essential in the explanation of the compression and rolling textures. The resolved shear stress contour diagram for each of these three slip systems is developed and the resulting tension and compression textures derived. Finally, the three slip systems are combined to give a tension and compression texture that agrees as much as possible with the observed texture.

$\{0001\}\langle 11\bar{2}0 \rangle$ slip. Slip on the base planes is simplified by the existence of only one active slip plane. The resolved shear stress contour diagram is shown in Figure 23. At both the $[0001]$ point and the $[10\bar{1}0]$ - $[11\bar{2}0]$ edge the resolved shear stress is zero. The slip systems active in the $\{0001\}\langle 11\bar{2}0 \rangle$ system are given in Table VI.

The tension and compression rotations for single slip (marked by the number I) and duplex slip (marked by the number II) are shown in Figures 24 and 25. As is seen the tension rotations lead to a moderate $[11\bar{2}0]$ texture plus a spread of orientations along the $[11\bar{2}0]$ - $[10\bar{1}0]$ edge. Compression rotations lead to a strong $[0001]$ texture. After the material reaches a $[0001]$ position in compression or a position along the $[10\bar{1}0]$ - $[11\bar{2}0]$ edge in tension, no further slip can occur since the resolved shear stress is zero.

$\{10\bar{1}1\}\langle 11\bar{2}0 \rangle$ slip. The $\{10\bar{1}1\}\langle 11\bar{2}0 \rangle$ system contains

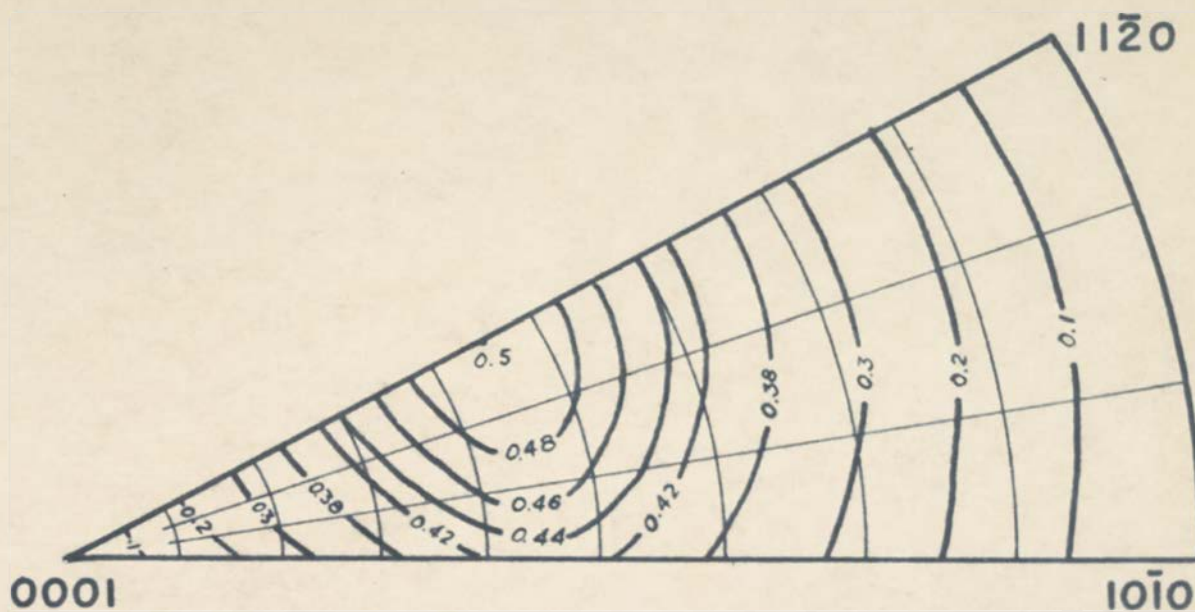


Figure 23. Resolved shear stress contours for {0001}<11 $\bar{2}$ 0> slip.

TABLE VI

ACTIVE SLIP ELEMENTS IN THE $\{0001\}\langle 11\bar{2}0 \rangle$ SLIP SYSTEM

Position	Active Slip System
$[0001]$	None--Fracture
$[10\bar{1}0]$	None--Fracture
$[11\bar{2}0]$	None--Fracture
$[0001]-[11\bar{2}0]$	$(0001)[11\bar{2}0]$
$[0001]-[10\bar{1}0]$	$(0001)[11\bar{2}0]; (0001)[2\bar{1}10]$
$[10\bar{1}0]-[11\bar{2}0]$	None--Fracture
$[0001]-[11\bar{2}0]-[10\bar{1}0]$	$(0001)[11\bar{2}0]$

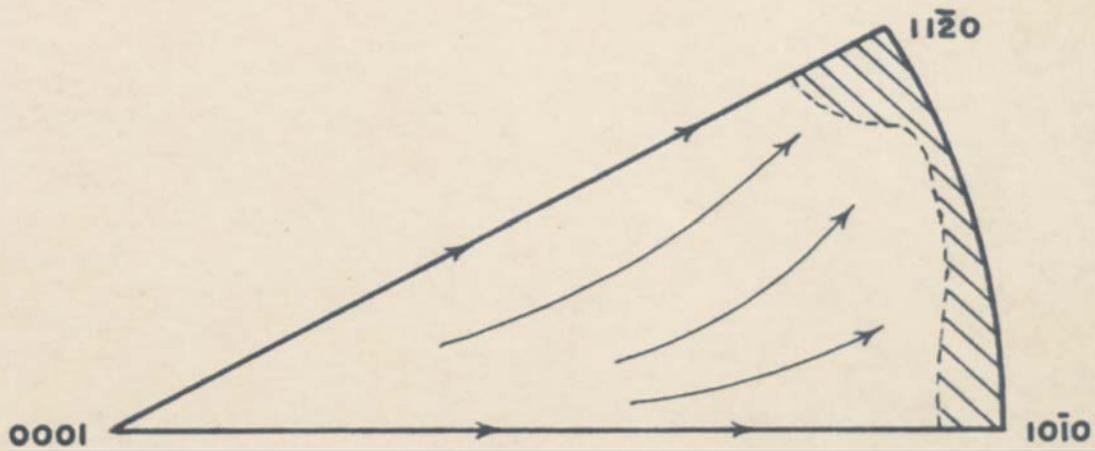
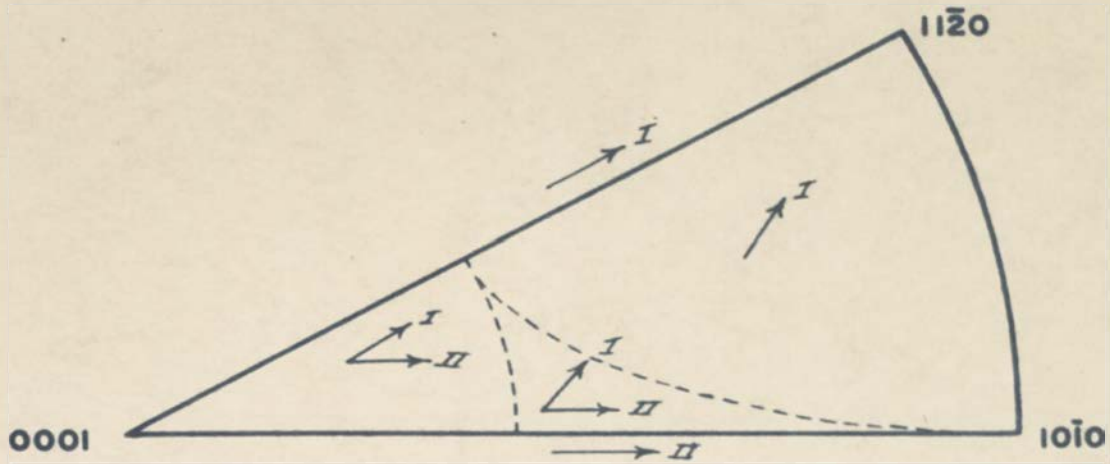


Figure 24. Tension slip rotations and tension texture resulting from $\{0001\}\langle 11\bar{2}0 \rangle$ slip.

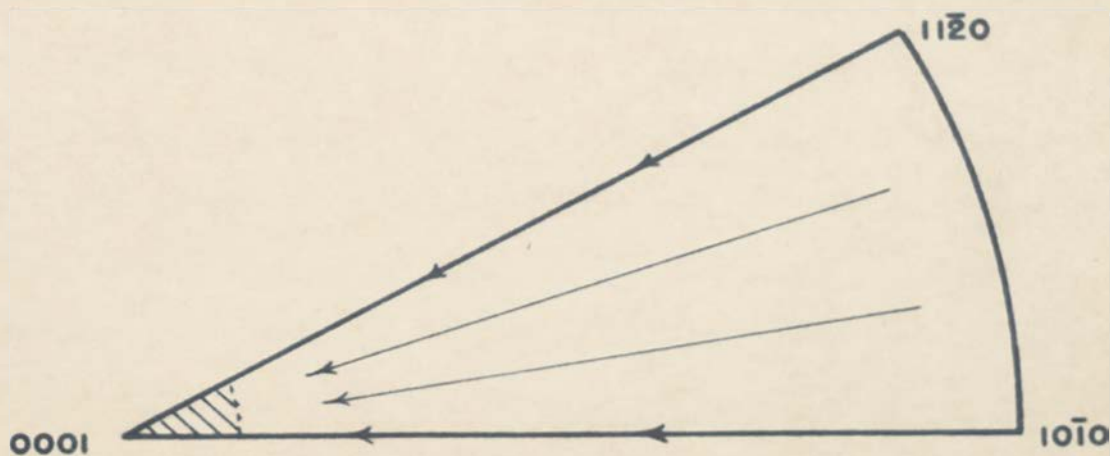
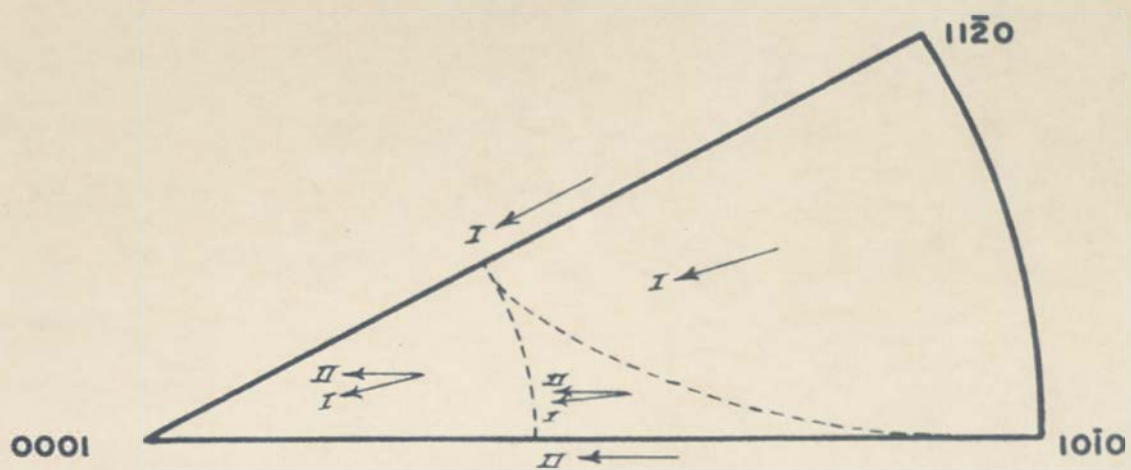


Figure 25. Compression slip rotations and compression texture resulting from $\{0001\}\langle 11\bar{2}0 \rangle$ slip.

six slip planes each of which has two possible slip directions. The resolved shear stress diagram for this system is shown in Figure 26. This diagram is more complicated than that for $\{0001\}$ slip since two different slip systems are active within the unit stereographic triangle. In addition, points B, $[11\bar{2}0]$, and $[10\bar{1}0]$ each support multiple slip in four slip systems. The active slip systems are given in Table VII.

The tension rotations and the resulting tension texture for $\{10\bar{1}1\}$ slip are given in Figure 27. Due to the unsymmetrical position of the slip planes at point B, multiple slip rotation, marked with the letter M, occurs. Examination of the tension rotations shows a strong $[10\bar{1}0]$ texture plus a weak $[11\bar{2}0]$ texture. Those orientations along the $[11\bar{2}0]$ - $[0001]$ line have a strong probability of rotation by duplex slip to the $[11\bar{2}0]$ point where they will be stable.

In the compression rotations, Figure 28, there exist a number of possible end positions. Duplex slip along the $[11\bar{2}0]$ -B edge will cause rotation of the stress axis toward the great circle joining the two active slip plane normals. This will give a strong preferred orientation at approximately thirty-two degrees from the $[11\bar{2}0]$ point. Since single slip will rotate most of the A-B- $[11\bar{2}0]$ - $[10\bar{1}0]$ region to the $[11\bar{2}0]$ -B edge, the concentration at thirty-two degrees should be the main texture in the $\{10\bar{1}1\}$ slip system. Subsidiary textures are probable at the points

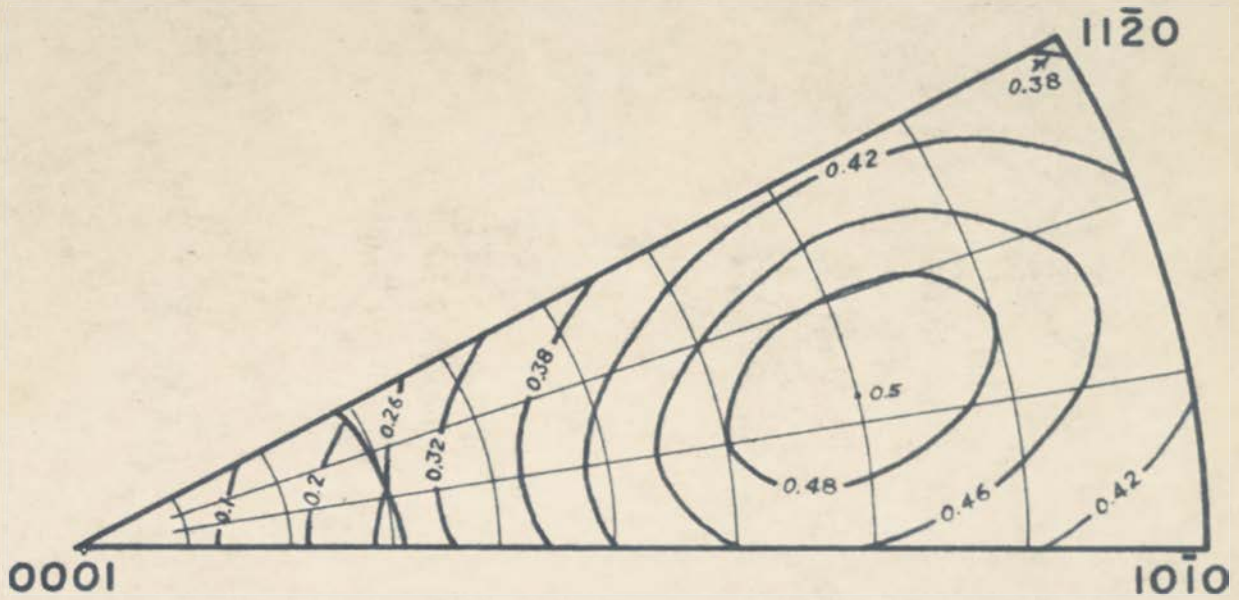


Figure 26. Resolved shear stress contours for $\{10\bar{1}1\}\langle 11\bar{2}0\rangle$ slip.

TABLE VII

ACTIVE SLIP ELEMENTS IN THE $\{10\bar{1}1\}\langle 11\bar{2}0\rangle$ SLIP SYSTEM

Position	Active Slip System
$[0001]$ ✓	None--Fracture
$[10\bar{1}0]$ ✓	$(01\bar{1}1)[2\bar{1}\bar{1}0]$; $(1\bar{1}01)[11\bar{2}0]$; $(01\bar{1}\bar{1})[2\bar{1}\bar{1}0]$; $(1\bar{1}01)[11\bar{2}0]$
$[11\bar{2}0]$ ✓	$(01\bar{1}1)[2\bar{1}\bar{1}0]$; $(10\bar{1}1)[\bar{1}2\bar{1}0]$; $(01\bar{1}\bar{1})[2\bar{1}\bar{1}0]$; $(10\bar{1}\bar{1})[\bar{1}2\bar{1}0]$
A ✓	$(01\bar{1}1)[2\bar{1}\bar{1}0]$; $(1\bar{1}01)[11\bar{2}0]$
B ✓	$(01\bar{1}1)[2\bar{1}\bar{1}0]$; $(10\bar{1}1)[\bar{1}2\bar{1}0]$; $(1\bar{1}01)[11\bar{2}0]$; $(1\bar{1}01)[11\bar{2}0]$
$[0001]$ -A- $[10\bar{1}0]$ ✓	$(01\bar{1}1)[2\bar{1}\bar{1}0]$; $(1\bar{1}01)[11\bar{2}0]$
$[11\bar{2}0]$ -B ✓	$(01\bar{1}1)[2\bar{1}\bar{1}0]$; $(10\bar{1}1)[\bar{1}2\bar{1}0]$
$[0001]$ -B ✓	$(1\bar{1}01)[11\bar{2}0]$; $(1\bar{1}01)[11\bar{2}0]$
$[10\bar{1}0]$ - $[11\bar{2}0]$ ✓	$(01\bar{1}1)[2\bar{1}\bar{1}0]$; $(01\bar{1}\bar{1})[2\bar{1}\bar{1}0]$
A-B ✓	$(01\bar{1}1)[2\bar{1}\bar{1}0]$; $(1\bar{1}01)[11\bar{2}0]$
$[0001]$ -A-B ✓	$(1\bar{1}01)[11\bar{2}0]$
A-B- $[11\bar{2}0]$ - $[10\bar{1}0]$	$(01\bar{1}1)[2\bar{1}\bar{1}0]$

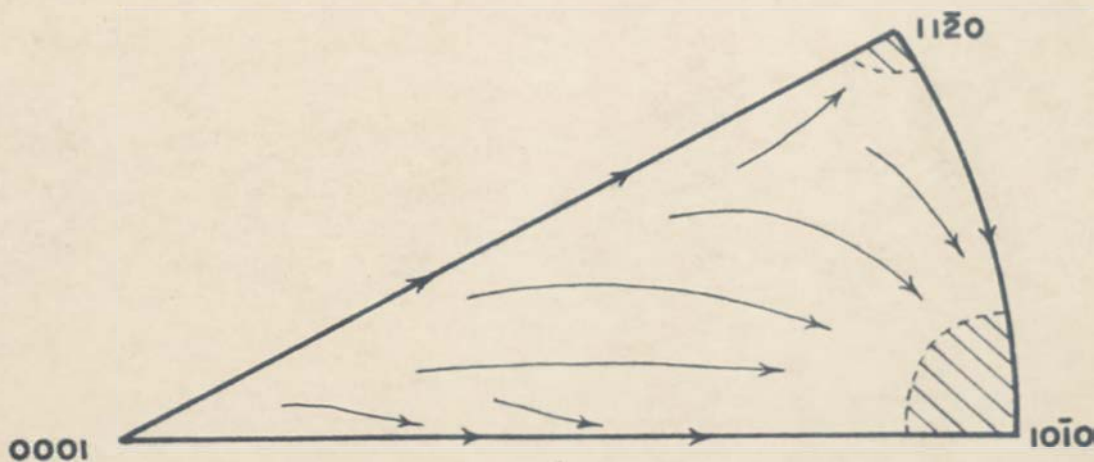
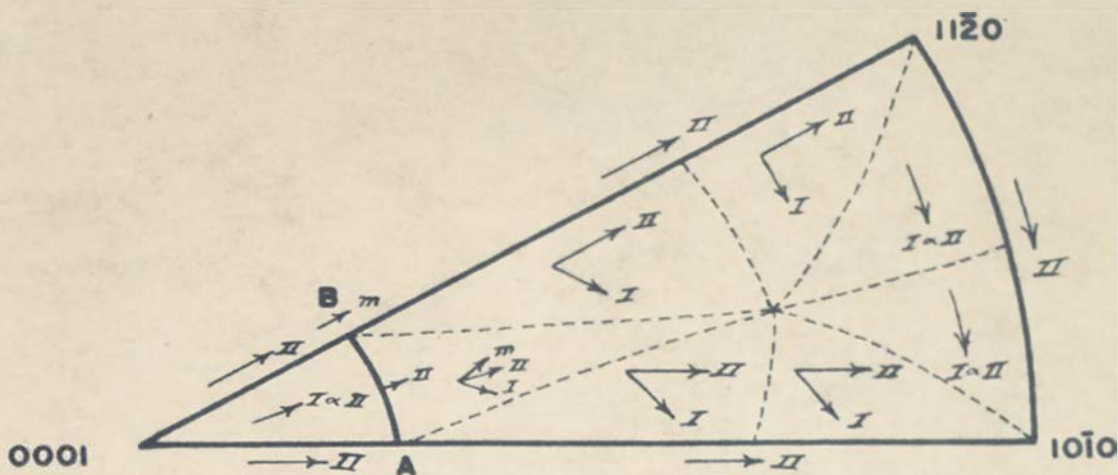


Figure 27. Tension slip rotations and tension texture resulting from $\{10\bar{1}1\}\langle 11\bar{2}0\rangle$ slip.

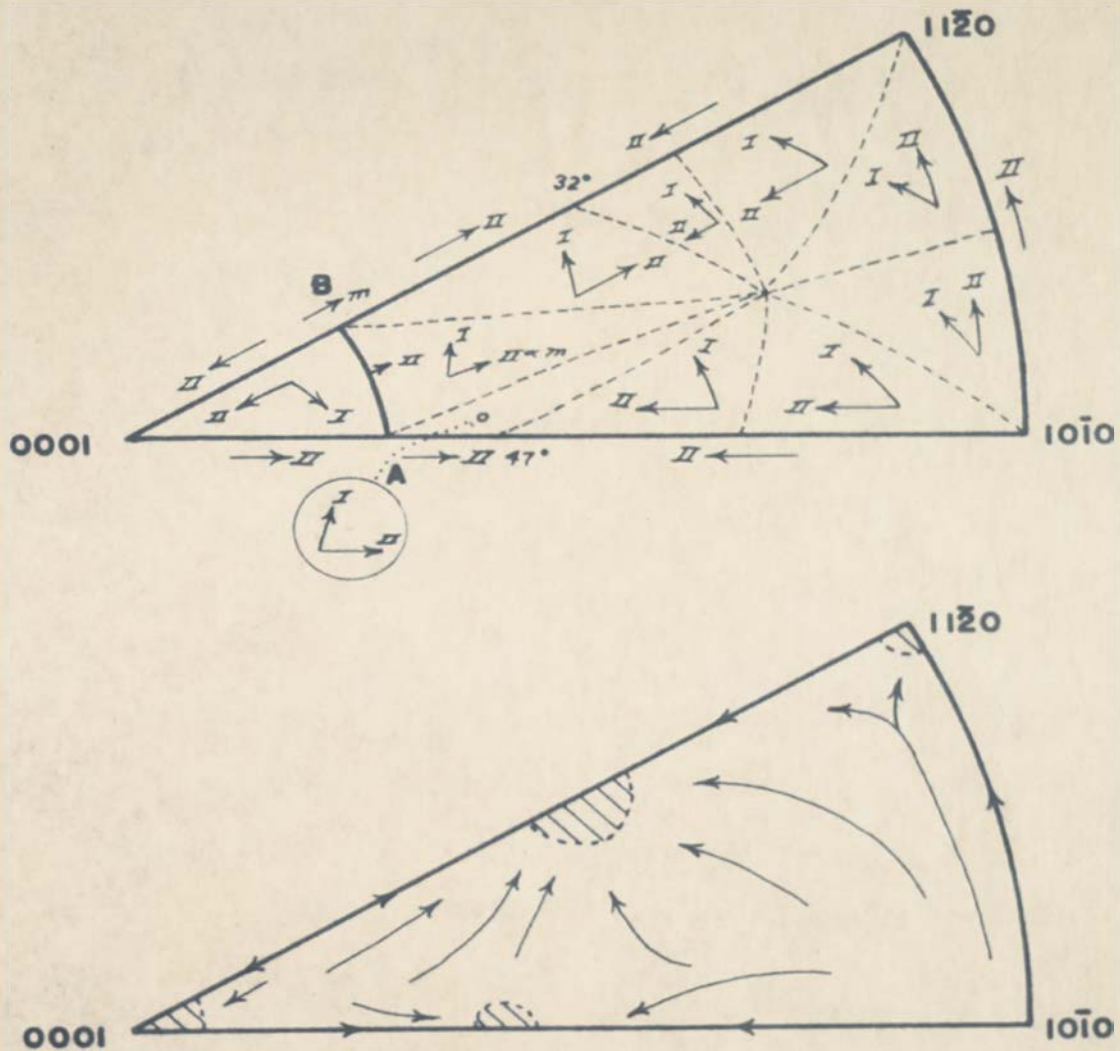


Figure 28. Compression slip rotations and compression texture resulting from $\{10\bar{1}1\}\langle 11\bar{2}0\rangle$ slip.

indicated in Figure 28.

$\{10\bar{1}0\}\langle 11\bar{2}0\rangle$ slip. This slip system is symmetrical about the midpoint between the $[10\bar{1}0]$ and $[11\bar{2}0]$ points as is shown in Figure 29. The active slip systems are given in Table VIII.

The tension and compression rotations are shown in Figures 30 and 31. The tension texture will be primarily $[10\bar{1}0]$ with some $[11\bar{2}0]$. The compression texture will be primarily $[11\bar{2}0]$ with some $[10\bar{1}0]$.

Combined slip system. Before the three slip systems are combined it is necessary to consider the experimental data. The tension texture of titanium has been shown to be primarily $[10\bar{1}0]$. Thus either $\{10\bar{1}0\}$ or $\{10\bar{1}1\}$ slip must predominate near the $[10\bar{1}0]$ - $[11\bar{2}0]$ edge. The compression texture has been shown to have a maximum in the 0001 pole figure thirty degrees from the axis of compression. The angle between this maximum and the compression axis decreased with increased reduction. A slight tendency for the compression axis to be on the $[0001]$ - $[11\bar{2}0]$ edge was also noticed. Since $\{10\bar{1}0\}$ slip can not produce rotation toward $[0001]$ in compression and since $\{10\bar{1}1\}$ slip tends to produce a 0001 maximum fifty-eight degrees from the axis of compression (see Figure 28), $\{0001\}$ slip must be active at least to a point within thirty-two degrees of the $[11\bar{2}0]$ point along the $[0001]$ - $[11\bar{2}0]$ edge.

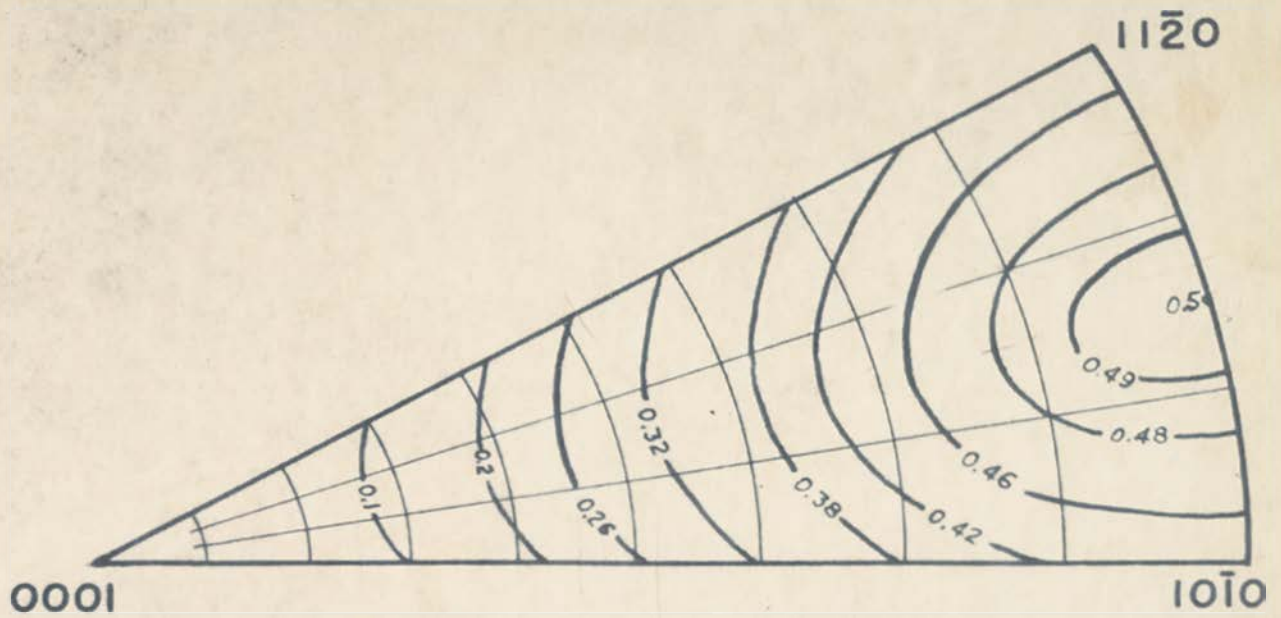


Figure 29. Resolved shear stress contours for $\{10\bar{1}0\} \langle 11\bar{2}0 \rangle$ slip.

TABLE VIII

ACTIVE SLIP ELEMENTS IN THE $\{10\bar{1}0\}\langle 11\bar{2}0\rangle$ SLIP SYSTEM

Position	Active Slip System
$[0001]$	None--Fracture
$[10\bar{1}0]$	$(01\bar{1}0)[2\bar{1}\bar{1}0]$; $(1\bar{1}00)[11\bar{2}0]$
$[11\bar{2}0]$	$(01\bar{1}0)[2\bar{1}\bar{1}0]$; $(10\bar{1}0)[\bar{1}2\bar{1}0]$
$[0001] - [11\bar{2}0]$	$(01\bar{1}0)[2\bar{1}\bar{1}0]$; $(10\bar{1}0)[\bar{1}2\bar{1}0]$
$[0001] - [10\bar{1}0]$	$(01\bar{1}0)[2\bar{1}\bar{1}0]$; $(1\bar{1}00)[11\bar{2}0]$
$[10\bar{1}0] - [11\bar{2}0]$	$(01\bar{1}0)[2\bar{1}\bar{1}0]$
$[0001] - [10\bar{1}0] - [11\bar{2}0]$	$(01\bar{1}0)[2\bar{1}\bar{1}0]$

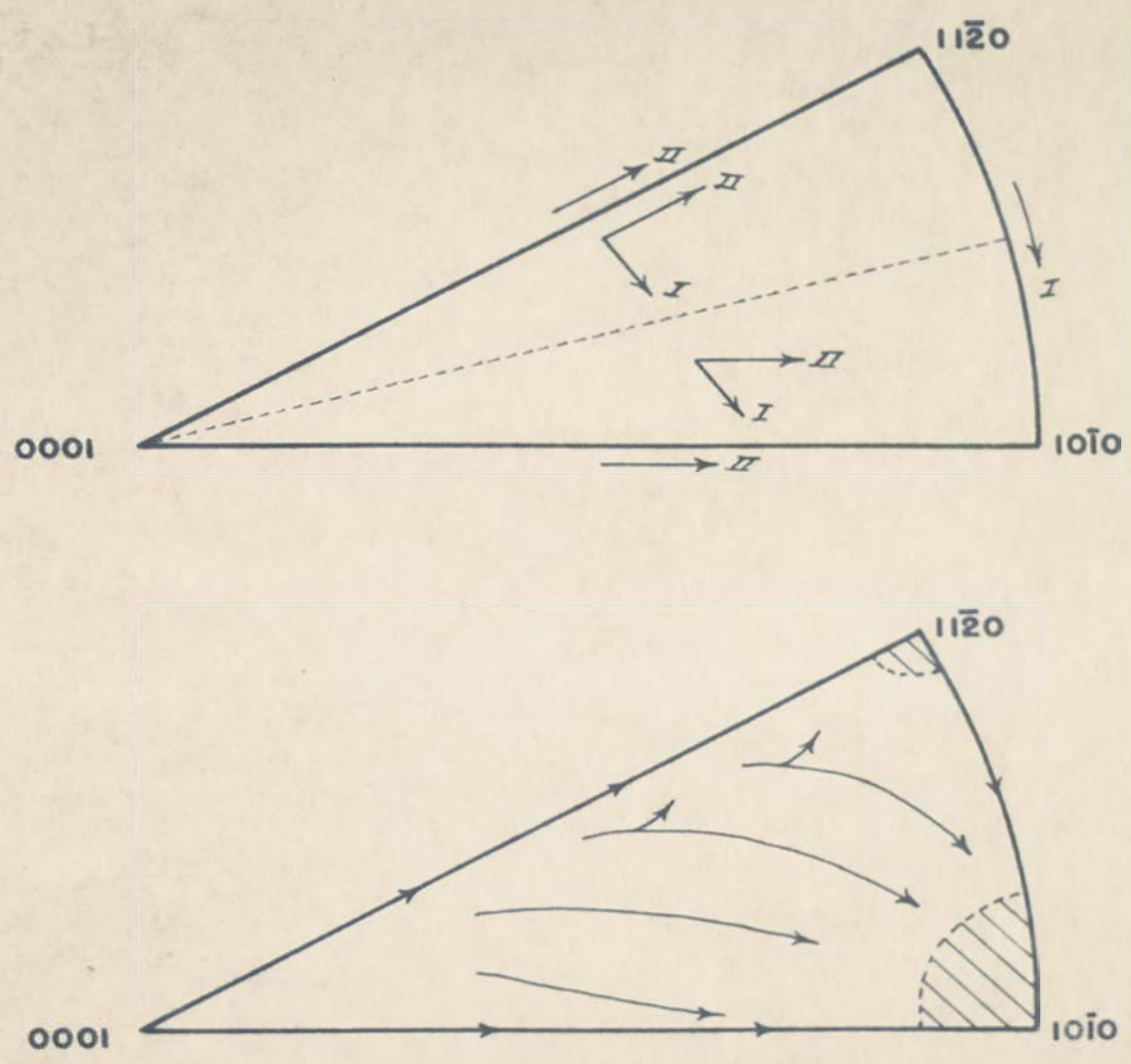


Figure 30. Tension slip rotations and tension texture resulting from $\{10\bar{1}0\}\langle 11\bar{2}0\rangle$ slip.

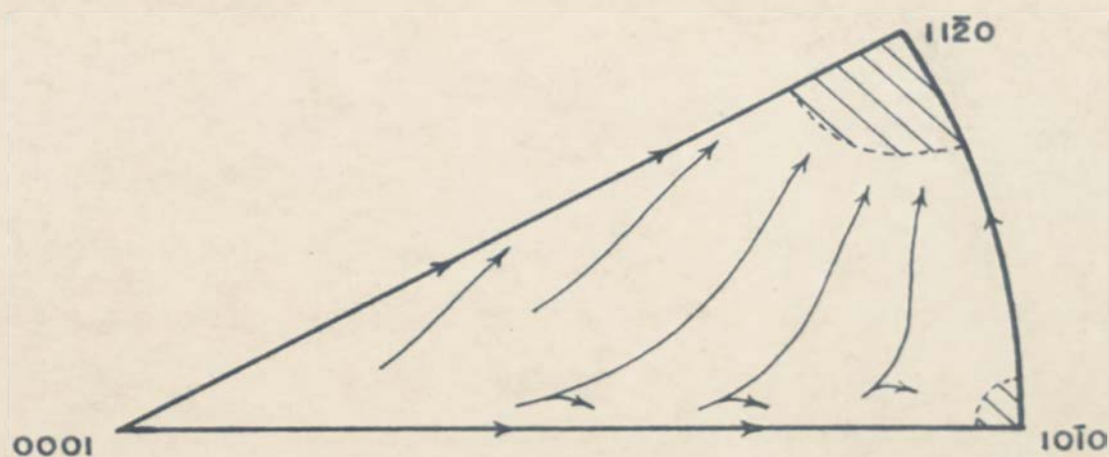
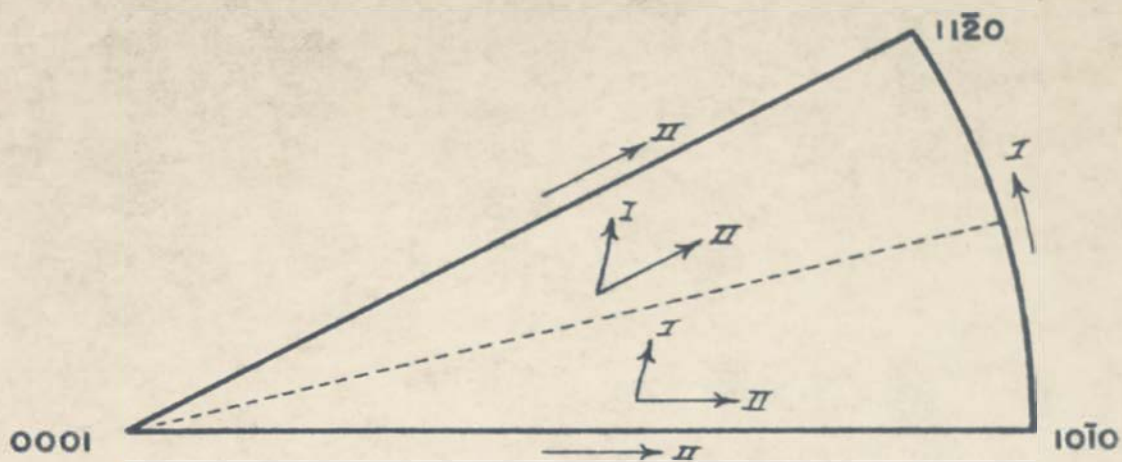
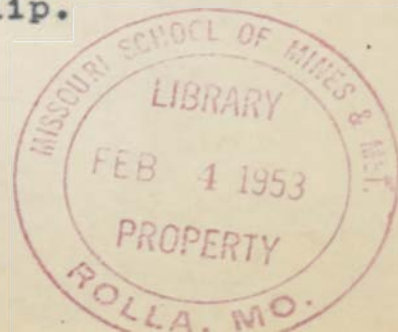


Figure 31. Compression slip rotations and compression texture resulting from $\{10\bar{1}0\}\langle 11\bar{2}0\rangle$ slip.



81370

The determination of slip elements of titanium (61) indicated that $\{0001\}$ slip was absent and $\{10\bar{1}0\}$ slip was the primary mechanism of slip. Because of these results the $\{0001\}$ - $\{10\bar{1}1\}$ slip boundary was adjusted so that the critical shear stress for $\{0001\}$ slip was as large with respect to the critical shear stress for $\{10\bar{1}1\}$ slip as possible without allowing $\{10\bar{1}1\}$ slip to form the maximum along the $[0001]$ - $[11\bar{2}0]$ edge thirty-two degrees from $[11\bar{2}0]$. This was accomplished by placing the boundary between the two systems thirty degrees from $[11\bar{2}0]$. Equation number one was used for this calculation and the following ratio of the critical shear stresses was obtained,

$$\tau_{s0001} = 1.1 \tau_{s10\bar{1}1} \quad 3.$$

Although the results of the above mentioned determination of slip elements in titanium indicated that $\{10\bar{1}0\}$ slip predominates at low reductions, the lack of appreciable $[11\bar{2}0]$ compression texture at higher reductions (see Chapter V) indicates that it is relatively unimportant or possibly completely absent at high reductions. For the purpose of this development the $\{10\bar{1}0\}$ - $\{10\bar{1}1\}$ slip boundary was calculated assuming that it crossed the $[0001]$ - $[11\bar{2}0]$ edge five degrees from the $[11\bar{2}0]$. This resulted in a ratio of shear stresses of,

$$\tau_{s10\bar{1}0} = 1.078 \tau_{s10\bar{1}1} \quad 4.$$

(61) Rosi, Dube, and Alexander, loc. cit.

The assumption that $\{10\bar{1}0\}$ slip is occurring is unnecessary at high reductions but it is included so that its effect at lower reductions may be considered.

Combining equations three and four gives the following relationship between the critical shear stresses for slip on the three slip systems,

$$\tau_{s0001} = 1.1 \tau_{s10\bar{1}1} = 1.02 \tau_{s10\bar{1}0} \quad 5.$$

The tension and compression textures resulting from the assumption that the above ratios of critical shear stress are correct are shown in Figures 32 and 33. The active slip systems are given in Table IX.

Examination of the tension rotations and the resulting tension texture given in Figure 32 shows that the texture will be predominately $[10\bar{1}0]$. A weak $[11\bar{2}0]$ texture is also evident.

The compression rotations and the compression texture as given in Figure 33 show a predominate 0001 texture plus a weak secondary $[11\bar{2}0]$ texture. Also of interest is the noticeable increase in density along the $[0001]$ - $[11\bar{2}0]$ edge which is the preferred route of rotation to the $[0001]$ position. Although the slip system developed here gives the desired rotation tendency for the observed compression texture, the maximum thirty degrees from $[0001]$ is not developed and must be a result of mechanical twinning.

TABLE IX

ACTIVE SLIP ELEMENTS IN THE COMBINED SLIP SYSTEM

Position	Active Slip System
[0001]	None--Fracture
[10 $\bar{1}0$]	(01 $\bar{1}0$)[2 $\bar{1}\bar{1}0$]; (1 $\bar{1}00$)[11 $\bar{2}0$]
[11 $\bar{2}0$]	(01 $\bar{1}0$)[2 $\bar{1}\bar{1}0$]; (10 $\bar{1}0$)[12 $\bar{1}0$]
W	(0001)[11 $\bar{2}0$]; (0001)[2 $\bar{1}\bar{1}0$]; (01 $\bar{1}1$)[2 $\bar{1}\bar{1}0$]; (1 $\bar{1}01$)[11 $\bar{2}0$]
X	(0001)[11 $\bar{2}0$]; (01 $\bar{1}1$)[2 $\bar{1}\bar{1}0$]; (10 $\bar{1}1$)[12 $\bar{1}0$]
Y	(01 $\bar{1}1$)[2 $\bar{1}\bar{1}0$]; (1 $\bar{1}01$)[11 $\bar{2}0$]; (01 $\bar{1}0$)[2 $\bar{1}\bar{1}0$]; (1 $\bar{1}00$)[11 $\bar{2}0$]
Z	(01 $\bar{1}1$)[2 $\bar{1}\bar{1}0$]; (10 $\bar{1}1$)[12 $\bar{1}0$]; (01 $\bar{1}0$)[2 $\bar{1}\bar{1}0$]; (10 $\bar{1}0$)[12 $\bar{1}0$]
[0001]-W	(0001)[11 $\bar{2}0$]; (0001)[2 $\bar{1}\bar{1}0$]
[0001]-X	(0001)[11 $\bar{2}0$]
W-X	(0001)[11 $\bar{2}0$]; (01 $\bar{1}1$)[2 $\bar{1}\bar{1}0$]
W-Y	(01 $\bar{1}1$)[2 $\bar{1}\bar{1}0$]; (1 $\bar{1}01$)[11 $\bar{2}0$]
X-Z	(01 $\bar{1}1$)[2 $\bar{1}\bar{1}0$]; (10 $\bar{1}1$)[12 $\bar{1}0$]
Y-Z	(01 $\bar{1}1$)[2 $\bar{1}\bar{1}0$]; (01 $\bar{1}0$)[2 $\bar{1}\bar{1}0$]
[10 $\bar{1}0$]-Y	(01 $\bar{1}0$)[2 $\bar{1}\bar{1}0$]; (1 $\bar{1}00$)[11 $\bar{2}0$]
[11 $\bar{2}0$]-Z	(01 $\bar{1}0$)[2 $\bar{1}\bar{1}0$]; (10 $\bar{1}0$)[12 $\bar{1}0$]
[10 $\bar{1}0$]-[11 $\bar{2}0$]	(01 $\bar{1}0$)[2 $\bar{1}\bar{1}0$]
[0001]-W-X	(0001)[11 $\bar{2}0$]
W-X-Z-Y	(01 $\bar{1}1$)[2 $\bar{1}\bar{1}0$]
Y-Z-[11 $\bar{2}0$]-[10 $\bar{1}0$]	(01 $\bar{1}0$)[2 $\bar{1}\bar{1}0$]

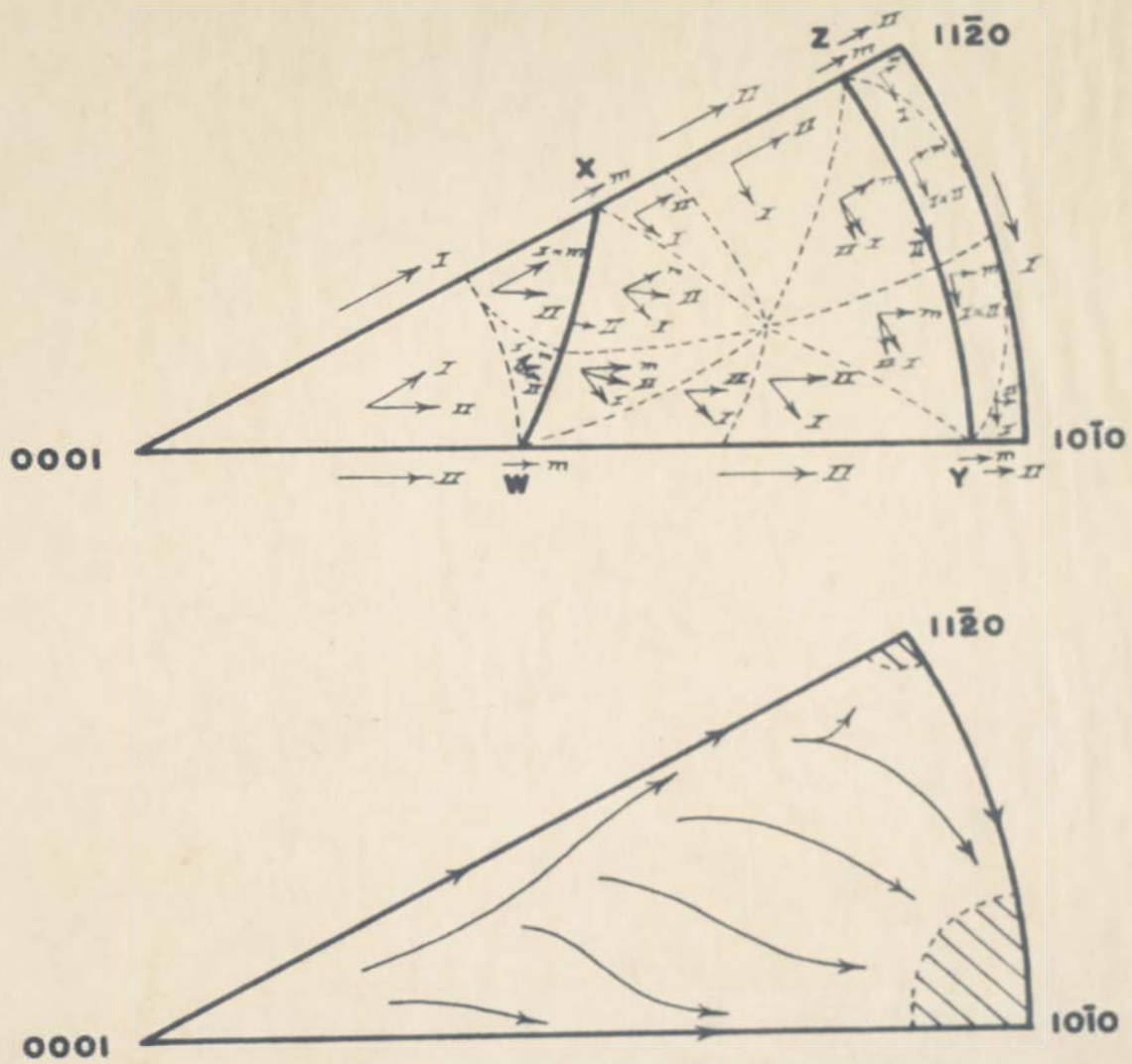


Figure 32. Tension slip rotations and tension texture resulting from the combined slip system.

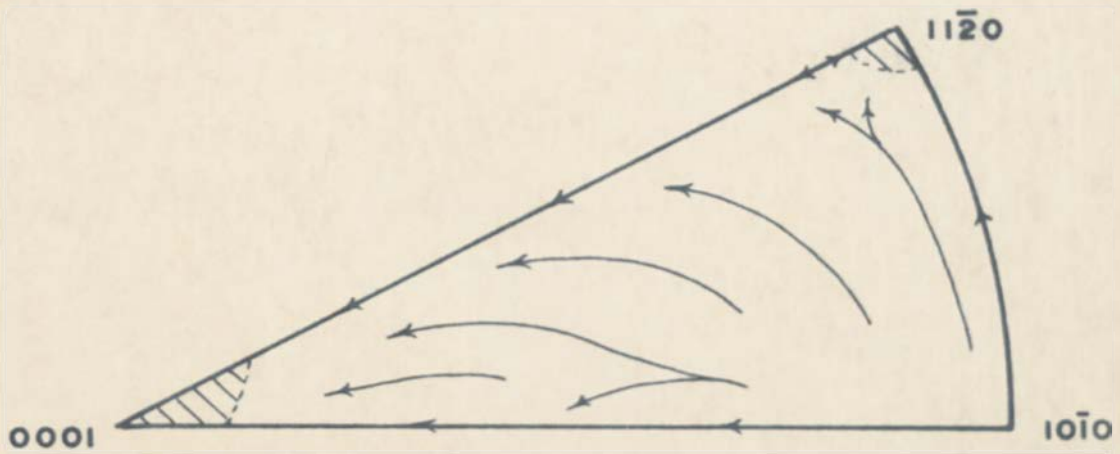
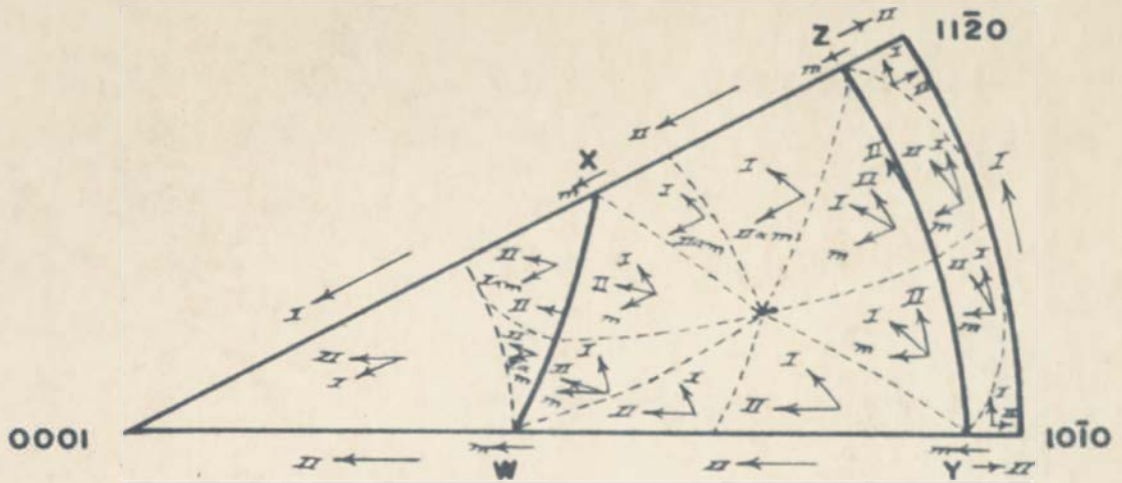


Figure 33. Compression slip rotations and compression texture resulting from the combined slip system.

D. DEFORMATION BY TWINNING

Hexagonal close-packed metals twin most easily on the $\{10\bar{1}2\}$ planes. It has been shown (62) that metals with a c/a ratio of less than 1.732 will not twin by $\{10\bar{1}2\}$ twinning when the axis of compression is along the c axis of the unit cell. Thus the minimum near $[0001]$ noted in the 0001 pole figure for compressed and for cold rolled titanium can not be the result of twinning on the $\{10\bar{1}2\}$ planes.

To explain the minimum evident in the compression texture a new type of twinning must be assumed which can twin in compression from the $[0001]$ position. Several types of twinning can be visualized which will twin from this position. The $\{10\bar{1}1\}$ twinning reported in magnesium (63) would be an example. Similarly, both the $\{11\bar{2}1\}$ and $\{11\bar{2}2\}$ twinning reported in titanium (64) have the ability to twin from a $[0001]$ position in compression.

A comparison of the twinning shear angles, the angle between the diagonals of the twinned and untwinned unit cell, of $\{10\bar{1}2\}$, $\{11\bar{2}1\}$, and $\{11\bar{2}2\}$ twinning is given in Figure 34. It seems likely from inspection of this illustra-

(62) C. S. Barrett, "The crystallographic mechanisms of translation, twinning and banding." The Cold Working of Metals, (Cleveland: American Soc. for Metals, 1949), p. 84

(63) E. Schiebold and G. Siebel, "Studies of magnesium and magnesium alloys." Z. Physik, Vol 69, pp. 458-82, 1931

(64) Rees, Dube, and Alexander, loc. cit.

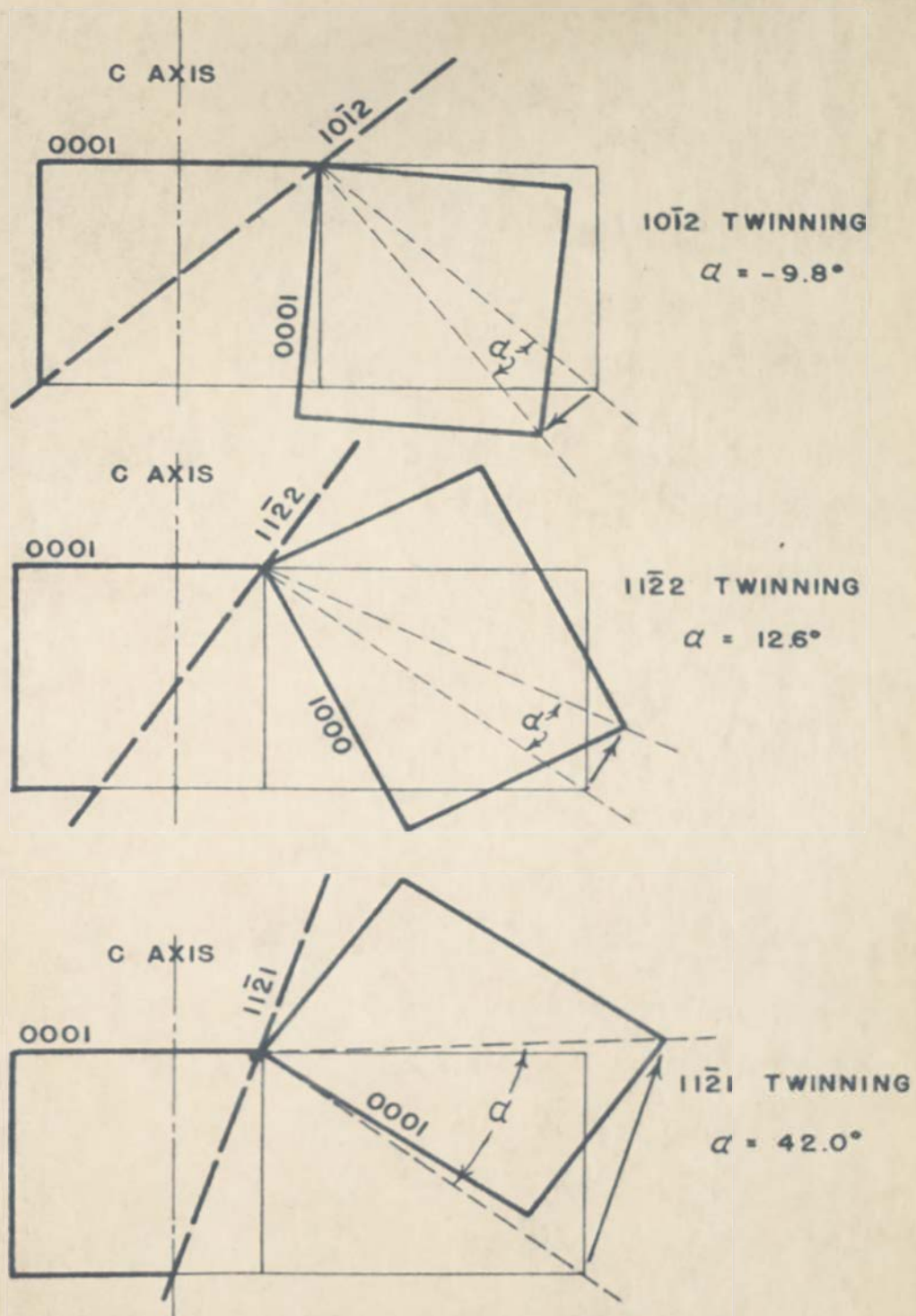


Figure 34. Twinning shear direction of twinning on $\{10\bar{1}2\}$, $\{11\bar{2}2\}$, and $\{11\bar{2}1\}$ planes of titanium.

tion that $\{11\bar{2}2\}$ twinning should occur much more readily than $\{11\bar{2}1\}$ twinning. Attempts to develop a satisfactory picture of the atom movements in $\{11\bar{2}1\}$ and $\{11\bar{2}2\}$ twinning such as has been done for $\{10\bar{1}2\}$ twinning (65) were unsuccessful.

For the purpose of this development of the twinning effects, the following assumptions were made: (1), $\{10\bar{1}2\}$ and $\{11\bar{2}2\}$ twinning are of about equal frequency and $\{11\bar{2}1\}$ twinning should be relatively rare, (2), the twinning shear stress of $\{11\bar{2}2\}$ twinning is in the direction shown in Figure 34, and the c axis, twin plane normal, and twinning shear direction are in the same plane, and (3), the critical shear stress for $\{10\bar{1}2\}$ twinning and $\{11\bar{2}2\}$ twinning are equal to the critical shear stress for $\{0001\}$ slip.

$\{10\bar{1}2\}$ twinning. For the purpose of calculation the assumption was made that the critical shear stress for twinning on the $\{10\bar{1}2\}$ planes was equal to the critical shear stress for slip on the $\{0001\}$ planes. Thus, from equation five,

$$\sigma_{t10\bar{1}2} = \sigma_{s0001} = 1.1 \sigma_{s10\bar{1}1} = 1.02 \sigma_{s10\bar{1}0} \quad \underline{6.}$$

The boundary between the slip and twinning areas were determined by use of the formulae,

$$\cos \gamma \cos \delta = n \cos \alpha \cos \lambda, \text{ in tension} \quad \underline{7.}$$

(65) Barrett, op. cit., pp. 78-86

$$\cos \gamma \cos \delta = -n \cos \alpha \cos \lambda, \text{ in compression } \underline{8.}$$

$$\text{where } n = C_t/C_s$$

The boundaries for twinning in both tension and compression based on the combined slip system shown in Figures 32 and 33 were calculated for all six of the possible $\{10\bar{1}2\}$ twinning systems. The results are given in Table X. The most favorable slip system is that which includes the most area of the unit stereographic triangle.

Each point in the twinning area will move the same angle beyond the twin plane normal as its initial angle from the twin plane normal. The twinning area, T, the active twin plane normal, marked by number, the new twinned orientation, T', and the new twinned orientation placed in the unit stereographic triangle, T^a, are shown in Figure 35.

It is seen that $\{10\bar{1}2\}$ twinning assists slip rotations by twinning toward the $[0001]$ in compression and toward the $[10\bar{1}0]$ - $[\bar{1}1\bar{2}0]$ edge in tension.

$\{11\bar{2}2\}$ twinning. The boundary conditions for $\{11\bar{2}2\}$ twinning were determined in the same manner as those for $\{10\bar{1}2\}$ twinning. In this case however, the signs of the two equations, 7 and 8, are reversed because of the change in the twinning shear direction (see Figure 34). The shear stress ratios were assumed to be,

$$C_{t11\bar{2}2} = C_{s0001} = 1.1 C_{s10\bar{1}1} = 1.02 C_{s10\bar{1}0} \quad \underline{9.}$$

The calculated positions of the boundaries for each of

TABLE X
INTERSECTIONS OF TWIN-SLIP BOUNDARIES FOR $\{10\bar{1}2\}$ TWINNING

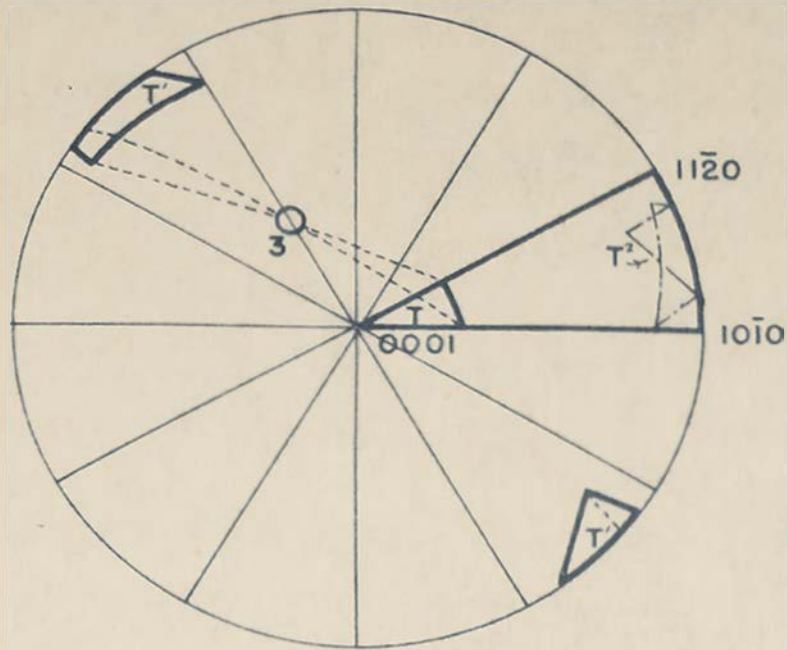
Twinning System	Tension	
	Angle from $[0001]$ along $[0001]-[10\bar{1}0]$	Angle from $[0001]$ along $[0001]-[11\bar{2}0]$
1	23°	22°
2	27°	22°
3	29° *	27° *
4	26°	24°
5	29°	24°
6	27°	27°

Twinning System	Compression		
	Angle from $[10\bar{1}0]$ along $[10\bar{1}0]-[0001]$	Angle from $[10\bar{1}0]$ along $[10\bar{1}0]-[11\bar{2}0]$	Angle from $[11\bar{2}0]$ along $[11\bar{2}0]-[0001]$
1	11° *	7° *	-
2	-	-	-
3	-	-	-
4	7°	7°	-
5	-	-	-
6	-	-	-

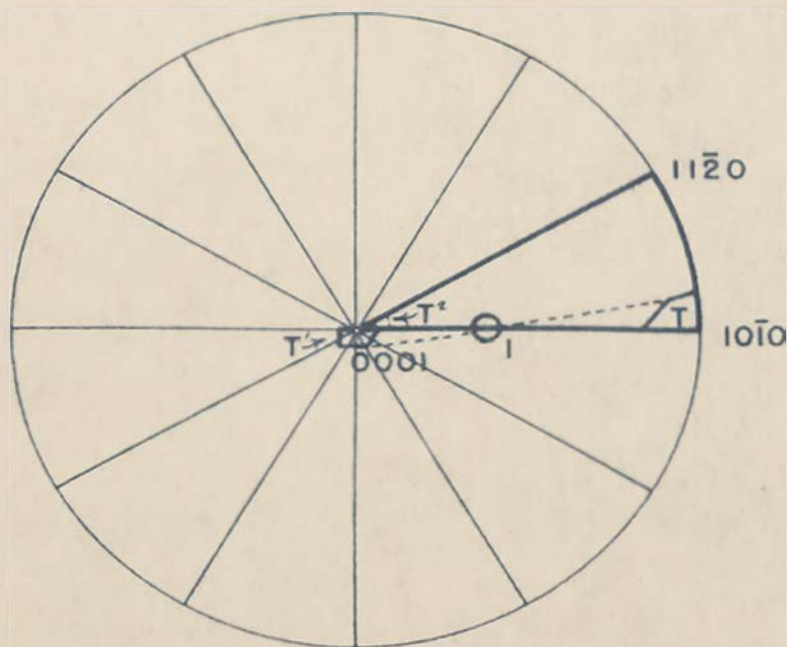
* Most favorable twinning system

These values calculated assuming $G_{t10\bar{1}2} = G_{s0001} = 1.1$

$G_{s10\bar{1}1} = 1.02 G_{s10\bar{1}0}$.



a. $\{10\bar{1}2\}$ twinning in tension



b. $\{10\bar{1}2\}$ twinning in compression

Figure 35. Reorientation resulting from $\{10\bar{1}2\}$ twinning from the combined slip system.

the six $\{11\bar{2}2\}$ twinning systems in tension and compression are given in Table XI.

The most favorable twinning system was determined in the same manner as before. The results of the twinning reorientations are given in Figure 36, using the same notations as in Figure 35. In this case, twinning opposes slip rotation in compression but in tension its only effect is to remove those poles in the subsidiary $[11\bar{2}0]$ texture.

$\{11\bar{2}1\}$ twinning. The geometrical analysis of the twinning shear shown in Figure 34 indicated that $\{11\bar{2}1\}$ twinning was much less likely to occur than $\{11\bar{2}2\}$ twinning. The magnitude of the twinning shear required for $\{11\bar{2}1\}$ twinning was over three times that required for $\{11\bar{2}2\}$ twinning. It should be noted that the method of prediction of the magnitude and direction of the twinning shear used in Figure 34 is purely geometrical. Future work on the mechanics of twinning may show this method of analysis to be in error. Thus, $\{11\bar{2}1\}$ rather than $\{11\bar{2}2\}$ twinning might actually be the more active twinning system. The only result of this change would be a slight readjustment of the critical shear stress ratios.

The agreement of the critical shear stress ratios predicted from the texture analysis (see equation nine) with the geometrically predicted twinning shears is good and strengthens the assumption that the geometrical methods

TABLE XI

INTERSECTIONS OF TWIN-SLIP BOUNDARIES FOR $\{11\bar{2}2\}$ TWINNING

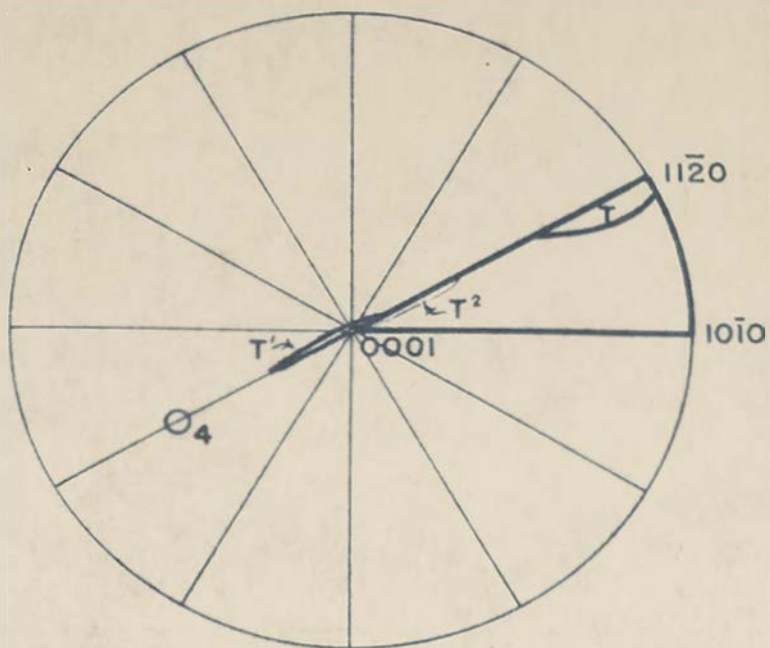
Twinning System	Tension	
	Angle from $[10\bar{1}0]$ along $[10\bar{1}0]-[0001]$	Angle from $[11\bar{2}0]$ along $[10\bar{1}0]-[11\bar{2}0]$ and $[11\bar{2}0]-[0001]$
1	-	1°
2	-	-
3	-	-
4	-	1° * 27° *
5	-	-
6	-	-

Twinning System	Compression	
	Angle from $[0001]$ along $[0001]-[10\bar{1}0]$	Angle from $[0001]$ along $[0001]-[11\bar{2}0]$
1	32° *	29° *
2	27°	28°
3	18°	19°
4	18°	16°
5	27°	19°
6	32°	28°

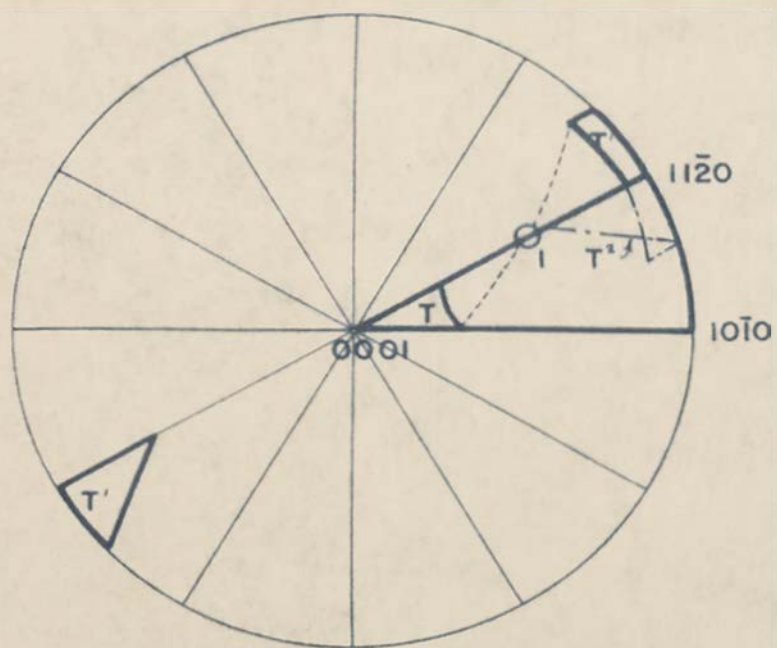
* Most favorable twinning system

These values calculated assuming $G_{t11\bar{2}2} = G_{s0001} = 1.1$

$G_{s10\bar{1}1} = 1.02 G_{s10\bar{1}0}$.



a. $\{11\bar{2}2\}$ twinning in tension



b. $\{11\bar{2}2\}$ twinning in compression

Figure 36. Reorientation resulting from $\{11\bar{2}2\}$ twinning from the combined slip system.

used in drawing Figure 34 are valid.

E. THE DEFORMATION TEXTURES OF TITANIUM

By use of the Calnan and Clews method, the known slip and twinning systems have been examined and the critical shear stress ratios necessary to give various phases of the observed textures calculated. These critical shear stress ratios made it possible to combine the three slip systems and two twinning systems considered and to consider their combined effect on the deformation process in titanium.

The tension texture of titanium. The results plotted in Figures 32, 35, and 36 for tension are combined in Figure 37. In this figure it is seen that $\{10\bar{1}2\}$ twinning aids in developing the $[10\bar{1}0]$ texture while $\{11\bar{2}2\}$ twinning prevents the formation of the subsidiary $[11\bar{2}0]$ texture. The net result of slip on three systems and twinning on two is a strong $[10\bar{1}0]$ tension texture. This texture should be developed early in the deformation process. As the critical shear stress on the $\{10\bar{1}0\}$ slip planes increases, the boundary between $\{10\bar{1}1\}$ and $\{10\bar{1}0\}$ slip moves toward the $[10\bar{1}0]$ - $[11\bar{2}0]$ edge. When the shear stress has increased until the two systems are equally favored at $[10\bar{1}0]$, when $\sigma_{s10\bar{1}1} = 0.878 \sigma_{s10\bar{1}0}$, there are six active and stable slip systems at $[10\bar{1}0]$. The $[10\bar{1}0]$ tension texture would therefore be expected to persist with no change until the mate-

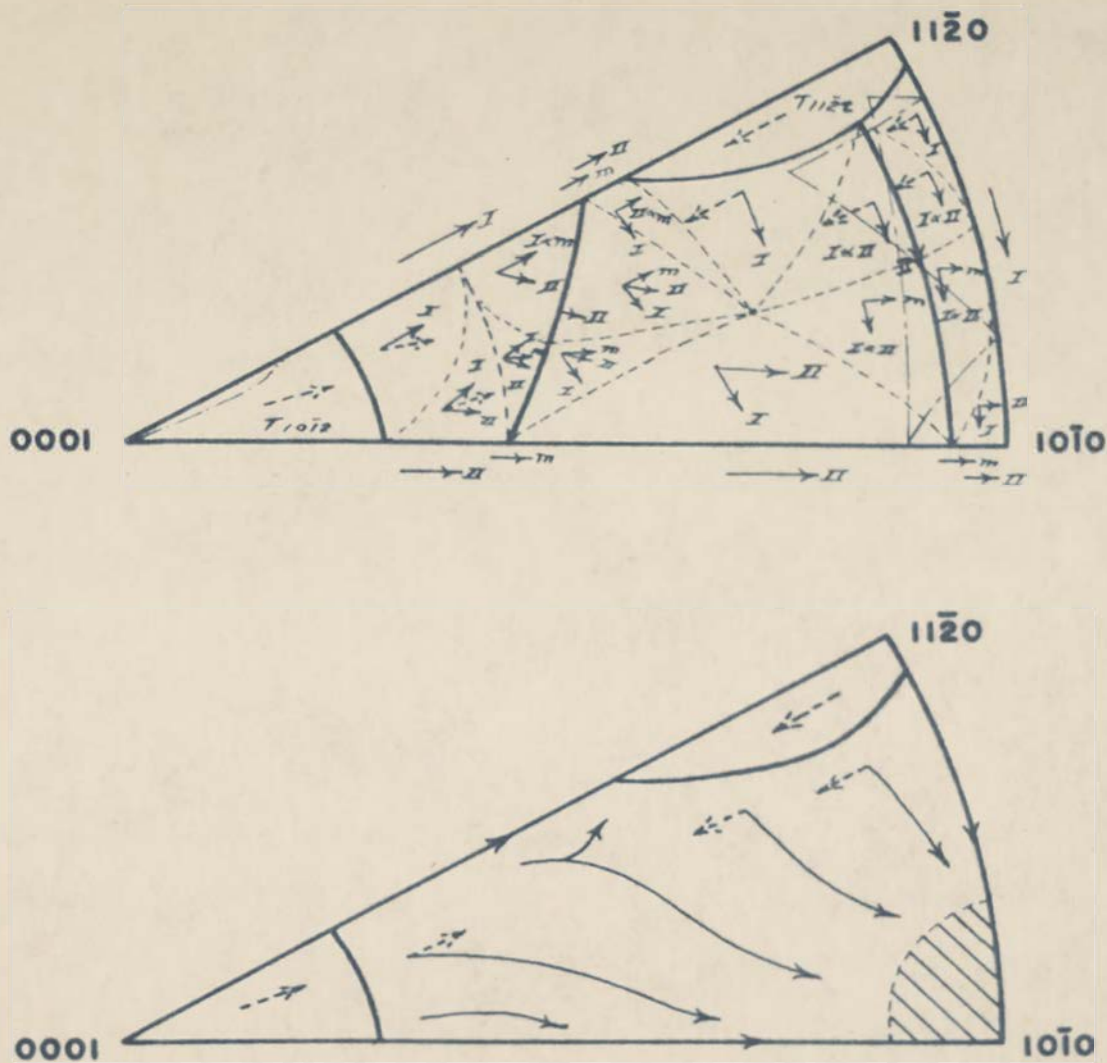


Figure 37. Tension texture resulting from combined slip on the $\{0001\}\langle 11\bar{2}0\rangle$, $\{10\bar{1}1\}\langle 11\bar{2}0\rangle$, and $\{10\bar{1}0\}\langle 11\bar{2}0\rangle$ slip systems and twinning from the $\{10\bar{1}2\}$ and $\{11\bar{2}2\}$ planes.

rial failed.

The compression texture of titanium. The data from Figures 33, 35, and 36 are combined in Figure 38. In this case $\{11\bar{2}2\}$ twinning is active in preventing the slip rotation from reaching the stable orientation. $\{10\bar{1}2\}$ twinning is of little importance in compression. As the slip rotations lead to the twinning region, the grains are twinned to a position near the $[11\bar{2}0]$ pole. Thus as deformation increases the slip rotations tend to be concentrated more completely along the $[11\bar{2}0]$ - $[0001]$ edge of the unit triangle. This accounts for the preferred orientation noticed in the $10\bar{1}0$ and $10\bar{1}1$ pole figures of compressed titanium (see Chapter V).

As the slip rotations lead toward the $[0001]$ position and the twinning reorientation leads away from this position, a spread of orientations from the slip-twinning boundary to the $[11\bar{2}0]$ position will occur. An equilibrium texture will arise near the slip-twinning boundary. This texture is seen in compression (Chapter V) and in cold rolling (Chapter VI). The decrease of the angle between the compression axis and the $[0001]$ with increased reduction may be attributed to a relative change in the ratio of the critical shear stress for $\{0001\}$ slip and $\{11\bar{2}2\}$ twinning such that the boundary between slip and twinning moves toward $[0001]$.

The lack of any appreciable $[11\bar{2}0]$ compression texture

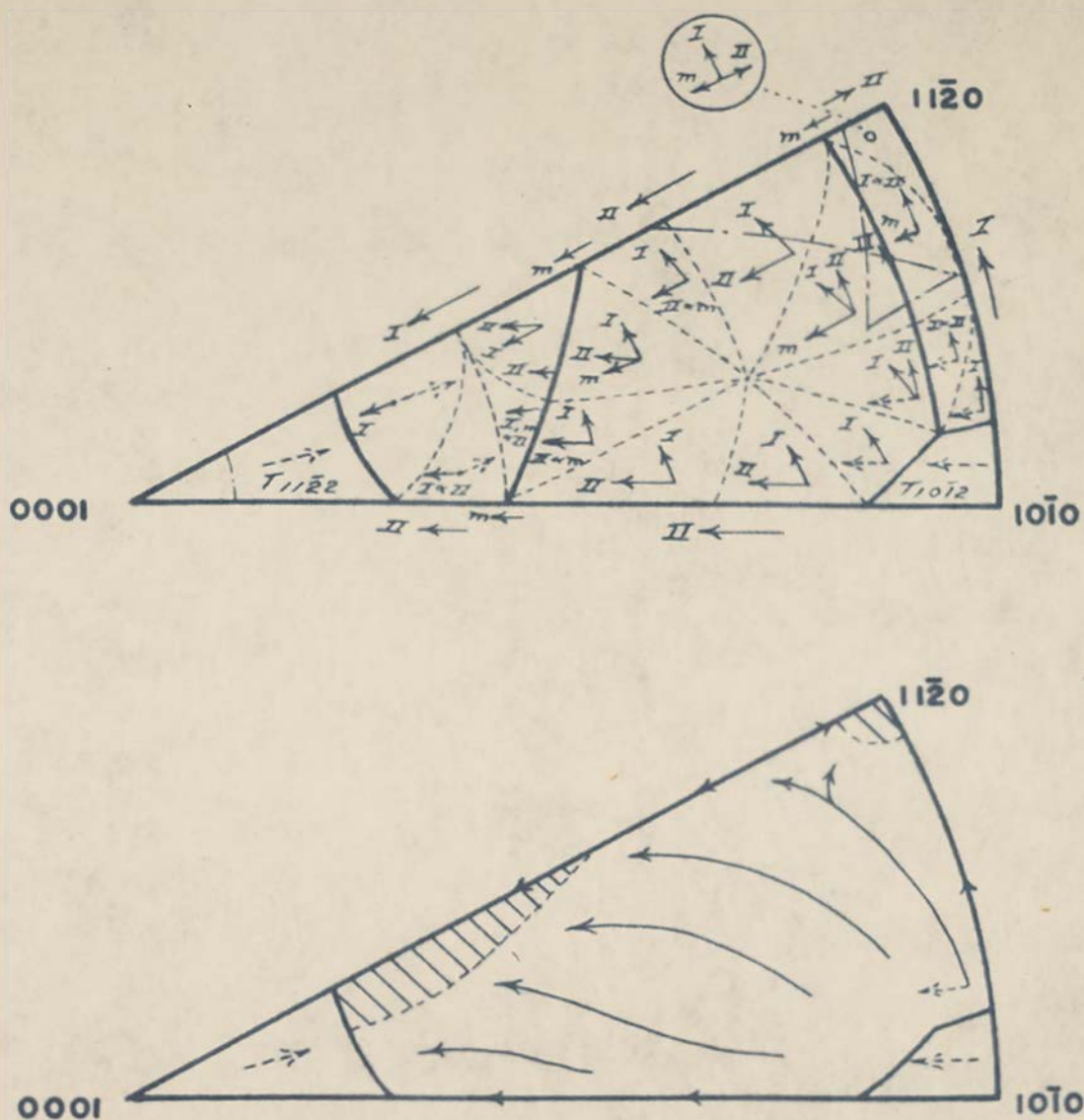


Figure 38. Compression texture resulting from combined slip on the $\{0001\}\langle 11\bar{2}0\rangle$, $\{10\bar{1}1\}\langle 11\bar{2}0\rangle$, and $\{10\bar{1}0\}\langle 11\bar{2}0\rangle$ slip systems and twinning from the $\{10\bar{1}2\}$ and $\{11\bar{2}2\}$ planes.

shows that $\{10\bar{1}0\}$ slip is probably completely absent at high reductions. The ability of the $\{10\bar{1}1\}$ slip system to trap the stress axis in the minimum occurring in the resolved shear stress diagram at $[11\bar{2}0]$ (see Figure 26) would be sufficient to account for the slight $[11\bar{2}0]$ texture apparent at high reductions.

The cold rolled texture of titanium. Cold rolling can be considered as tension in the rolling direction and compression on the rolling plane (66). In Figure 39 the compression texture is plotted in the unit stereographic triangle. The axis of compression lies somewhere along the line $[11\bar{2}0]$ - $[0001]$ between points N_1 and N_3 . Since the rolling direction is ninety degrees from the rolling plane normal, and thus from the compression axis, the rolling direction must lie on the great circle which lies ninety degrees from the compression axis. The great circles for the compression axes N_1 , N_2 , and N_3 are ABC, ADC, and A- $[0001]$ -C respectively. These circles intersect at point C which is a $\langle 10\bar{1}0 \rangle$ direction. Thus when the transverse plane contains a $\langle 11\bar{2}0 \rangle$ direction and the rolling direction is $\langle 10\bar{1}0 \rangle$ both the tension and compression texture are satisfied simultaneously.

(66) F. Wever, "Textures of metals after cold deformation." Trans. AIME, Vol 93, pp. 51-75, 1931

In Figure 40 the compression and tension rotations and the twinning reorientations are shown in a 0001 pole figure. If random initial orientation is assumed, the following tendencies are apparent. Since tension rotation tends to move a $\langle 10\bar{1}0 \rangle$ direction into the rolling direction, the 0001 poles should move to the transverse axis along the line of most rapid descent, a great circle passing through the rolling direction and the 0001 pole being considered. Compression rotations tend to move the 0001 poles toward the rolling plane normal. The tension and compression rotations are marked T and C in Figure 40. The resultant 0001 pole rotation is shown by the arrow marked R. Tension twinning from the $\{10\bar{1}2\}$ planes (Figure 35) will tend to remove all 0001 poles within approximately twenty-nine degrees of the rolling direction to a position near the transverse direction. Compression twinning from a region within thirty degrees of the rolling plane normal will twin the 0001 poles to a position near the circumference (Figure 36). Twinning reorientations are indicated by dashed arrows in Figure 40. Those poles falling within the $\{10\bar{1}2\}$ tension twinning area near the rolling direction will be twinned to the transverse direction depicting the area enclosed by the long dashes. As the resultant slip rotations tend to move the 0001 poles toward the transverse axis, and from there toward the rolling plane normal, an equilibrium state will gradually be established in which the 0001 poles rotate by compression

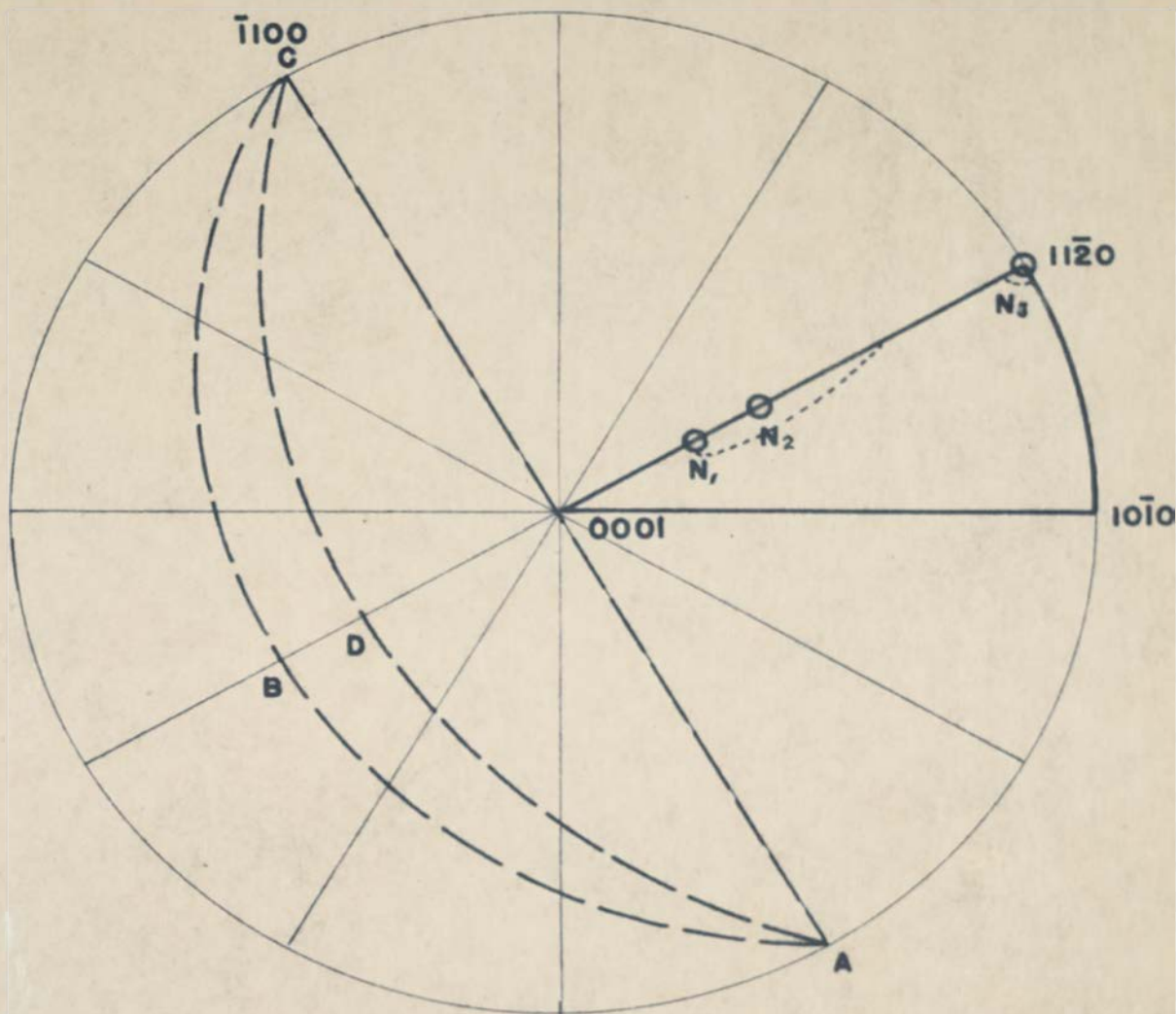


Figure 39. Stereographic plot of the compression texture of titanium. Great circles drawn ninety degrees from the compression axes (N_1 , N_2 , and N_3) intersect at a common point (C). Since this point is a $\langle 10\bar{1}0 \rangle$ direction both the compression and tension tendencies are satisfied.

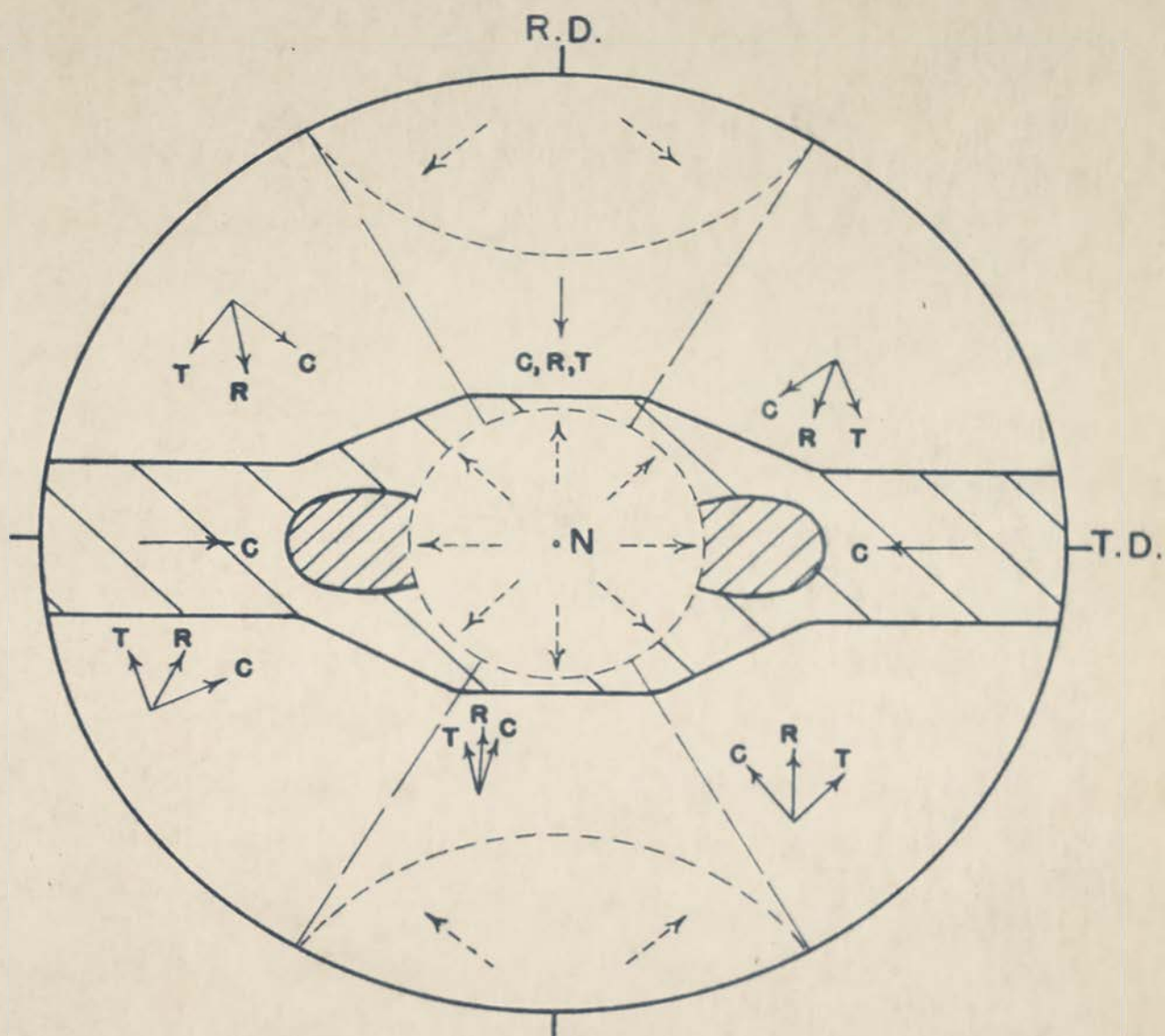


Figure 40. Form of the 0001 pole figure of titanium resulting from tension in the rolling direction and compression along the rolling plane normal.

toward the rolling plane normal and by twinning are removed to the transverse direction to again rotate toward the rolling plane normal. The resulting 0001 pole figure will have a shape such as that indicated in Figure 40.

This texture is seen to resemble the actual cold rolling texture determined in Chapter VI.

F. DISCUSSION

It should be emphasized that the agreement of the theoretically developed texture with that actually observed is the result of the choice of assumptions and does not indicate that the assumptions made are correct. The validity of the assumptions made can not be determined until more complete information is available on the actual modes of slip and twinning in titanium.

The method developed by Galnan and Clews is seen to be quite versatile allowing not only the prediction of the deformation texture when the modes of deformation are known but also the prediction of the modes of deformation when the deformation texture is known. The ability of their method to give an indication of the ratio of critical shear stresses among various systems may also prove of value as more accurate deformation textures are determined.

As an example of the latter point, consider the pole figures given in Figure 20, Chapter VI. The appearance of a pronounced maximum at the transverse direction in the

sample with the lower reduction in area and its absence at higher reduction in area is a strong indication that the $\{10\bar{1}0\}$ slip system becomes less favored as the deformation increases. Thus it must be assumed that the critical shear stress for $\{10\bar{1}0\}$ slip is increasing at a faster rate than that for $\{10\bar{1}1\}$ slip.

The second maximum at twenty degrees from the rolling plane normal in the rolling direction in commercial titanium sample number three (Figures 19 and 20, Chapter VI) may possibly be due to a similar change in critical shear stress ratio, in this case possibly due to an impurity present in the titanium lattice. Consideration of Figure 40 shows that if the critical shear stress for $\{10\bar{1}2\}$ twinning were sufficiently high that no $\{10\bar{1}2\}$ twinning occurred, a maximum, consisting of the poles originally within the dash enclosed area, would be formed along the rolling axis. The difference in the angle of the maxima from the rolling plane normal in the transverse and rolling directions, thirty and twenty degrees respectively, could be due to the fact that in the rolling direction both a tension and compression slip component tend to rotate the 0001 pole toward the rolling plane normal while in the transverse direction, only a compression rotation is present.

The change in the shear stress ratios between two types of slip or between slip and twinning allows changes in the deformation texture with increased reduction to be considered.

The assumption that the actual boundary may be located exactly requires the consideration of an additional factor. In the analysis of the compression texture, for example, the slip-twinning boundary is placed thirty degrees from the [0001] to agree with experimental results. The ability of T_e to move away from T_a is not considered. If it is assumed that the actual boundary is ten degrees from [0001] in Figure 38, the decrease in intensity from thirty to ten degrees in the measured texture can be attributed to the variation in movement of T_e from T_a . That is, if T_e is assumed to have a probability of further movement rather than slip decreasing with increased distance from T_a and equal to zero when T_e has moved twenty degrees from T_a , both the maximum at thirty degrees and the variation between thirty and ten degrees would be explained. It should be remembered that movement of T_e does not imply movement of T_a . A crystallite oriented so that T_a was at thirty degrees could conceivably twin from this position even though the slip-twinning boundary was at ten degrees if T_e is allowed sufficient freedom of movement. This will introduce the effect of freedom of movement of T_e to the already discussed change of ratio of shear stresses which should be considered in placing boundaries. Since there is presently no provision for considering the maximum movement of T_e or the effect of increased deformation on the maximum movement in the method of analysis developed by Calnan and Clews this

factor has been neglected. As more critical studies of the deformation textures of metals are conducted, the movement of T_e may be found to give an indication of the reasons for the differences in the deformation textures among metals of the same crystal structure.

The Calnan and Clews method of texture analysis has sufficient flexibility that new discoveries in single crystal studies may be included using only minor adjustments. For example, bending and kinking could be fitted into the analysis if the experimental data indicated that they were necessary for an accurate texture determination.

CHAPTER VIII

SUMMARY AND CONCLUSIONS

A. SUMMARY

The textures of titanium deformed by compression and cold rolling were examined using a new X-ray technique. This X-ray technique permitted rather exact textures to be determined.

The pole figures of iodide titanium compressed to eight different reductions were determined. Both compression between parallel plates and compression rolling were used to compress the titanium samples. The change in texture with increased reduction was studied.

Samples of iodide titanium and three grades of commercial titanium were examined after cold rolling. The different textures developed by the various samples were determined. The effect of amount of reduction on the texture developed on cold rolling was studied.

The Calnan and Clews method of deformation texture analysis was examined and used to determine the probable origin of the tension, compression, and cold rolled texture of titanium. The mechanisms of slip and twinning in titanium were considered. Resolved shear stress contours were determined for the $\{0001\}\langle 11\bar{2}0 \rangle$, $\{10\bar{1}1\}\langle 11\bar{2}0 \rangle$, and $\{10\bar{1}0\}\langle 11\bar{2}0 \rangle$ slip systems. Twinning from the $\{10\bar{1}2\}$, $\{11\bar{2}2\}$, and $\{11\bar{2}1\}$

planes was considered. The final adjusted slip and twinning mechanisms were used to show how the 0001 pole figure of cold rolled titanium could have been developed.

B. CONCLUSIONS

The compression texture of titanium can be described as a [0001] rotated thirty degrees from the compression axis. As the amount of reduction increased the angle of rotation decreased. There was apparently a slight tendency for the rotation of the [0001] from the compression axis to occur about a $\langle 10\bar{1}0 \rangle$ rotation axis.

The cold rolled texture of titanium consisted of a (0001)[$10\bar{1}0$] texture rotated thirty degrees in the transverse direction. The degree of preferred orientation was greatest in the $10\bar{1}0$ pole figure in which the $\langle 10\bar{1}0 \rangle$ poles showed a very strong tendency to be in the rolling direction. The 0001 maximum was an equilibrium type maximum existing between the stable slip and twinning end positions.

The compression and cold rolled textures were shown to be those which would result if $\{0001\}\langle 11\bar{2}0 \rangle$, $\{10\bar{1}1\}\langle 11\bar{2}0 \rangle$, and $\{10\bar{1}0\}\langle 11\bar{2}0 \rangle$ slip plus $\{10\bar{1}2\}$ and $\{11\bar{2}2\}$ twinning were active simultaneously. The critical shear stresses were found to be related according to the following equation,

$$C_{s0001} = 1.1 C_{s10\bar{1}1} = 1.02 C_{s10\bar{1}0} = C_{t10\bar{1}2} = C_{t11\bar{2}2}$$

$\{10\bar{1}0\}$ slip was not present to any great extent at high reductions but was important at lower reductions.

The Calnan and Clews method of texture analysis was found to satisfactorily handle the deformation process of titanium. This method should be extremely valuable for future work since it can handle most types of deformation in its present form and can be modified when necessary to consider special cases.

The appearance of a pronounced double maximum in the 0001 pole figure in both the compression and cold rolling texture of titanium suggests that the textures of beryllium and zirconium should be re-examined using the more exact Geiger counter technique to determine whether the reported rolling texture, (0001)[10 $\bar{1}$ 0] with a spread in the transverse direction, is accurate. Both of these metals would be expected to show a double maximum.

BIBLIOGRAPHY

- Ashburn, A., "How to work titanium and its alloys." J. Amer. Machinist, Vol 95, p. 145, June 11, 1951
- Backofen, W. A., "The torsion texture of copper." Trans AIME, Vol 188, p. 1454, 1950
- Bakarjian, P. W., "Preferred orientation in rolled magnesium and magnesium alloys." Trans AIME, Vol 147, p. 266, 1942
- Barrett, C. S., "The crystallographic mechanisms of translation, twinning, and banding." Cold Working of Metals, Cleveland: American Society for Metals, 1949
- _____, "The stereographic projection." Trans AIME, Vol 124, p. 52, 1937
- _____, "The structure of iron after compression." Trans AIME, Vol 135, p. 296, 1939
- _____, The Structure of Metals, New York: McGraw-Hill Book Company, 1943
- _____, and L. H. Levenson, "Determination of orientation by etch pits." Trans AIME, Vol 137, p. 76, 1940
- Becker, K., R. O. Herzog, W. Jancke, and M. Polanyi, "Methods for the arrangement of crystal elements." Z. Physik, Vol 5, p. 61, 1921
- Boas, W. and E. Schmid, "The interpretation of deformation textures in metals." Z. tech. Physik, Vol 12, p. 71, 1931
- Bounds, A. M. and H. W. Cooper, "Annealing of titanium and zirconium." Met. Prog., Vol 59, p. 69, 1951
- Brown, A. F., "Slip bands and hardening processes in aluminum." J. Inst. Met., Vol 80, p. 115, 1951
- Burgers, W. J. and F. M. Jacobs, "Structure of rolled and drawn zirconium." Metallwirtschaft, Vol 14, p. 285, 1935
- Caglioti, V. and G. Sachs, "The structure of rolled zinc and magnesium." Metallwirtschaft, Vol 11, p. 1, 1932

- Calnan, E. A. and C. J. B. Clews, "Deformation textures in face-centered cubic metals." Phil. Mag., Vol 41, p. 1085, 1950
- _____, "The development of deformation textures in metals. Part II. Body-centered cubic metals." Phil. Mag., Vol 42, p. 616, 1951
- _____, "The development of deformation textures in metals. Part III. Hexagonal metals." Phil. Mag., Vol 42, p. 919, 1951
- Carpenter, J. R. and G. W. Luttrell, "Bibliography on titanium (to Jan. 1, 1950)." Geol. Sur., Circ. No. 87, 19 pp., 1951
- Carver, C. B., "Differentiation of grain size and phases in titanium." Met. Prog., Vol 59, p. 371, 1951
- Clark, H. T., Jr., "The textures of cold rolled and annealed titanium." Trans AIME, Vol 188, p. 1154, 1950
- Cook, M. and T. L. Richards, "Fundamental aspects of cold working of metals." J. Inst. Met., Vol 78, p. 463, 1951
- Dean, R. S., J. R. Long, F. S. Wartsman, and E. L. Anderson, "Preparation and properties of ductile titanium." Met. Tech., Vol 13, TP 1961, 1946
- _____ and B. Silkes, "Metallic titanium and its alloys." Bur. of Mines, Inf. Circ. 7381, 38 pp., 1946
- Decker, B. F., "Validity of pole figures." J. Appl. Phy., Vol 16, p. 309, 1945
- _____, E. T. Asp, and D. Harker, "Preferred orientation determination using a Geiger counter X-ray diffraction goniometer." J. Appl. Phy., Vol 19, p. 388, 1948
- DuMont, C. S., "Bibliography on titanium production and properties of titanium." Met. Prog., Vol 55, p. 368, 1949
- _____, "Bibliography on titanium, production, properties, and uses (1900-1946)." Battelle Memorial Institute, 180 pp., 1949
- Dunkerley, F. J., F. Pledger, V. Damiano, and J. Fulton, "Grain-growth and recrystallization characteristics of zirconium." Trans AIME, Vol 191, p. 1003, 1951

- Duwez, P. and J. L. Taylor, "The structure of intermediate phases in alloys of titanium with iron, cobalt, and nickel." Trans AIME, Vol 188, p. 1173, 1950
- Edmunds, G. and M. L. Fuller, "Relation of crystal orientation to bending qualities of a rolled zinc alloy." Trans AIME, Vol 99, p. 175, 1932
- Finlay, W. L., J. Resketo, and M. Vordahl, "Optical metallography of titanium." Ind. Engr. Chem., Vol 42, p. 218, 1950
- Fuller, M. L. and G. Edmunds, "Crystal orientations developed by progressive cold rolling of an alloyed zinc." Trans AIME, Vol 111, p. 146, 1934
- Gruner, P. and T. Bruggemann, "Source of rolling defects." Stahl u. Eisen, Vol 71, p. 20, 1951
- Hibbard, W. R., Jr., "A theory of deformation textures in metals," Rev. Met., p. 131, Feb. 1951
- _____, A. L. Kearney, W. H. Hawley, Jr., and E. C. Burke, "Solid solution alloys of aluminum with lithium and indium." Trans AIME, Vol 191, p. 978, 1951
- _____, and M. K. Yen, "Wire textures of copper and its binary and solid solution alloys with aluminum, nickel, and zinc." Trans AIME, Vol 175, p. 126, 1948
- Hill, R., The Mathematical Theory of Plasticity, London: Oxford University Press, 1950
- Hu, H., P. R. Sperry, and P. Beck, "Rolling textures in face-centered cubic metals." J. of Met., Vol 4, No. 1, p. 76, 1952
- Jacquet, P. A., "Electrolytic oxidation and polishing of titanium and their application in inspection of microstructures." Comptes Rendu, Vol 232, p. 71, 1951
- Leighly, H. P., "Etching of titanium." Met. Prog., Vol 60, p. 79, 1951
- Malts, J. and V. DePierre, "Heat treatment and structure of commercial titanium." Met. Prog., Vol 58, p. 862, 1950
- Mark, H., M. Polanyi, and E. Schmid, "Processes in the stretching of zinc crystals." Z. Physik, Vol 12, p. 58, 1923

- McElgin, J., "Experience growing in forming, machining titanium alloys." Steel, Vol 129, p. 68, 1951
- McGeary, R. K. and B. Lustman, "Preferred orientation in zirconium." AECD-2951, March 1950
- Meier, J. W., "Bibliography on titanium metal and alloys (1946-1950)." Can. Dept. of Mines and Tech. Surveys, Inf. and Mem. 303, 1951
- Morrell, L. G. and J. P. Hanawalt, "X-ray study of the plastic working of magnesium alloys." J. Appl. Phys., vol 3, p. 161, 1932
- Habarro, F. R. H., "Influence of grain boundaries on the plastic properties of metals." United Trade Press, (London), p. 38, 1950
- Neil, D. J., "A sheet specimen scanner for X-ray diffraction." Can. Inst. of Tech., Vol 29, p. 84, 1951
- Norton, J. T., "A technique for quantitative determination of textures of sheet metals." J. Appl. Phys., Vol 19, p. 1176, 1948
- Pickus, M. R. and C. H. Mathewson, "On the theory of the origin of rolling textures in face-centered cubic metals." J. Inst. Met., Vol 64, p. 237, 1939
- Polakowski, N. H., "The compression test in relation to cold rolling." J. Iron and Steel Inst., Vol 163, p. 250, 1949
- Polanyi, M., "Deformation, rupture, and hardening of crystals." Trans. Far. Soc., Vol 24, p. 72, 1928
- _____, "Structure changes in metals through cold working." Z. Physik, Vol 17, p. 42, 1923
- Roth, H. P., "Metallography of zirconium." Met. Prog., Vol 58, p. 709, 1950
- _____, "Microstructure of titanium." Met. Prog., Vol 59, p. 878, 1951
- Schmid, E. and W. Boas, Plasticity of Crystals, London: F. A. Hughes and Company, 1950, (English translation)
- Schulz, L. G., "A direct method of determining preferred orientation in flat reflection samples using a Geiger counter X-ray spectrometer." J. Appl. Phys., Vol 20, p. 1030, 1949

- _____, "Determination of preferred orientation in flat transmission samples using a Geiger counter X-ray spectrometer." J. Appl. Phy., Vol 20, p. 1033, 1949
- Smigelskas, A. and C. S. Barrett, "Preferred orientation in rolled and recrystallized beryllium." Trans AIME, Vol 185, p. 145, 1949
- Sutcliffe, D. A., J. I. M. Forsyth, and J. A. Reynolds, "Electrolytic polishing of titanium." Metallurgia, Vol 41, p. 283, 1950
- Taylor, G. I., "Mechanism of plastic deformation of crystals." Proc. Royal Soc., Vol A145, p. 362, 1934
- _____, "Plastic strain in metals." J. Inst. Met., Vol 62, p. 307, 1938
- _____, "Resistance to shear in metal crystals." Trans Far. Soc., Vol 24, p. 121, 1928
- "Tentative method for preparing quantitative pole figures of metals." ASTM, E81-49T, 1949
- Uspinskij, N. and Konobejewski, Lecture before the Russian Physical Lebedev Society, April 30, 1920, Moscow
- "Vacuum melting of titanium and zirconium." Steel, Vol 126, p. 77, June 18, 1951
- Wassermann, G., Textures of Metallic Materials, Berlin: Julius Springer, 1939
- Wever, F., "Texture of metals after cold deformation." Trans AIME, Vol 93, p. 51, 1931
- _____, "The structure of cubically crystallizing metals after rolling." Z. Physik, Vol 28, p. 69, 1924
- _____, and W. E. Schmid, "Texture of cold-deformed metals." Z. Metallkunde, Vol 22, p. 133, 1930
- Williams, W. L., "How titanium behaves at temperatures to 900°F." Iron Age, p. 81, June 14, 1951
- Wood, J. K., "An analytical discussion of the construction of pole figures." J. Appl. Phy., Vol 19, p. 784, 1948
- Werner, H. W., "Thermoelectric properties of titanium with special reference to the allotropic modification." Aust. J. Sci. Res., Vol 4A, p. 62, 1951

Yen, M. K., Interim report to Watertown Arsenal, WHL 401-
14/4, March 20, 1950

_____ and J. P. Nielsen, Discussion of paper by Clark,
Trans AIME, Vol 191, p. 549, 1951

A P P E N D I X

APPENDIX I

X-RAY TECHNIQUE

A universal specimen mount which combined the best features of the transmission specimen mount described by Decker et al (67) and the reflection mount described by Schulz (68) was developed for use in the pole figure studies conducted. This specimen mount allowed the complete pole figure to be determined using the Schulz-Decker technique. This method is both faster and more accurate than the usual photographic methods.

A description of the construction and use of the universal specimen mount has been published in a University of Missouri Bulletin (69) and in a national magazine (70).

(67) B. F. Decker, E. T. Asp, and D. Harker, "Preferred orientation determination using a Geiger counter X-ray diffraction goniometer." J. Appl. Phy., Vol 19, pp. 388-92, 1948

(68) L. G. Schulz, "A direct method of determining preferred orientation of a flat reflection sample using a Geiger counter X-ray spectrometer." J. Appl. Phy., Vol 20, pp. 1030-33, 1949, (Referred to hereafter as Schulz, Part I.)

(69) D. N. Williams and D. S. Eppelsheimer, "Universal specimen mount for pole figure determination using the Schulz-Decker technique." Bulletin, Univ. of Mo., Sch. of Mines and Met., Tech. Series No. 79, Jan. 1952

(70) D. N. Williams and D. S. Eppelsheimer, "Universal specimen mount for pole figure determination using the Schulz-Decker technique." to be published in Rev. Sci. Inst., April or May, 1952

The following discussion parallels that given in the above publications.

A. CONSTRUCTION OF THE SPECIMEN MOUNT

Schulz (71) has shown that if the value of μt is controlled in the method developed by Decker et al (72) by control of the sample thickness, intensity readings may be used directly without absorption corrections when the angle of rotation is small. The X-ray beam is regulated by means of the standard slit system. (A Norelco instrument is assumed.) Vertical slits are used at both the tube and the Geiger counter entrance. In most cases, satisfactory readings are obtained using the smallest tube slit (0.075 centimeter) and a slightly larger counter slit.

To complete the pole figure, Schulz suggested a method of mounting the sample to allow reflection patterns to be made (73). This method involves the use of three horizontal slits to control the shape of the incident beam, one at the tube, one between the tube and the sample, and one at the counter. A beam diverging in the horizontal plane and parallel in the vertical plane is obtained. With this in-

(71) L. G. Schulz, "Determination of preferred orientation in flat transmission samples using a Geiger counter X-ray spectrometer." *J. Appl. Phy.*, Vol 20, pp. 1033-36, 1949, (Referred to hereafter as Schulz, Part II.)

(72) Decker, Asp, and Harker, loc. cit.

(73) Schulz, Part I, loc. cit.

cident beam, absorption changes are eliminated. The only other requirement is that the sample must be of sufficient thickness to give complete absorption of the incident beam.

In determining the data for a pole figure it is necessary to mount the sample in such a manner that two axes of rotation are obtained for both the transmission and reflection samples. For simplicity, the axis which allows angular changes around any of the concentric latitude circles in the polar net drawn on the projection plane will be referred to as the axis of rotation. The axis which allows angular changes which change the diameter of the concentric latitude circles will be referred to as the axis of revolution. In the transmission method the axis of revolution is vertical and in the plane of the sample, and the axis of rotation is perpendicular to the plane of the sample. In the reflection method, the axis of revolution is horizontal and in the plane of the sample, and the axis of rotation is perpendicular to the plane of the sample.

To obtain these conditions a specimen mount was constructed consisting of the following parts: (See Figure 41)
1.--A base which is mounted on the spectrometer; 2.--A ring which revolves about a vertical axis in the base and which may contain one of two other rings which are free to rotate within it; 3.--The transmission ring; 4.--The reflection ring in which is placed a pin whose top half is free to rotate; and 5.--A horizontal slit which is used as the

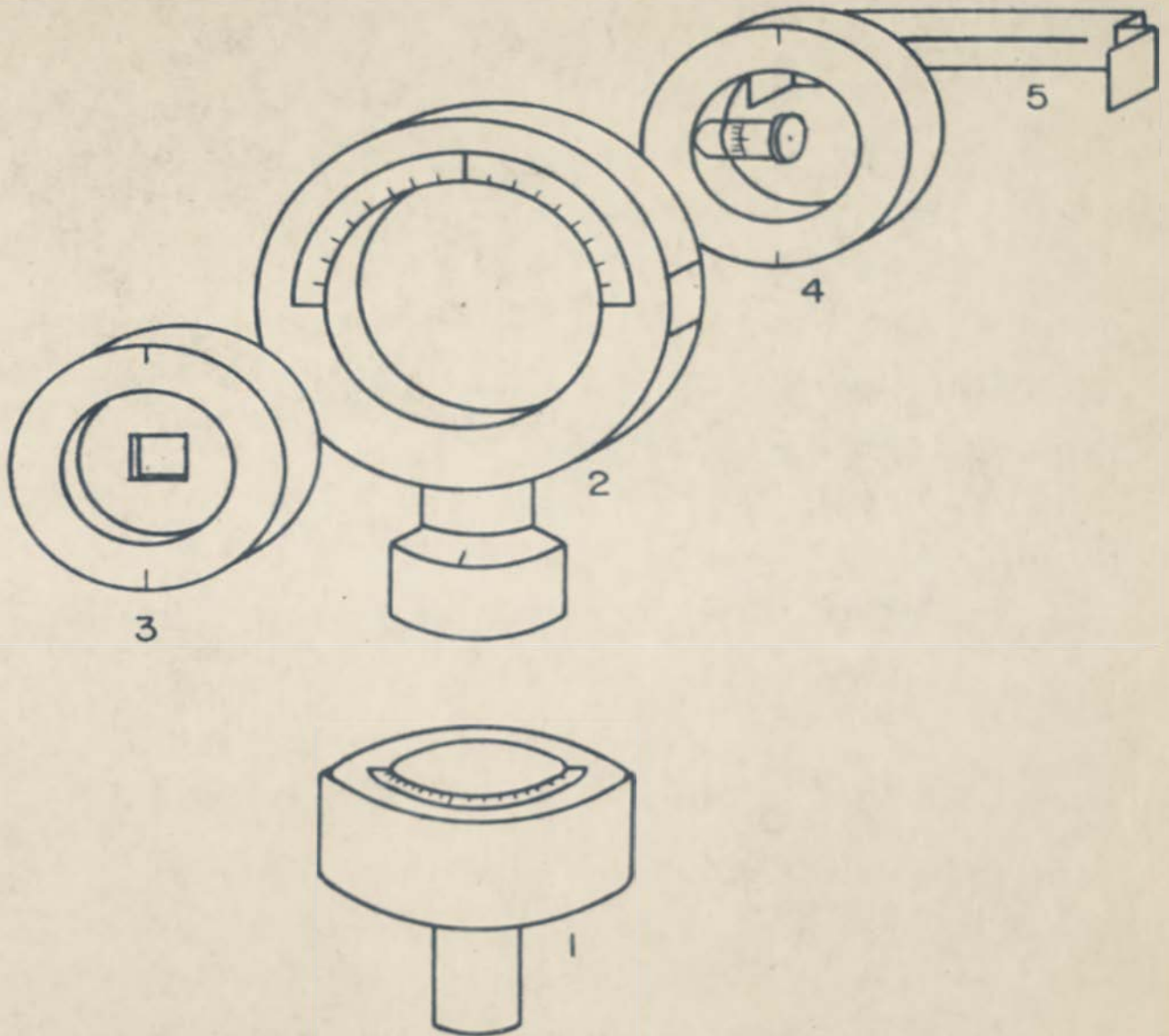


Figure 41. The five parts of the universal specimen mount.

second slit in the reflection method and which is held to ring 2 by a slight spring pressure.

In making transmission patterns (Decker technique) parts 1, 2, and 3 are used. Parts 1 and 2 give the necessary movement for the axis of revolution. Parts 2 and 3 give the necessary movement for the axis of rotation.

In making reflection patterns (Schulz technique) parts 1, 2, 4, and 5 are used. The ring 2 is set at the zero mark in the base and is not moved during the examination of the sample. The axis of revolution is given by movement of ring 4 in ring 2. The axis of rotation is obtained by movement of the top half of the mounting pin in ring 4 with respect to the bottom half.

A scale is placed on mount 1 running from $+90^\circ$ to -90° with an index mark placed on the base of ring 2. A scale is placed on one half of the mounting pin of ring 4 with an index mark on the other half of the mounting pin.

When the Geiger counter of the Norelco instrument is moved through an angle of 2θ , the mount 1 will move through an angle of θ . Thus the diameter of the projection of the reflection circle on the projection plane corresponds to the diameter of the polar net making a special pole figure net for each material and wave length unnecessary.

B. USE OF THE SPECIMEN MOUNT

The Schulz-Decker technique requires that two samples

be prepared. One sample is used with the transmission sample holder and the other with the reflection sample holder. After the transmission and reflection patterns have been determined the readings are corrected for absorption when necessary and the data plotted. The pole figures are plotted directly over a polar stereographic net.

Making transmission patterns. By means of the graph given by Schulz (74) and reproduced in this section (see Figure 42) the proper value of μt to correspond to the value of θ being used is chosen. The sheet sample is then etched to sufficient thickness to give this value of μt and mounted over the hole in ring 3. The parts 1, 2, and 3 are assembled and the intensity of the reflection with the sample in various positions is taken. The positions of the sample (A), reference sphere (B), and projection plane (E) are shown in Figure 43. The axis of revolution is a-a' and the axis of rotation is b-b'. Since the sample as shown in Figure 43 has the rolling direction vertical, the reflection picked up by the Geiger counter (H) will correspond to the intensity of reflection of the plane whose normal intersects the reference sphere at point (C). This point will project to point (D) on the projection plane (E). If the sample is rotated about b-b' by rotation of ring 3 within ring 2

(74) Schulz, Part II, loc. cit.

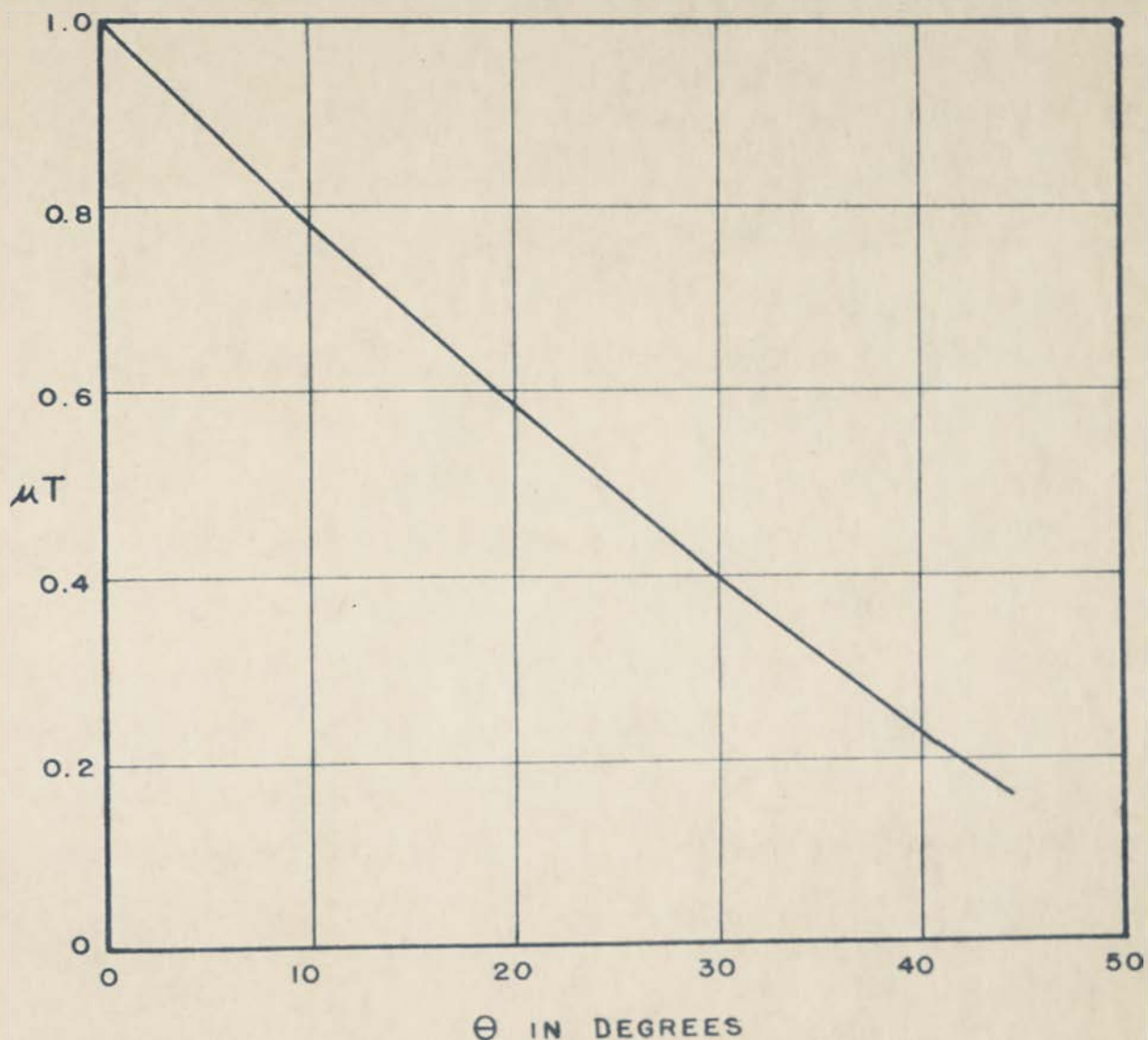


Figure 42. Graph showing the optimum value of μt for various values of θ . With these values of μt the counting rate is nearly independent of the values of the angle of revolution up to about 25° . From Schulz, Part II.

successive points may be plotted along the circumference of the projection of the reflection circle (J). If the sample is revolved 10° counter-clockwise as seen from above by revolving ring 2 in mount 1, a reading is obtained for the intensity of a point which will plot on the 10° latitude circle and in the transverse direction of the polar stereographic net. If the sample is again rotated about the axis b-b', successive points are obtained on the circumference of the 10° latitude circle. Similarly, by a 20° revolution followed by rotation about the axis b-b', readings are obtained for the 20° latitude circle. The transmission method is not used beyond a revolution of 25° unless it is desired to check the reflection readings. If readings are made beyond 25° for check purposes or if a sufficiently thin sample can not be prepared, a correction must be made of the observed intensities. Intensity corrections can be made using the formula developed by Decker et al (75),

$$(I_{\pm a}) = (I_{\pm a})_{\text{obs.}} \times I_0/I_{\pm a}$$

where,

$$I_0/I_{\pm a} = \frac{\mu t \exp[-\mu t/\cos \theta]}{\cos \theta} \times \frac{[\cos(\theta \pm a)/\cos(\theta \mp a)] - 1}{\exp[-\mu t/\cos(\theta \pm a)] - \exp[-\mu t/\cos(\theta \mp a)]}$$

in which μ is the absorption coefficient, t the sample thickness, and θ the Bragg angle. When viewing the sample from above when it is in place on the machine, $+a$ is a

(75) Decker, Asp, and Harker, loc. cit.

counter-clockwise revolution and $-a$ is a clockwise revolution. This formula was found to give accurate values when a was between $+20^\circ$ and -50° .

The necessary rotation and revolution to cover each quadrant of the projection can be determined from Figure 43 by geometrical considerations.

A picture of the universal specimen mount as it is used in making transmission intensity patterns, is shown in Figure 45.

Making reflection patterns. The size of the slit 5 is made equal to one of the tube slits. When examining titanium it was necessary to use the medium tube slit (0.150 centimeter) to obtain a sufficiently strong diffracted beam. The slit on the Geiger counter is kept about twice as wide as the tube slit and slit 5. All slits are mounted horizontally and vertical wedges are used at the tube and at the counter.

A circular sample is cut, using laminated sheets if necessary, and mounted parallel to the top surface of the mounting pin in ring 4. Ring 4 is then placed in ring 2. Ring 2 is kept stationary in mount 1 at the zero position. Slit 5 is placed in position on ring 2.

The position of the sample (A) with respect to the reference sphere (B) and the projection plane (E) is shown in Figure 44. The axis of revolution is $a-a'$. The axis of

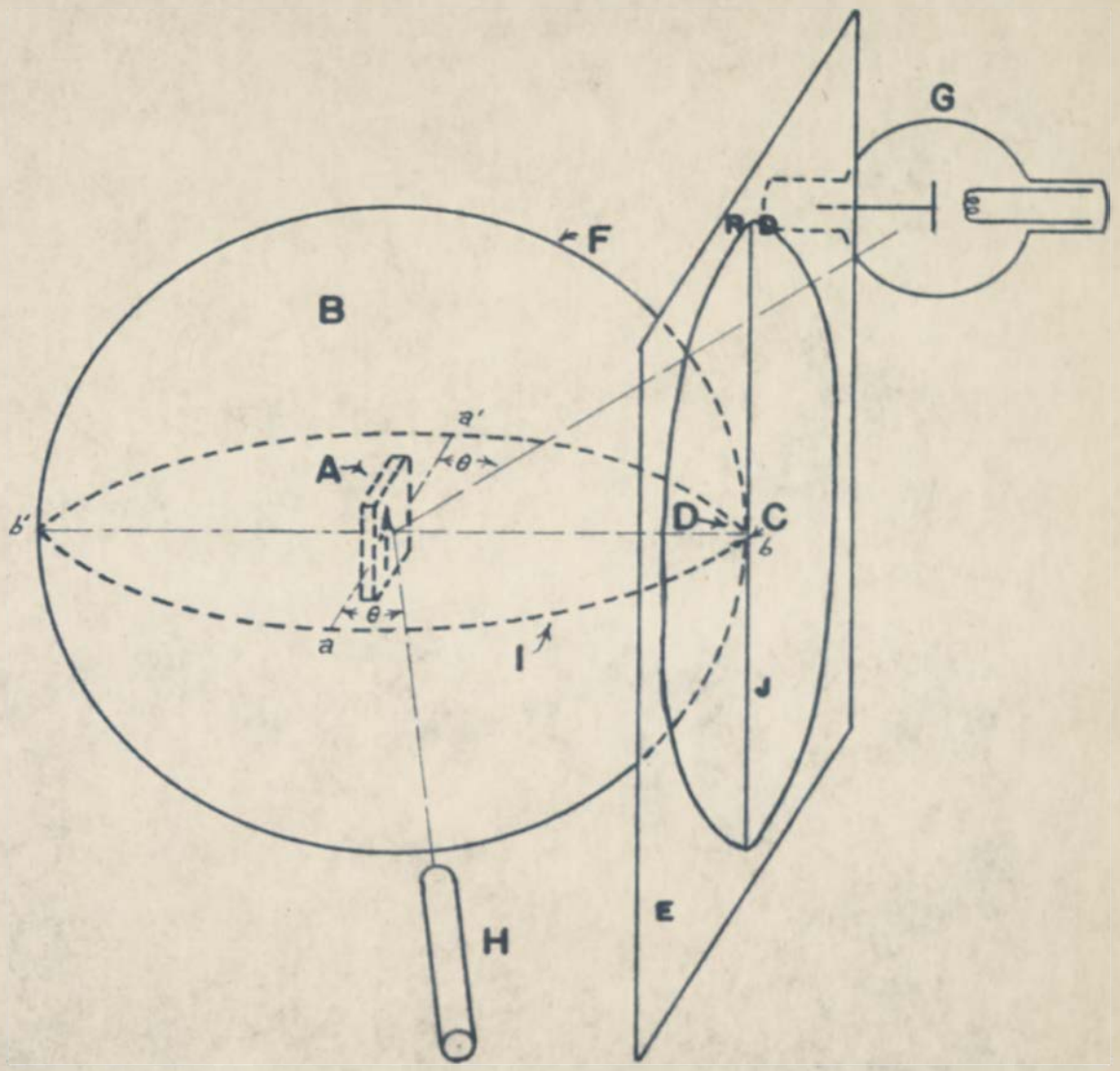


Figure 44. Location of the various elements in the reflection method.

The following symbols are used to identify the various elements in Figure 43 and Figure 44.

- a-a' Axis of revolution.
- b-b' Axis of rotation.
- A Sample.
- B Reference sphere.
- C Intersection of pole of reflecting plane with the reference sphere.
- D Projection of (C) on the projection plane.
- E Projection plane.
- F Reflection circle.
- G X-ray tube.
- H Geiger counter.
- I Intersection of the horizontal plane of the X-ray beam with the reference sphere.
- J Projection of the reflection circle (F) on the projection plane.
- R.D. Rolling direction of the sheet. The rolling direction is marked by an arrow on the sample (A) and by the letters R.D. on the projection plane (E).

rotation is $b-b'$. The positions of the reference sphere and projection plane were changed from those in Figure 43 to make the geometry involved in sample movement clearer. The sample as shown will give an intensity reading corresponding to point (D) on the projection plane. When the sample is correctly placed in position as shown in Figure 44, constant intensity readings should occur on rotation about axis $b-b'$ since the reflecting plane is perpendicular to the axis of rotation.

By revolution of the sample about axis $a-a'$ by moving ring 4 within ring 2 counter-clockwise 10° as one looks toward the tube, readings will be obtained on the 80° latitude circle of the polar stereographic net. Since the rolling direction is vertical in the sample as shown in Figure 44, the reading corresponds to a position 100° away from the rolling direction (R.D.) on the projection of the reference circle (J). A clockwise revolution gives readings in the opposite direction from the center of the polar stereographic net. If the sample is revolved 10° counter-clockwise and then rotated about the axis $b-b'$, successive readings are obtained along the circumference of the 80° latitude circle. Similarly, readings may be taken along the remaining latitude circles until the 20° latitude circle is reached.

Consideration of Figure 44 will show the direction of revolution and rotation necessary for each point on the

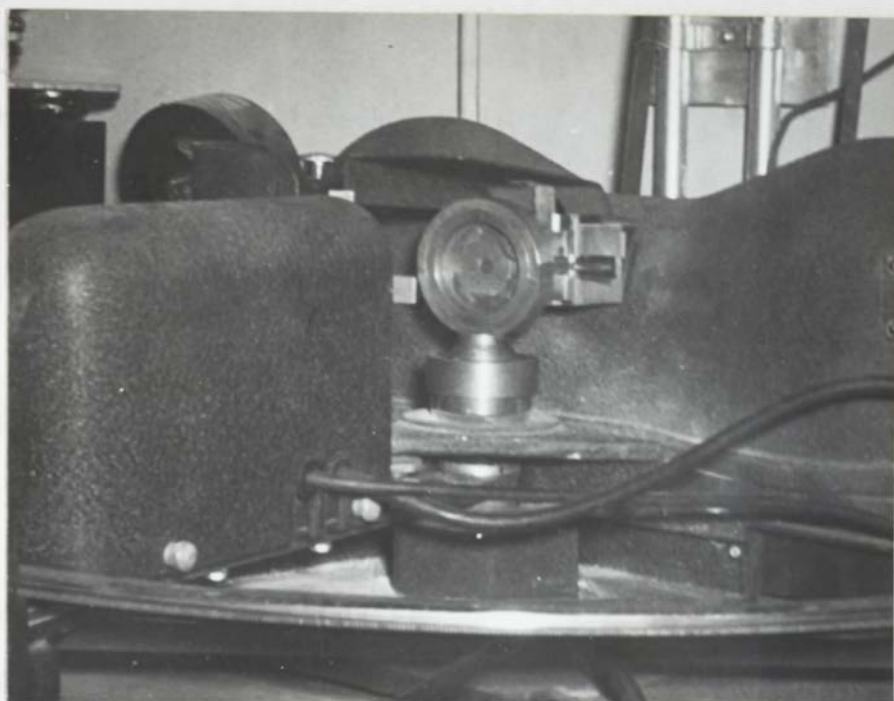


Figure 45. The universal specimen mount in position for measurement of transmission intensities.

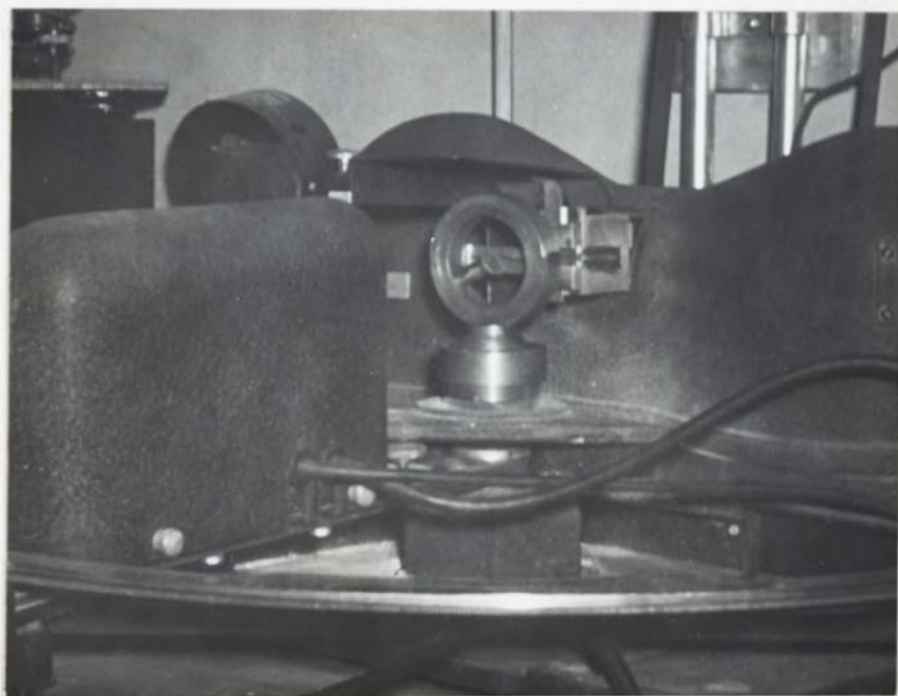


Figure 46. The universal specimen mount in position for measurement of reflection intensities.

polar stereographic net.

A picture of the universal specimen mount as it is used in making reflection intensity patterns is shown in Figure 46.

Plotting of the data. Readings may be taken either by stopping the Geiger counter at the correct value of 2θ or by running the Geiger counter a few degrees to cover the desired angle after each movement of the sample. The latter method appears to give more consistent results.

The data taken from the transmission and reflection intensity readings are plotted directly over a polar stereographic net. By examining the readings at 20° latitude circle obtained by the two methods, or between 20° and 50° if transmission readings are made to 50° , the necessary correction to make their intensities equal is calculated. The transmission readings are then corrected to correspond with the reflection readings.

If in plotting the data, a certain area seems to warrant increased coverage, this may be easily done.

APPENDIX II

INTERPRETATION AND ADJUSTMENT OF DATA

The 1011 pole figure of a cold rolled sample of commercial titanium is used for this demonstration of the necessary correction of data. In the examination of titanium, the high scattering power made reflection readings beyond an angle of revolution of 50° unreliable. The transmission readings were therefore made to -50° and the measured intensities corrected for absorption. The readings at 50° were then used to correlate the readings from the two patterns. In the following sections, all of the necessary steps to plot a pole figure from the data of the X-ray patterns are discussed.

A. TABULATION OF INTENSITY DATA

As in Appendix I, the angles along the concentric latitude circles will be referred to as angles of rotation and angles along the diameters of the polar stereographic net will be referred to as angles of revolution.

In Figure 47, a portion of the transmission pattern is reproduced. This illustration shows the readings taken with an angle of revolution of -20° and angles of rotation at 10° intervals between the transverse direction (T.D.) and the rolling direction (R.D.) of the sheet. A segment of the titanium pattern was run at each angle of revolution to

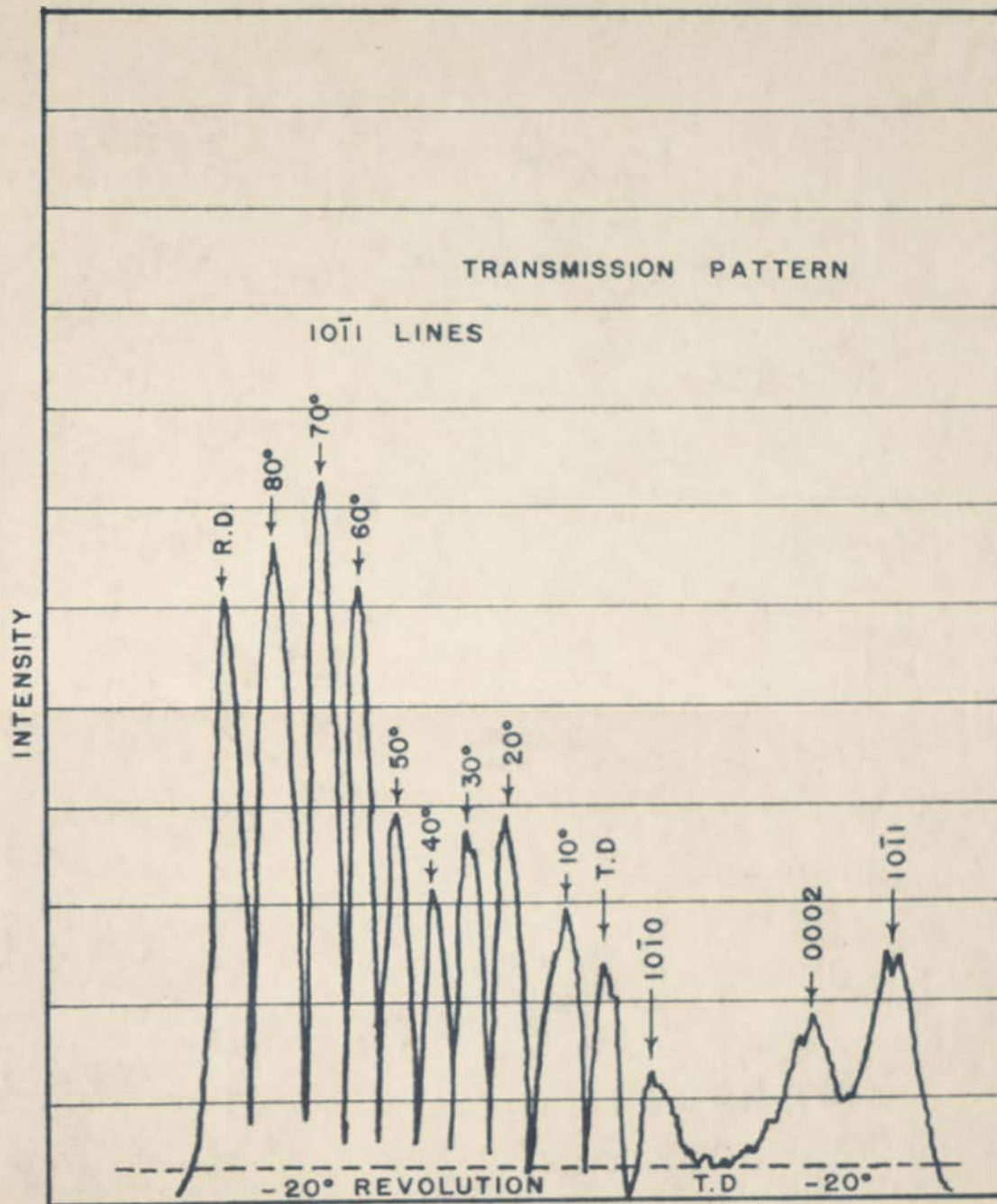


Figure 47. Part of the transmission pattern of a cold rolled sample of commercial titanium.

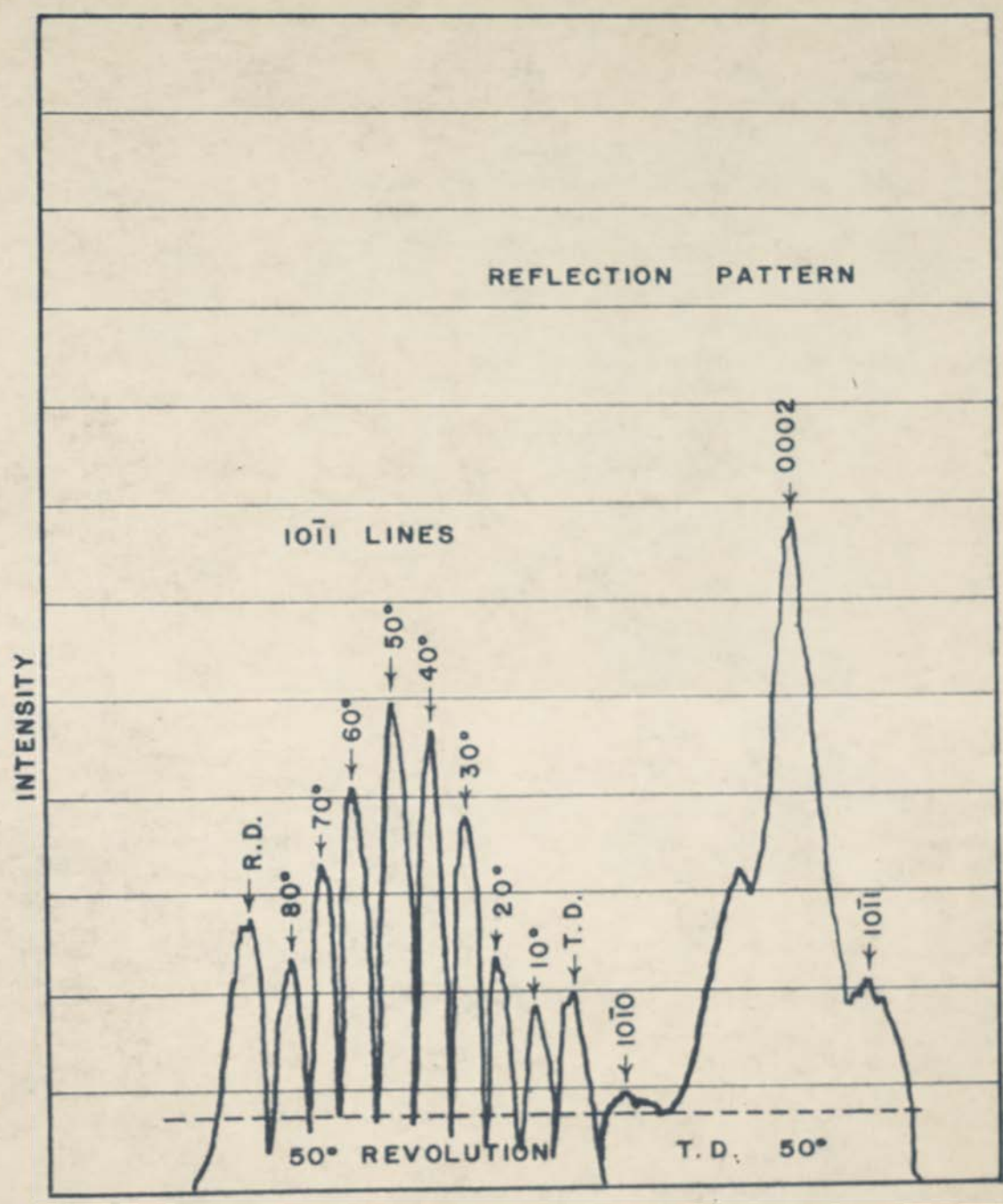


Figure 48. Part of the reflection pattern of a cold rolled sample of commercial titanium.

TABLE XII

$10\bar{1}1$ INTENSITIES FROM TRANSMISSION PATTERN

Angle of Revolution	T.D.	Angle of Rotation								R.D.
		10°	20°	30°	40°	50°	60°	70°	80°	
0°	47	65	68	77	54	41	38	20	10	10
-10°	31	51	58	52	44	42	52	34	27	26
-20°	<u>20</u>	<u>25</u>	<u>36</u>	<u>33</u>	<u>27</u>	<u>35</u>	<u>58</u>	<u>68</u>	<u>63</u>	<u>57</u>
-30°	10	16	18	21	21	22	34	46	39	42
-40°	8	8	15	16	15	13	14	18	17	22
-50°	5	5	11	13	18	15	13	13	9	8

TABLE XIII

$10\bar{1}1$ INTENSITIES FROM REFLECTION PATTERN

Angle of Revolution	T.D.	Angle of Rotation								R.D.
		10°	20°	30°	40°	50°	60°	70°	80°	
50°	<u>13</u>	<u>10</u>	<u>16</u>	<u>31</u>	<u>40</u>	<u>42</u>	<u>33</u>	<u>26</u>	<u>17</u>	<u>21</u>
55°					37	55	44			
60°	1	8	12	13	29	40	49	41	30	33
70°	5	7	8	6	8	7	13	17	12	12
80°	1			3			3			3
90°	2			1			1			2

determine the background intensity. This pattern appears at the right side of Figure 47. The background intensity is marked by a dashed line. The intensity of each line is determined by measuring its height above the background line. The measured transmission intensities are given in Table XII. The values which are underlined are those which were obtained from the lines shown in Figure 47.

In Figure 48, a portion of the reflection pattern of the sample of cold rolled titanium is shown. The measured reflection intensities are given in Table XIII.

B. CORRECTION OF TRANSMISSION READINGS FOR ABSORPTION

The transmission readings in Table XII require an absorption correction before being correlated with the reflection readings. The Decker absorption correction formula and method of determining μt were used for this correction (76). Measurements of the intensity of a strong line from a brass sample were made with the counter open and then with the counter covered by the transmission sample. These intensity readings were designated I_0 and I respectively and were used to calculate μt . The calculation is shown below,

$$I_0 = 165$$

(76) B. F. Decker, E. T. Asp, and D. Harker, "Preferred orientation determination using a Geiger counter X-ray diffraction goniometer." J. Appl. Phy., Vol 19, pp. 388-92, 1948

TABLE XIV

CORRECTION FACTOR FOR TRANSMISSION INTENSITIES

Angle of Revolution	Correction Factor (f)*
0°	1.00
-10°	1.08
-20°	1.21
-30°	1.43
-40°	1.90
-50°	3.08

* The values of f were determined by solving the Decker absorption equation,

$$f = \frac{\mu t \exp[-\mu t / \cos \theta]}{\cos \theta} \times \frac{[\cos(\theta - a) / \cos(\theta + a)] - 1}{\exp[-\mu t / \cos(\theta - a)] - \exp[-\mu t / \cos(\theta + a)]}$$

where μt is 1.523, a is the angle of revolution, and θ , the Bragg angle for the 1011 line of titanium, is 20.08°.

TABLE XV
CORRECTED TRANSMISSION INTENSITIES

Angle of Revolution	T.D.	Angle of Rotation								R.D.
		10°	20°	30°	40°	50°	60°	70°	80°	
0°	47	65	86	77	54	41	38	20	10	10
-10°	33	55	62	56	47	45	56	37	29	28
-20°	24	30	43	40	33	42	70	82	76	69
-30°	14	23	26	30	30	32	49	66	56	60
-40°	15	15	28	30	28	25	27	34	32	42
-50°	15	15	34	40	56	46	40	40	28	25

$$I = 36$$

$$\ln(I_0/I) = \mu t = \ln(4.58)$$

$$\mu t = 1.523$$

$$\text{and since } \mu = 918/\text{cm},$$

$$t = 0.00166 \text{ centimeter}$$

This value of μt was substituted into the Decker correction formula along with the value of θ for the $10\bar{1}1$ line of titanium and the correction factor determined. The Decker correction formula and the calculated values of the correction factor are given in Table XIV. The corrected transmission intensity reading, I_0 , was found by multiplying the observed intensity reading, I_{obs} , by the correction factor, f . ($I_0 = I_{\text{obs}} \times f$) The corrected values of the observed intensities tabulated in Table XII are given in Table XV.

C. CORRELATION OF PATTERNS

After correction of the transmission intensities for absorption, the transmission and reflection intensity readings obtained at an angle of revolution of 50° were compared and a factor calculated to make them correspond.

The transmission readings at 50° were divided by the reflection readings at 50° in the following manner,

Rotation	T.D.	10°	20°	30°	40°	50°	60°	70°	80°	R.D.	
Trans.	15	15	34	40	56	46	40	40	28	25	
Refl.	13	10	16	31	40	42	33	26	17	21	
$f_1 = \left(\frac{\text{Trans}}{\text{Refl}}\right)$		1.15	1.50	2.13	1.29	1.40	1.10	1.21	1.54	1.65	1.19

The highest two and the lowest two readings were discarded and the remaining six averaged. The average value of f_1 in this case was 1.35. Removing the four readings most apt to be in error before averaging prevents one or two bad intensity readings from effecting the final pole figure. This is especially necessary when the transmission correction factor is large, as in this example in which it was 3.08.

The reflection readings were multiplied by f_1 to make them correspond to the transmission readings. The values of the readings at 50° were obtained by taking the mean value of the transmission and reflection readings after correction,

Rotation	T.D.	10°	20°	30°	40°	50°	60°	70°	80°	R.D.
Trans.	15	15	34	40	56	46	40	40	28	25
Refl.	18	14	22	42	54	57	45	35	23	28
Mean	16	14	28	41	55	52	42	38	26	26

The correlated intensity values are given in Table XVI.

D. PLOTTING OF DATA

The intensity values given in Table XVI were reduced to make the maximum intensity have a value of seventy intensity units. This choice of maximum intensity is arbitrary and was made for convenience of plotting. The values were reduced by multiplying all of the values in Table XVI by the value of the ratio of the maximum in Table XVI to the desired maxi-

TABLE XVI
CORRELATED INTENSITY VALUES

Angle of Revolution	T.D.	Angle of Rotation								R.D.
		10°	20°	30°	40°	50°	60°	70°	80°	
0°	47	65	86	77	54	41	38	20	10	10
10°	33	55	62	56	47	45	55	37	29	28
20°	24	30	43	40	33	42	70	82	76	69
30°	14	23	26	30	30	32	49	66	56	60
40°	15	15	28	30	28	25	27	34	32	42
50°	16	14	28	41	55	52	42	38	26	26
55°					50	75	60			
60°	1	11	16	18	29	54	66	56	41	45
70°	7	9	11	8	11	9	18	23	16	16
80°	1			4			4			4
90°	3			1			1			3

TABLE XVII

FINAL ADJUSTED 10^{11} INTENSITY VALUES

Angle of Revolution	T.D.	Angle of Rotation								R.D.
		10°	20°	30°	40°	50°	60°	70°	80°	
0°	38	53	70	63	44	33	31	16	8	8
10°	27	45	50	46	38	37	46	30	24	23
20°	20	24	35	33	27	34	57	67	62	56
30°	11	19	21	24	24	26	40	54	46	49
40°	12	12	23	24	23	20	22	28	26	34
50°	13	11	23	33	45	42	34	31	21	21
55°					41	61	49			
60°	1	9	13	15	24	44	54	46	33	37
70°	6	7	9	7	9	7	15	19	13	13
80°	1			3			3			3
90°	2			1			1			2

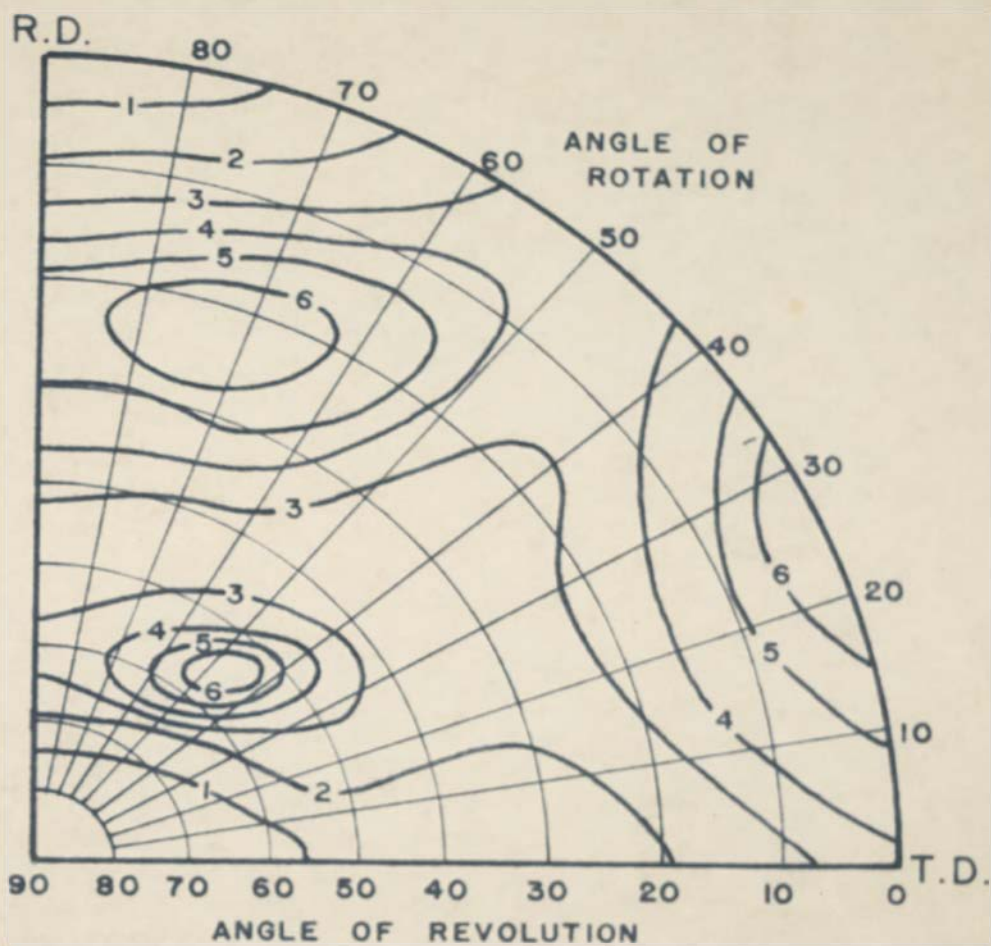


Figure 49. $10\bar{1}1$ pole figure resulting from a plot of the intensity values given in Table XVII.

sum, 70/86. The new adjusted values are given in Table XVII. The pole figure was constructed by placing each intensity value over its correct point on a polar stereographic net and drawing constant intensity contour lines. The pole figure resulting from a plot of the data given in Table XVII is shown in Figure 49. The polar stereographic net has been reproduced with the pole figure and the angles of rotation and revolution indicated. The contour lines for intensities of 60, 50, etc. are shown on the pole figure by the numbers 6, 5, etc.

APPENDIX III

THE RECRYSTALLIZATION TEXTURE OF COMMERCIAL TITANIUM

The annealed texture of iodide titanium has been examined by Clark (77) who reported only the 0001 pole figure but indicated that the annealed texture tended toward the (0001)[10 $\bar{1}0$] with a transverse rotation. The pole figures reported for annealed zirconium on the other hand showed a definite (0001)[11 $\bar{2}0$] with a transverse rotation (78). No studies of commercial titanium have been reported in the literature. Since cold rolled samples of commercial titanium were available from the deformation texture studies, a brief examination of the annealed texture was undertaken.

Samples of commercial titanium grade number two were annealed at three different temperatures after cold rolling to determine the annealed texture of commercial titanium. This commercial grade of titanium was used because of its fine annealed grain size.

A. EXPERIMENTAL PROCEDURE

Samples of the cold rolled commercial titanium, having

(77) H. T. Clark, Jr., "The textures of cold rolled and annealed titanium." Trans AIME, Vol 188, pp. 1154-56, 1950

(78) R. K. McGeary and B. Lustman, "Preferred orientation in zirconium." AEGD-2951, March 1950

a texture such as that shown in Figure 18, Chapter VI, were annealed for one-half hour in helium at temperatures of 650°C, 800°C, and 880°C. All of these temperatures were below the transformation temperature.

The cold rolled samples were etched slightly to 0.021 centimeter. The etched samples were placed in the furnace at temperature, held one-half hour, and cooled in helium according to the procedure outlined in Chapter III.

The annealed samples were then etched to remove the slight scale produced in the furnace and mounted for X-ray examination. The Schulz-Decker technique was used (see Appendix I). Because of the small grain size of the annealed samples (less than 0.015 millimeter) no scanning was necessary. Readings were taken from the $10\bar{1}0$ and 0001 planes and the pole figures constructed.

The $10\bar{1}0$ and 0001 pole figures of commercial titanium annealed at 650°C, 800°C, and 880°C are given in Figures 50, 51, and 52 respectively.

B. DISCUSSION OF RESULTS

The pole figures shown in Figures 50, 51, and 52 showed the same general texture. There were apparently at least three ideal textures represented. These were: (1), (0001) $[10\bar{1}0]$ rotated 30° in the transverse direction; (2), (0001) $[11\bar{2}0]$ rotated 30° in the transverse direction; and (3), $(0001)[10\bar{1}0]$ rotated 30° in the transverse direction fol-

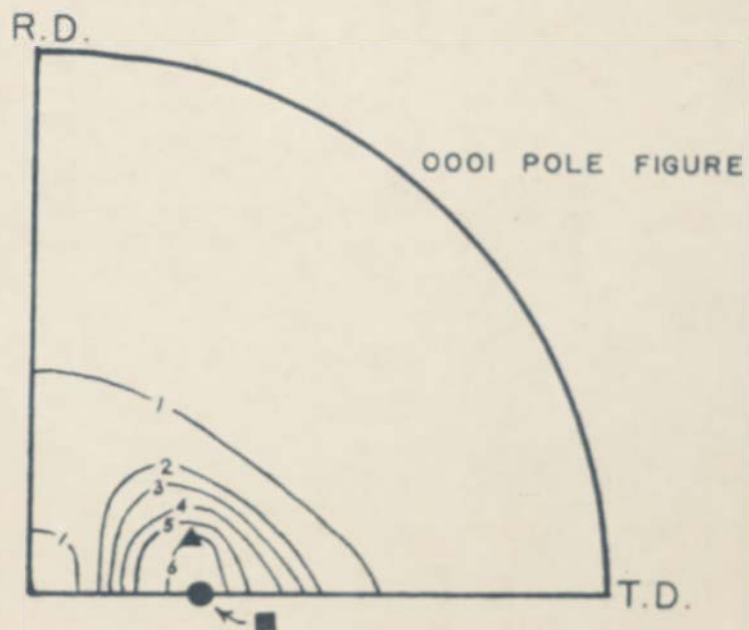
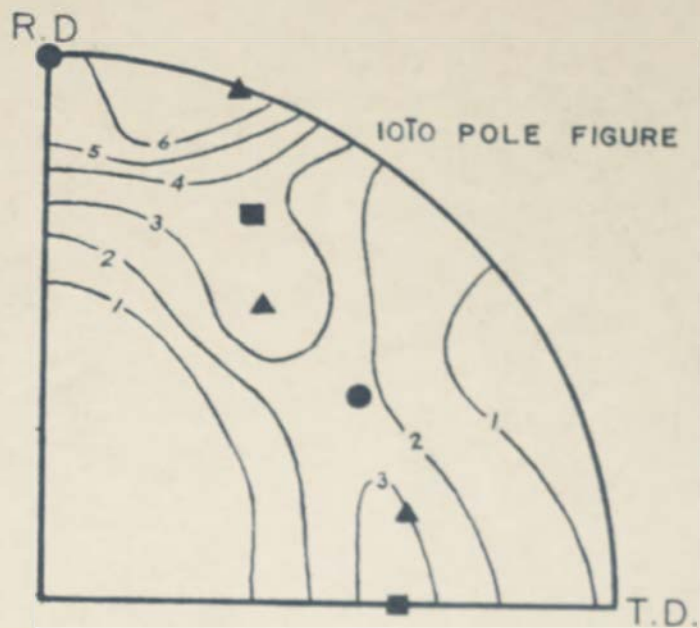


Figure 50. Pole figures of commercial titanium annealed one-half hour at 650°C. ●--(0001)[10 $\bar{1}$ 0] rotated 30° in T.D. ■--(0001)[11 $\bar{2}$ 0] rotated 30° in T.D. ▲--(0001)[10 $\bar{1}$ 0] rotated 30° in T.D. and 20° about rolling plane normal.

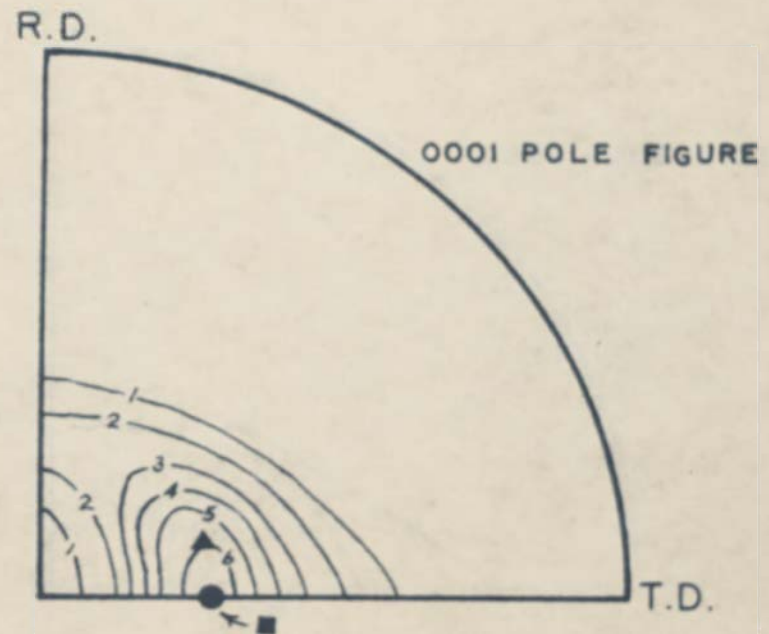
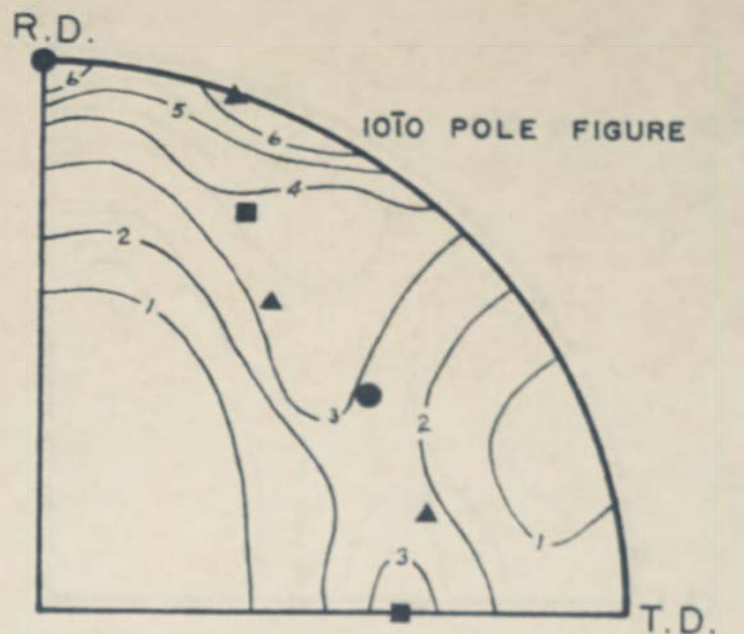


Figure 51. Pole figures of commercial titanium annealed one-half hour at 800°C. ●--(0001)[1010] rotated 30° in T.D. ■--(0001)[1120] rotated 30° in T.D. ▲--(0001)[1010] rotated 30° in T.D. and 20° about the rolling plane normal.

lowed by a rotation of 20° about the rolling plane normal. (This texture could also have resulted from a double rotation of the $(0001)[11\bar{2}0]$ texture.) Texture number one was designated by a circle, number two by a square, and number three by a triangle in the pole figures.

Texture number one was the same as the cold rolled texture and presumably was due to recrystallization in place. Texture number two was the same as the texture reported for recrystallized zirconium (79). Texture number three was a new texture as yet unreported in the literature.

The change of recrystallization texture with change in the recrystallization temperature was slight. Examination of the pole figures indicated that a slight increase in texture number three at the expense of texture number one was occurring as the annealing temperature was raised.

A spread of orientations between these three ideal textures was seen in the pole figures. This suggested that one of them may have been a transition texture existing between the other two. That is, texture number one may have been changing to texture number three which was itself changing to texture number two. There were not sufficient data in the pole figures from which the ideal final texture and the transition texture, if one existed, could be determined.

(79) McGeary and Lustman, loc. cit.

The 0001 pole figures of commercial titanium did not show the same tendencies as those reported by Clark for iodide titanium (80). The iodide texture still showed considerable spread toward the transverse direction in the 0001 pole figure but had lost those orientations near the rolling plane normal after annealing. In commercial titanium the opposite tendency was noted.

C. SUMMARY

1. The texture of commercial titanium initially having the normal cold rolled texture, $(0001)[10\bar{1}0]$ rotated 30° in the transverse direction, was determined after annealing one-half hour at 650°C , 800°C , and 880°C .

2. Three ideal components were recognizable in the annealed texture. These were: (1), $(0001)[10\bar{1}0]$ rotated 30° in the transverse direction; (2), $(0001)[11\bar{2}0]$ rotated 30° in the transverse direction; and (3), $(0001)[10\bar{1}0]$ rotated 30° in the transverse direction and 20° about the rolling plane normal. This texture could also have been the result of a double rotation of the $(0001)[11\bar{2}0]$.

3. The annealed textures were relatively unaffected by annealing temperature in the range examined.

(80) Clark, *loc. cit.*

VITA

The author was born on December 31, 1927, in Salt Lake City, Utah. He graduated from the Belle Plaine High School of Belle Plaine, Iowa, in June, 1945, and entered the army immediately. In September, 1947, he entered the Michigan College of Mining and Technology and graduated with a degree of Bachelor of Science in Metallurgical Engineering in April, 1950. He received a degree of Master of Science from the same institution in August, 1950. In September, 1950, he received the National Lead Company Research Fellowship at the Missouri School of Mines and Metallurgy.